R005-01
B 会場 ：11/4　PM1 （13:45-15:30）
13:45〜14:00

SS-520-3 号機観測ロケット実験フライト結果の概要

#齋藤　義文 [1)], 小嶋　浩嗣 [2)], 小川　泰信 [3)], 浅村　和史 [4)], 阿部　琢美 [5)], 石坂　圭吾 [6)], 栗田　怜 [7)], 熊本　篤志 [8)], 頭師　孝拓 [9)], 田中　真 [10)], 滑川　拓 [11)], 野村　麗子 [12)], 細川　敬祐 [13)], 松岡　彩子 [14)], 横田　勝一郎 [15)],Moen Joran[16)],Miloch　Wojciech J.[17)]
([1 宇宙研,([2 京大・生存圏,([3 極地研,([4 宇宙研,([5 ＪＡＸＡ宇宙科学研究所,([6 富山県大・工,([7 京都大学 生存研,([8 東北大・理・地球物理,([9 奈良高専,([10 東海大・情教セ,([11 東大・理・地惑,([12JAXA,([13 電通大,([14 京都大学,([15 大阪大,([16 オスロ大学,([17University of Oslo

Overview of the SS-520-3 Sounding Rocket Experiment

#Yoshifumi Saito[1)], Hirotsugu Kojima[2)], Yasunobu Ogawa[3)], Kazushi Asamura[4)], Takumi Abe[5)], Keigo Ishisaka[6)], Satoshi Kurita[7)], Atsushi Kumamoto[8)], Takahiro Zushi[9)], Makoto Tanaka[10)], Taku Namekawa[11)], Reiko Nomura[12)], Keisuke Hosokawa[13)], Ayako Matsuoka[14)], Shoichiro Yokota[15)], Joran Moen[16)], Wojciech J. Miloch[17)]
([1ISAS,([2RISH, Kyoto Univ.,([3NIPR,([4ISAS/JAXA,([5ISAS/JAXA,([6Toyama Pref. Univ.,([7RISH, Kyoto Univ.,([8Dept. Geophys, Tohoku Univ.,([9National Institute of Technology , Nara Col,([10Tokai Univ.,([11Earth and Planetary Science, Tokyo Univ.,([12JAXA,([13UEC,([14Kyoto University,([15Osaka Univ.,([16University of Oslo,([17University of Oslo

In order to understand the particle acceleration processes that cause the ion outflow by making in-situ observation of the wave-particle interaction in the polar cusp, SS-520-3 sounding rocket was successfully launched from Ny-Alesund on 4 November 2021.

Although SS-520-3 was planned to be launched in December 2017, the launch was postponed due to mal-function of the timer equipment that was found during the final stage of the integration test. After fixing the timer equipment problem, we had no launch opportunity until 2021. During the postponement period, the solar activity decreased to the solar minimum around the end of 2019 and started to recover afterwards. It was good for the SS-520-3 sounding rocket experiment that the solar activity in November 2021 recovered to the level similar to that in December 2017. The opportunities that satisfy the launch condition were rare around the solar minimum since the latitude of cusp became higher comparing the apex latitude of SS-520-3.

An M-class flare occurred two days before the scheduled two-week launch window that started on 3 November. A halo CME was observed in conjunction with this flare and reached Earth around 2000 UT on November 3, which triggered the magnetic storm on November 4.

SS-520-3 was launched at 10:09:25UT with the launcher setting Azimuthal angle of 202.4deg. and Elevation angle of 80.7deg. The condition of the ionosphere before and after the launch was monitored by 32 m and 42m antennas of the EISCAT Svalbard Radar and the launch timing was decided mainly by confirming that the electron temperature increased at the altitude of 350km where the apex of the rocket was traced down along the magnetic field line. The trajectory of the rocket was mostly as planned with the apex altitude of 742.011km (at +487.0s 10:17:32UT) and the impact range of 1353.861km (at +993.5s 10:25:59UT).

SS-520-3 was equipped with 9 onboard instruments including DFG: Digital Flux Gate magnetometer, LFAS: Low Frequency Analyzer System, TSA: Thermal ion Spectrum Analyzer, LEP: Low Energy Particle experiment, IMS: Ion Mass Spectrometer, FLP: Fast Langmuir Probe, NLP: Needle Langmuir Probe, NEI/PWM: Plasma and Wave Monitor, and SAS: Sun Aspect Sensor. Judging from the obtained data, SS-520-3 succeeded in flying in the mantle, cusp, and LLBL during the time period around the Apex above 700km altitude and afterwards. All the onboard instruments succeeded in obtaining data during the SS-520-3 flight in the cusp.

SS-520-3 sounding rocket experiment is a part of the comprehensive observation campaign including ground-based radar and optical observations. SS-520-3 sounding rocket experiment is also one of the projects participating in “A Grand Challenge Initiative (GCI) Cusp program” that is a large-scale international collaboration for targeting advancement in the common understanding of cusp region space physics.

極域カスプにおける電離大気の流出メカニズムを解明する目的で、2021 年 11 月 4 日に Ny-Alesund から SS-520-3 号機観測ロケットが打ち上げられた。元々、SS-520-3 号機観測ロケットは 2017 年 12 月に打ち上げる予定であったが、噛み合わせ試験の最終段階でタイマー装置に不具合が見つかったため、打ち上げが延期されることになった。その後、タイマー装置の不具合の改修は完了したものの、いくつかの理由から 2021 年まで打ち上げることができなかった。打ち上げの延期が続く中、2019 年末頃に太陽活動は低下して太陽活動極小となり、その後再び回復に向かった。太陽極小期には SS-520-3 の最高高度の緯度に比べてカスプの緯度が高くなり打ち上げ条件を満たす機会が少なくなっていたため、2021 年 11 月の太陽活動が、2017 年 12 月と同程度に回復したことは SS-520-3 号機観測ロケット実験にとって好都合であった。

11 月 3 日からの 2 週間に予定されていた打ち上げ期間が始まる 2 日前に M クラスフレアが発生した。このフレアに伴ってハロー CME が観測され、11 月 3 日の 2000UT 頃に地球に到達したことで 11 月 4 日には磁気嵐が発生した。

R005-02
B 会場 ：11/4　PM1 （13:45-15:30）
14:00〜14:15

#阿部　琢美 [1)]
(1 ＪＡＸＡ宇宙科学研究所

Variation of ion current in the current – voltage characteristics obtained by Langmuir Probe onboard “SS-520-3” sounding rocket

#Takumi Abe[1)]
(1ISAS/JAXA

Ion outflow along the geomagnetic lines of force from the polar ionosphere have been reported since 1970's based on the sounding rocket and satellite observations. The ionospheric cusp is known as a particular region where the largest flux of the ionospheric ion is observed. In November, 2021, in Svalbard, Norway, JAXA and the related organizations conducted a sounding rocket "SS-520-3" campaign whose purpose is to elucidate the plasma acceleration/heating mechanism responsible for the ion outflow/upflow in the ionospheric cusp region. A combination of the high time resolution in-situ rocket measurements and the ground-based optical and radar observations makes it possible to approach such an important science topic. In comparison with other experiments, the feature of this campaign is to try to make an in-situ measurement of wave-particle interaction which is believed to play a primary role in the ion energization. Sounding rocket "SS-520-3" was launched at 11:09:25 CET from the SvalRak facility at Ny-Alesund in Svalbard, Norway, after confirming that the rocket would traverse a region of the ion upflow. A total of 9 science instruments were installed on the rocket. Observations of thermal plasmas by FLP (Fast Langmuir Probe) instrument onboard the rocket will be discussed in this presentation.

A cylindrical probe with a length of 200 mm and a diameter of 3 mm was adopted to the FLP. The probe is directly biased by a triangular voltage with an amplitude of 4 V with respect to the rocket potential and a period of 100 msec so as to provide the current-voltage relationship. A current incident to the probe was sampled with a rate of 6400 Hz and amplified by two different gains (low and high) so that it can measure in a wide range of the plasma density. In order to measure the ion current as well as the electron current, the amplifier has an offset voltage of +0.5 V. The electron temperature and number density can be derived from a relationship between the incident current versus voltage applied to the probe.

The obtained FLP data were good enough in quality to estimate electron temperature and density. In our study, ion current in addition to electron current is subject to be analyzed since the main objective of this rocket campaign is to investigate the thermal ion upflow in the cusp region. Results obtained so far from our analysis are summarized as follows:

1) The FLP successfully made its measurement during both upleg and downleg of the rocket flight, which means that the local electron temperature and density can be estimated.

2) The observed electron density is larger than the predicted value, which suggests a possible traverse of the rocket through a region of the electron precipitation.

3) The ion current exhibits unusual behavior in the current – voltage characteristics. The cause of such a particular component is now investigated.

4) A ratio of electron to ion random currents significantly changed during the flight, which may be caused by a change in a ratio of electron to ion temperature. However, the ratio may be related to an existence of the ion upflow somewhere along the rocket trajectory.

In this presentation, we will focus on a spatial/temporal variation of ion current in the current - voltage characteristics. A latest result from our analysis of FLP data will be presented in more detail.

R005-03
B 会場 ：11/4　PM1 （13:45-15:30）
14:15〜14:30

#頭師　孝拓[1)], 石坂　圭吾[2)], 笠原　禎也[3)], 尾崎　光紀[3)], 栗田　怜[5)], 八木谷　聡[3)], 加藤　雄人[4)], 小嶋　浩嗣[5)], 阿部　琢美[6)], 細川　敬祐[7)], 小川　泰信[8)], 齋藤　義文[6)]
([1] 奈良高専,[2] 富山県大・工,[3] 金沢大,[4] 東北大・理・地球物理,[5] 京大・生存圏,[6] ＪＡＸＡ宇宙科学研究所,[7] 電通大,[8] 極地研

Plasma wave and DC electric field observations by the SS-520-3 sounding rocket

#Takahiro Zushi[1)], Keigo Ishisaka[2)], Yoshiya Kasahara[3)], Mitsunori Ozaki[3)], Satoshi Kurita[5)], Satoshi Yagitani[3)], Yuto Katoh[4)], Hirotsugu Kojima[5)], Takumi Abe[6)], Keisuke Hosokawa[7)], Yasunobu Ogawa[8)], Yoshifumi Saito[6)]
([1]National Institute of Technology , Nara Col,[2]Toyama Pref. Univ.,[3]Kanazawa Univ.,[4]Dept. Geophys., Grad. Sch. Sci., Tohoku Univ.,[5]RISH, Kyoto Univ.,[6]ISAS/JAXA,[7]UEC,[8]NIPR

The SS-520-3 sounding rocket experiment was planned to clarify the ion outflow phenomenon in the polar cusp region. Heating/acceleration transverse to the geomagnetic field lines is known as one of the acceleration processes for obtaining the velocity for the ions to flow out, and the wave-particle interaction is considered the primary mechanism of the heating/acceleration. For this reason, an instrument for DC electric field and plasma waves, called Low-Frequency wave Analyzer System (LFAS) is on board the SS-520-3. LFAS is composed of three blocks: electric field sensors (LFAS-S), pre-amplifiers (LFAS-Pre), and receivers. LFAS has two types of receivers with different observation bands: Electric Field Detector (EFD) covers DC and the ELF range (DC − 400 Hz), and WaveForm Capture (WFC) covers the VLF range (10 Hz − 10 kHz). In addition, WFC has Software Wave-Particle Interaction Analyzer (SWPIA) to measure wave-particle interaction directly. SWPIA generates clock signals for synchronous observation between plasma wave and particle. The signal is sent to two particle instruments: Thermal and Supra-thermal ion energy-mass Analyzer (TSA) and low-energy Ion energy-Mass Spectrometer (IMS). The sounding rocket was launched on 4th November 2021 from Ny Alesund, Spitsbergen, Norway. During the flight, two receivers of LFAS including SWPIA were successfully worked. However, problems with LFAS-S caused two of the four sensor elements to not extend and one to extend later than scheduled. As a result, LFAS observed the electric field in an orthogonal monopole configuration. In the presentation, we will show the detailed design and the initial result of LFAS.

R005-04
B 会場 ：11/4　PM1 （13:45-15:30）
14:30〜14:45

観測ロケット S-310-44 号機実験で観測されたエネルギー分布の特徴について

#梅岡　大貴 [1)], 阿部　琢美 [2)], 三宅　亙 [1)]
[(1] 東海大・工,[(2] ＪＡＸＡ宇宙科学研究所

The characteristics of electron energy distribution observed in the S-310-44

#Daiki Umeoka[1)], Takumi Abe[2)], Wataru Miyake[1)]
[(1]Tokai Univ.,[(2]ISAS/JAXA

Many sounding rockets have been launched in the mid-latitudes around Japan. The electron temperature and density have been measured most frequently. Analysis of the electron temperature data shows that the electron temperature increases locally in the lower ionosphere around noon in winter. It is known that this phenomenon is most likely to be observed when a rocket passes near the center of the Sq current system that locates in the mid-latitudes of the winter hemisphere. Ground-based observations of the magnetic field and theoretical studies have shown that this Sq current system exists in the ionosphere E region at an altitude of approximately 100-140 km, counterclockwise in the northern hemisphere and clockwise in the southern hemisphere on the day side. The S-310-44 sounding rocket experiment aimed to elucidate the generation mechanism of such a high-temperature layer of plasma near the center of the Sq current system in the lower ionosphere. In this study, the current-voltage characteristics and electron energy distribution of the Fast Langmuir Probe (FLP) data acquired in this experiment are analyzed, and the scientific characteristics of the observation results are discussed. The FLP on board S-310-44 differs from ordinary Langmuir probes. An AC voltage of a small amplitude is superimposed on the applied voltage. By extracting the second harmonic components of the current variation in this way, the second differential coefficient of the probe's V-I characteristic can be estimated (second harmonic method) and the energy distribution derived. In this study, the energy distribution was first obtained from the second harmonic component of the probe current and the probe voltage, and an unusual energy distribution was found at a certain altitude. In the S-310-44 experiment, two peaks were observed in each voltage sweep after 90 sec from the rocket launch (altitude above 110 km), whereas the energy distribution of ionospheric electrons only shows a single peak that suggesting that electrons obey to a Maxwellian distribution. To investigate the cause of this unusual distribution, the spin phase was calculated when multiple peaks were observed. This is because the current values of the peaks vary with the spin period and have a maximum in a particular direction. The results of this analysis show that the low-energy peak has a maximum in the direction of the rocket RAM (south-east), which suggests that it is affected by the wake around the rocket, and that the probe measures background ionospheric electrons. On the other hand, the high-energy peak has a current maximum when the probe is pointing westwards and its behavior is different from that of the low-energy peak. This may be due to plasma other than the usual ionospheric electrons. In the presentation, the characteristics of this high-energy peak will be discussed in detail.

日本付近の中緯度において，これまで多くの観測ロケットが打ち上げられてきた．その中で最も多く測定が行われてきたのが電子温度と電子密度である．この電子温度データを解析した結果，冬季の正午前後において電離圏下部付近で電子温度が局所的に上昇する事例が報告されている．この現象はロケットが冬半球の中緯度帯に発生する Sq 電流系中心付近を通過したときに観測される可能性が高いことが分かっている．この Sq 電流系は磁場の地上観測や理論的な研究から，およそ高度 100〜140km の電離圏 E 領域において，昼側で北半球では反時計回り，南半球では時計回りに存在することがわかっている．このような電離圏下部の Sq 電流系中心付近に発生するプラズマの高温度層の発生メカニズムを解明することを目的として行われたのが S-310-44 号機型観測ロケット実験である．本研究ではこの実験で取得された高速ラングミュアプローブ（以下 FLP）の取得データを用いて，その電流-電圧特性および電子エネルギー分布について解析を行い，観測結果の科学的特徴について議論する．S-310-44 号機に搭載された FLP は一般のラングミュアプローブとは異なり，印加する電圧に微小振幅の交流電圧を重畳している（交流重畳法）．この方法によって変化する電流の 2 次高調波成分を取り出すことでプローブの V-I 特性の 2 次微分係数を推定し，エネルギー分布を導き出すことができる．本研究では，まずプローブ電流の 2 次高調波成分とプローブ電圧からエネルギー分布を求めたが，ある高度において通常とは異なるエネルギー分布が見つかった．電離圏電子のエネルギー分布は，通常マクスウェル分布に従うような単一のピークしか観測されないのに対し，S-310-44 号機実験では，ロケット発射から 90 秒後（高度 110 km 以上）の各電圧掃引で二つのピーク（エネルギー分布の異なる二つの分布）が観測されている．ピークの電流値はスピン周期で変化するが，このような通常とは異なる分布の原因を調べるために，電流最大値が観測されたときのスピン位相を計算した．この解析の結果，低エネルギー側のピークはロケットの進行方向（南東方向）で最大となることからロケット周囲のウエークの影響を受けていると思われる．これは背景の電離圏電子を捉えていたものと推測される．一方で，高エネルギー側のピークはプローブが西方向を向いている時に電流最大値をもち低エネルギー側のピークと振る舞いが異なっている．これは通常の電離圏電子以外のプラズマによるものではないかと考える．講演ではこの高エネルギー側ピークの特徴について詳しく述べる．

R005-05
B 会場 ：11/4　PM1 （13:45-15:30）
14:45〜15:00

観測ロケット S-520-32 号機と自前開発機器によるロケット－地上間の電離圏全電子数観測

#山本　衛 [1)], 高橋　透 [2)], 芦原　佑樹 [3)]
([1] 京大・生存圏研,([2]ENRI,([3] 奈良高専

Ionospheric TEC measurement with S-520-32 sounding rocket and in-house developed equipment

#Mamoru Yamamoto[1)], Toru Takahashi[2)], Yuki Ashihara[3)]
([1]RISH, Kyoto Univ.,([2]ENRI, MPAT,([3]NIT Nara

This presentation reports the first results from the rocket-to-ground total electron content (TEC) measurement with the JAXA sounding rocket S-520-32. The rocket will be launched in August or September 2022 from JAXA Uchinoura Space Center (USC). The rocket consists of a dual-band (150MHz and 400MHz) beacon (DBB) transmitter and antennas that are developed in-house at Kyoto University. To support the experiment we deploy four DBB receivers in Uchinoura, Tarumizu, Satsuma-Sendai, and Kirishima.

We measure TEC from the phase variation of two radio signals that propagate from the sounding rocket to the ground. We have been developing digital beacon receivers for the ground site. But for this experiment, we newly developed a transmitter and antennas on board the rocket. The transmitter generates 1W at both frequencies based on a unique phase-locked loop LSI Si5338 that can generate at most four different timing signals that are almost perfectly phase coherent. The antenna is a compact inverse-L type that is attached to the skin of the rocket, and two sets of antenna elements for 150MHz and 400MHz signals are arranged in each antenna body. Using four antenna elements we transmit right-handed circular polarized radio signals to the ground. This development was fully conducted in-house mainly at Kyoto University.

In the presentation, we will show the setup of both the on-rocket transmitter and on-ground receiver. Preliminary results from the experiment would be included as far as these in-house equipments worked fine during the rocket flight.

観測ロケット S-520-32 を使用したロケットから地上までの電離圏の全電子数 (TEC) 観測の最初の結果を報告する。この観測ロケットは、2022 年 8 月または 9 月に JAXA 内之浦宇宙空間観測所 (USC) から打上げられる。ロケットには、京都大学で独自に開発された 2 周波 (150MHz および 400MHz) ビーコン (DBB) 送信機とアンテナが搭載されている。実験のために、内之浦、垂水、薩摩川内、霧島に 4 台の DBB 受信機を配備している。

観測ロケットから地上に伝搬する 2 波の電波の位相差から TEC を推定できる。我々は地上用のディジタルビーコン受信機を開発してきました。しかし今回の実験のために、ロケット搭載用の送信機とアンテナを新たに開発しました。送信機は、ほぼ完全に位相同期が取れた最大 4 つの異なるタイミング信号を生成できる独自のフェーズロックループ LSI Si5338 から信号を生成し、両方の周波数で 1W を出力する。アンテナはロケット外壁に取付けるコンパクトな逆 L 型で、1 台のアンテナ本体に 150MHz 用と 400MHz 用の 2 組のアンテナ素子が配置されている。4 つのアンテナ素子を使用して、右旋円偏波の電波を地上に送信する。これらの開発は、京都大学を中心に完全に所内で行われた。

発表では、ロケットに搭載された送信機と地上の受信機の両方のセットアップを示す。さらに、これらの新規開発機器がロケット飛行中に正常に機能する限り、実験の予備結果を示す予定である。

R005-06
B 会場 ：11/4　PM1 （13:45-15:30）
15:00〜15:15

S-520-32 観測ロケット搭載 GNSS 受信機による TEC の初期解析

#上垣　柊季 [1)], 芦原　佑樹 [2)], 上谷　仁亮 [1)], 石坂　圭吾 [3)]
([1] 奈良高専 専攻科,[2] 奈良高専,[3] 富山県大・工

Initial analysis of GNSS-TEC observed with S-520-32 sounding rocket

#Hiiragi Uegaki[1)], Yuki Ashihara[2)], Hitoaki Uetani[1)], Keigo Ishisaka[3)]
([1]Faculty of Advanced Engineering, NIT Nara,[2]NIT Nara,[3]Toyama Pref. Univ.

Earth's upper atmosphere is ionized due to X-rays and ultraviolet rays contained in sunlight and it forms cold plasma region which is called ionosphere. Ionospheric disturbances causes satellite-based communication failure and positioning error of GNSS. Spatial structure observation of ionospheric electron density is indispensable for elucidating the generation process. Ionospheric observations are often performed by ground-based remote sensing methods such as Ionosonde and GNSS-TEC. Ionosonde can observe altitudes below the electron density peak in the F region, and GNSS-TEC can observe the total electron content on the propagation path between satellite to receiver. However, the spatial structure of electronic density is not known from them.

For this reason, we proposed rocket GNSS-TEC tomography method as a new approach to the ionospheric observation. To evaluate this method, S-520-32 sounding rocket is equipped with a GNSS-TEC receiver and fly over the boundary between the E and F regions of the ionosphere. Then we can obtain TEC data separated in F region and E region.In this presentation, we show the initial analysis results obtained on S-520-32, and discuss.

地球の上層大気は、太陽光線に含まれる X 線や紫外線などにより電離され、電離圏と呼ばれる弱電離プラズマを形成する。電離圏擾乱は衛星通信障害や GNSS の測位誤差を引き起こすが、その生成過程の解明には電離圏電子密度の空間構造観測が不可欠である。電離圏観測は、Ionosonde、GNSS-TEC 等により、地上からのリモートセンシング手法で行われるのが一般的である。しかし、Ionosonde は F 領域の電子密度ピーク以下の高度について、GNSS-TEC は伝搬経路上の全電子数について観測できるが、電離圏の空間構造は得られない。

本研究では電離圏観測手法の新たなアプローチとしてロケット GNSS-TEC トモグラフィ法を提案する。観測ロケット S-520-32 号機に GNSS-TEC 受信機を搭載し、電離圏 E 領域と F 領域の境界を飛翔することで、E 領域、F 領域を分離した TEC データを取得する。本発表では、S-520-32 号機で得られた初期解析結果を示し、考察する。

R005-07
B 会場 ：11/4　PM2 （15:45-18:15）
15:45〜16:00

S-520-32 号機観測ロケットにより観測された中規模伝搬性電離圏擾乱発生時の電場の初期解析

#松山　実由規 [1)], 石坂　圭吾 [2)], 芦原　佑樹 [3)], 山本　衛 [4)], 熊本　篤志 [5)], 白澤　秀剛 [6)], 阿部　琢美 [7)]
(1 富山県大,(2 富山県大・工,(3 奈良高専・電気,(4 京大・生存圏研,(5 東北大・理・地球物理,(6 東海大・情報教育センター,(7 ＪＡＸＡ宇宙科学研究所

Initial Analysis of Electric Field Observation during MSTID Occurrence by S-520-32 Sounding Rocket

#Miyuki Matsuyama[1)], Keigo Ishisaka[2)], Yuki Ashihara[3)], Mamoru Yamamoto[4)], Atsushi Kumamoto[5)], Hidetaka Shirasawa[6)], Takumi Abe[7)]
(1Toyama Pref. Univ.,(2Toyama Pref. Univ.,(3Elec. Eng., NIT Nara,(4RISH, Kyoto Univ.,(5Dept. Geophys, Tohoku Univ.,(6ICT Edu. Center, Tokai Univ.,(7ISAS/JAXA

The Medium-Scale Traveling Ionospheric Disturbance (MSTID) is a plasma instability which occurs in the middle latitude ionospheric F region mainly at night in summer. It is a wave structures of electron density elongated northwest to southeast, 100-200 km horizontal wavelength and southwestward propagation. In the past, it was thought to be generated by the Perkins instability. The wave front directions of the MSTID and Perkins instability correspond, but their growth rates and propagation directions do not. Therefore, as a mechanism to compensate for this, it is thought to be generated by projected the polarization electric field by imbalance structure of the sporadic E layer onto the F region. In order to verify this assumption, S-520-32 sounding rocket will be launched from Uchinoura Space Center of JAXA. This rocket will observe horizontal and vertical structure of electron density in the E /F regions. In addition to the electron density structure, the rocket will observe the in-situ electric field by the Electric Field Detector (EFD). The electric field observation is one of the important parameters of this rocket, and can allows us to confirm whether a polarized electric field is actually generated during the MSTID occurrence. In this case, the electric field generated in the northeast-southwest (southwest-northeast) direction, which is tuned to the wave structure of the electron density, is expected to be observed. In this presentation, we will show the initial analysis of the electric field.

中規模伝搬性電離圏擾乱（MSTID）とは中緯度電離圏 F 領域で主に夏季夜間に発生するプラズマ不安定現象である．この現象は電子密度の北西-南東方向の波状構造を持ち，波長 100-200km で南西方向に伝搬する．MSTID の生成機構として，Perkins 不安定が昔から提唱されている．波面の向きは一致しているが，その成長率や伝搬方向が一致しない．そこで，これを補う機構として，スポラディック E 層の不均一構造に起因する分極電場が磁力線に沿って F 領域に投影される E-F 領域カップリング現象が提唱された．この検証のために，MSTID 発生時の E 領域および F 領域で同時に電子密度の鉛直・水平構造を観測する S-520-32 号機観測ロケットが内之浦宇宙空間観測所打ち上げられる．本ロケットでは電子密度構造のほかに，電場観測装置（EFD）によってその場の電場を観測する．電場の観測は，本ロケット実験にとって重要なパラメータの一つであり，MSTID 発生時に実際に分極電場が発生しているかどうか確認することができる．この場合，電子密度の波状構造に同調した北東-南西（南西-北東）方向に発生している電場が観測されると考えられる．本発表では，S-520-32 号機観測ロケット実験により観測された MSTID 発生時の電場の初期解析結果を示す．

R005-08
B 会場 ：11/4　PM2 （15:45-18:15）
16:00〜16:15

#高橋　透 [1)], 斎藤　享 [2)], 山本　衛 [3)], 篠原　学 [4)]
([1] 電子航法研,[2] 電子航法研,[3] 京大・生存圏研,[4] 鹿児島高専

VHF to UHF scintillation by using satellite and rocket beacon signals

#Toru Takahashi[1)], Susumu Saito[2)], Mamoru Yamamoto[3)], Manabu Shinohara[4)]
([1]ENRI, MPAT,[2]ENRI, MPAT,[3]RISH, Kyoto Univ.,[4]NIT Kagoshima,

The ionosphere plays an important role as a communication path between a ground-ground and satellite-ground. The irregularity of the plasma density in the ionosphere is often generated from a few tens of kilometers to a few meters. Notably, irregularities on the scale sizes of hundreds of meters to a few kilometers cause fluctuation in the radio wave transmitted from the Global Navigation Satellite System (GNSS) satellites. Previous studies presented small-scale ionospheric irregularities were generated by cascading of the large-scale irregularities. Therefore, it is essential to observe large (a few km) scale irregularities simultaneously with small (several 100s m) scale irregularities.

The beacon satellites is transmitting the VHF (150 MHz) and UHF (400 MHz) signals and National Oceanic and Atmospheric Administration (NOAA) satellites is transmitting the 137 MHz signal. The km scale irregularities cause the scintillation of those signals and thus we observe the variation of beacon signal amplitude to evaluate the km scale irregularity generation and growth simultaneous with the GNSS signal observation. In addition, the sounding rocket S-520-32 will be launched from Uchinoura, Kagoshima, which aims to observe irregularities associated with the Es layer and medium-scale traveling ionospheric disturbances (MSTIDs) and it will transmit dual-band beacon signals (150 and 400 MHz) in August or September 2022. We will try to observe the beacon signals from the sounding rocket.

The beacon receiver was developed at Chofu, Tokyo, as a test observation. After that, we relocated the beacon receiver to the National Institute of Technology, Kagoshima College, Kirishima (31.73 N, 130.73 E) in July 2022. The scintillation caused by the equatorial anomaly expanding northward is likely to be observed in there. In addition, the beacon signals transmitting from S520-32 can be observed.

In this presentation, we will describe our system and present observation results conducted at Chofu, Kirishima. The results of the rocket campaign will also be presented. The results are compared with the ROTI (rate of TEC index) map, which represents the existence of ionospheric irregularities. Future plans to extend our observation to equatorial regions will also be presented.

R005-09
B 会場 ：11/4　PM2 （15:45-18:15）
16:15〜16:30

観測ロケット搭載超高層大気観測用真空計の容器設計に関する研究

#飛田　奈々美 [1)], 阿部　琢美 [2)], 三宅　亙 [3)]
([1] 東海大・工,([2] ＪＡＸＡ宇宙科学研究所,([3] 東海大・工

Design of container for ionization gauge on a sounding rocket to observe the upper atmosphere

#Nanami Tobita[1)], Takumi Abe[2)], Wataru Miyake[3)]
([1]Tokai Univ.,([2]ISAS/JAXA,([3]Tokai Univ.

In a thermospheric atmosphere, the ionized atmosphere can move in a different direction from the neutral atmosphere by electromagnetic forces. When collisions between the ionized and neutral particles are dominant, momentum is transported, further complicating the particle motion in this system. Although there are many unique phenomena in the upper atmosphere, these remain unsolved due to this complexity.

There are various methods for observing the thermospheric atmosphere, but it is possible to estimate the atmospheric density if the pressure is measured and the temperature is known. We adopted the ionization gauge because of its small size, simple structure, and reliability as a way of measuring atmospheric pressure in the thermosphere on a sounding rocket, to estimate the density of the neutral atmosphere in the lower thermosphere. Since information on the neutral atmospheric wind is also important for studying the mechanism of phenomena, we would like to challenge the possibility of obtaining information not only on the atmospheric density but also on the atmospheric wind speed. To enable estimation of atmospheric wind velocity from the gauge measurements, we discuss a design of a gauge container so that we can find the direction of atmospheric wind observed on a rocket: a structure of a container that allows the internal pressure to vary depending on the direction of the incident direction.

For the direction of the expected atmospheric flow on a rocket, we referred to the attitude and orbit data of the S-520-26, which was launched from USC in 2012. The angle between the axis of the rocket and the velocity vector was calculated using the data: latitude, longitude, altitude, elevation angle, and azimuth angle of the rocket position at 179-461 seconds after the launch. The calculated angle showed a sinusoidal change due to the rocket's corning motion, with a gradually increasing central value. Since the thermal velocity of atmospheric particles is generally less than that of the rocket, the direction of the atmospheric flow on the rocket is the opposite direction of the rocket's velocity vector. Therefore, this calculated angle is the angle of the incoming wind with respect to the rocket axis during the flight.

Our calculation shows that the inflow direction is 30-45 degrees to the gas inlet at altitudes below 200 km during the ascending. Therefore, the gauge should be designed so that the pressure value varies with the angle in the range.

We designed and prepared three different containers in which the pressure value of the ionization gauge changes according to the influent angle of the gas and conducted experiments using the Space Science Chamber at ISAS to reproduce the lower thermospheric atmospheric environment. A small chamber was set up inside the space science chamber, and gas was introduced from outside of the Chamber and flowed out through a nozzle to create an artificial gas flow. A gauge was placed in front of the nozzle, and the pressure was measured with an internal sensor. The rotary table to which a container was fixed was rotated in a 5-degree step from -70 to 70 degrees, and the pressure was measured.

We compared a gradient of the measured pressure with angle. The container structure with the largest gradient was determined to be the most suitable container design for the purpose.

When an ionization gauge is directly mounted, it is difficult to accurately measure the background pressure of atmospheric particles because the translational kinetic energy of the particles generated by the supersonic movement is added to the thermal kinetic energy. A spherical container, called the Paterson probe, is used to make measurements without being affected by the energy generated by the rocket's motion. Two types of containers, in which ion gauge was put, were installed on the S-520-32: this spherical gauge container and the gauge container designed in this study. By comparing the two, the background pressure and the pressure dependent on the dynamic pressure on the rocket will be measured. In this report, we present the results of the measurements.

熱圏大気中では，電離大気は電磁気的な力を受けて，中性大気とは異なる方向に運動することができる．電離大気と中性大気の衝突が優勢な場合は運動量が輸送され，この系の粒子の運動はさらに複雑になる．超高層大気領域特有の現象は多数あるが，これに起因して未解明の現象が多い．

熱圏大気の観測には様々な方法があるが，圧力を測定し，温度が分かっていれば大気密度を推定することが可能になる．我々は観測ロケット上で熱圏大気の圧力を測る手段として，小型で構造が比較的単純，かつ信頼性のある電離真空計を採用し，熱圏下部の中性大気密度の推定を行うこととした．中性大気の風に関する情報は現象のメカニズムを研究する上で重要であるため，大気密度に加えて大気風速に関する情報を得る可能性についても挑戦したい．真空計による圧力測定から大気風速の推定を可能にするために，ロケット上で観測される大気風の方向検知が可能な容器，すなわち風の到来方向によって内部の圧力が変動するような構造の真空計収納容器の設計に関して検討を行った．

本研究ではまず，過去に打ち上げられた観測ロケットのデータから，真空計を搭載したときに予想される大気流の方向の計算を行った．その結果を受け，その範囲で風の流入方向が変化した際に，それに応じて測定圧力が有意に変化するような真空計の収納容器の検討を行った．

ロケットの飛翔中に入ってくる大気流の方向については，2012 年に内之浦宇宙空間観測所から打ち上げられた，観測ロケット S-520-26 号機の姿勢データおよび軌道情報を用いて計算を行った．打ち上げから 179〜461 秒後におけるロケット位置の緯度・経度・高度，および仰角・方位角のデータを使用し，ロケットの機軸と速度ベクトルのなす角度を求めた．算出した角度は，ロケットのコーニング運動により正弦波的な変化を示しながら中心値は徐々に大きくなっていく変化を示した．一般には，大気粒子の熱速度はロケットの速度よりも小さいことから，ロケット上で観測される大気流の方向はロケットの速度ベクトルの逆方向となる．したがって，この角度はロケットの飛翔中に入ってくる風の機軸に対する入射角を指すことになる．

ここで，観測ロケットの測定は，下降時より上昇時の測定の方がより重要である．使用したデータでは 179 秒以前の姿勢が計算されていないが，高度の時間変化のデータから，上昇時における高度 200 km 以下では真空計のガス流入口が機軸方向を向いている場合は 30〜45 度の方向から流入すると推測できる．したがって，30〜45 度の範囲で，角度に応じて圧力値が変化するような真空計の設計を行えばよいと考えられる．

ガスの入射角に応じて真空計の圧力値が変化する容器 3 種類を設計・製作し，宇宙科学研究所にある大型のスペースサイエンスチェンバーを使用して熱圏下部大気環境を再現し，実験を行った．スペースサイエンスチェンバー内部に小チャンバーを設置し，スペースサイエンスチェンバー外部からガスを導入してノズルから噴出させ，人工的に高真空中での大気の流れを作り出す．ノズル正面に真空計容器を設置し，内部のセンサで圧力を測定した．収納容器を固定した回転台を-70〜70 度の範囲で 5 度ずつ回転させ，その際の圧力を測定した．風の入射角の範囲として 30 度から 45 度に注目し圧力の変化率を計算し比較を行った．この変化率が最も大きくなった収納容器構造を目的に適した容器設計として結論づけた．

一般にロケットのような超音速の飛翔体上で大気圧力を測定する場合，大気粒子は観測ロケットの速度によって生じた粒子の並進運動エネルギーが熱運動エネルギーに加わってしまい，正確な圧力を測定することが困難である．このロケットの運動によって生じるエネルギーが影響を与えないように測定することが可能なものとして，球型のパターソンプローブがある．我々は上に述べた容器およびパターソンプローブの 2 種類の容器内部に圧力センサを収納して観測ロケット S-520-32 号機に搭載した．両者を比較することで，背景圧力と機上での動圧に依存する圧力を測定する予定である．講演では測定結果を報告する．

R005-10
B 会場 ：11/4　PM2 （15:45-18:15）
16:30〜16:45

トンガ海底火山噴火後の磁気リップルの全球的振幅増大

#家森　俊彦 [1)], 青山　忠司 [2)], 横山　佳弘 [3)],Pangsapa　Vijak[4)],Jarupongsakul　Thanawat[5)], 佐納　康治 [6)], 小田木洋子 [7)], 田中　良和 [1)], 田口　聡 [8)], 齊藤　昭則 [9)], 穂積　コンニャナット [10)]
([1] 京大,[2] エフ・ファクトリー (株),[3] スウェーデン宇宙物理研究所,[4] チュラロンコン大・理,[5] チュラロンコン大・理,[6] 朝日大・経営,[7] 京大・理・地磁気センター,[8] 京大理,[9] 京都大・理・地球物理,[10]NICT

Global enhancement of magnetic ripples after the 2022 Hunga Tonga Hunga Ha'apai volcanic eruption

#Toshihiko Iyemori[1)], Tadashi Aoyama[2)], Yoshihiro Yokoyama[3)], Vijak Pangsapa[4)], Thanawat Jarupongsakul[5)], Yasuharu Sano[6)], Yoko Odagi[7)], Yoshikazu Tanaka[1)], Satoshi Taguchi[8)], Akinori Saito[9)], Kornyanat Hozumi[10)]
([1]Kyoto Univ.,[2]F-Factory Co., Ltd.,[3]Swedish Institute of Space Physics,[4]Chulalongkorn Univ.,[5]Faculty of Science, Chulalongkorn Univ.,[6]Asahi Univ.,[7]WDC for Geomagnetism, Kyoto Univ.,[8]Grad school of Science, Kyoto Univ.,[9]Dept. of Geophysics, Kyoto Univ.,[10]NICT

After the huge eruption of the Hunga Tonga Hunga Ha'apai submarine volcano on January 15, 2022, a pressure wave so called "Lamb wave" went around the Earth. After the passage of the pressure wave, the Swarm satellites observed amplitude enhancement of magnetic ripples and electron density fluctuations in low and middle latitudes on the dayside, and the enhancement lasted two or three days. At a low latitude observatory in Phimai, Thailand, after the passage of pressure waves, an enhancement of short period oscillations of GPS-TEC and that of geomagnetic field were observed, and they lasted at least a few hours after the passage of the wave front. From these event analyses, it is suggested that the pressure wave which went around the Earth caused short period oscillations of magnetic field and electron density in the upper atmosphere which at least lasted a few hours after the passage of the pressure wave front.

2022 年 1 月 15 日の 04:14UT 頃に開始したトンガ海底火山噴火後、2〜3 日間にわたり、昼間側中低緯度の電離圏 F 領域では磁気リップルの全球的振幅増大が Swarm 衛星により観測された。他方、タイ・ピマーイでの気圧・地磁気・GPS-TEC 観測では、噴火により発生した気圧波 (Lamb 波) の到達後数時間、気圧波により励起されたと考えられる地磁気変動や TEC 変動が検出された。地球を周回した気圧波と衛星による磁気リップルの観測、地上観測との関係を中心に解析した結果を示す。

R005-11
B 会場 ：11/4　PM2 （15:45-18:15）
16:45〜17:00

HF ドップラー観測により得られた 2022 年トンガ噴火に伴うドップラーシフトの周期的変動

#中田　裕之 [1)], 細川　敬祐 [2)], 斎藤　享 [3)], 大塚　雄一 [4)], 冨澤　一郎 [5)]
([1] 千葉大・工,[2] 電通大,[3] 電子航法研,[4] 名大・宇地研,[5] 電通大・宇宙電磁環境

Periodic variations of Doppler shift observed with HF Doppler sounding in association with the 2022 Tonga volcanic eruption

#Hiroyuki Nakata[1)], Keisuke Hosokawa[2)], Susumu Saito[3)], Yuichi Otsuka[4)], Ichiro Tomizawa[5)]
([1]Grad. School of Eng., Chiba Univ.,[2]UEC,[3]ENRI, MPAT,[4]ISEE, Nagoya Univ.,[5]SSRE, Univ. Electro-Comm.

The Tonga volcanic eruption that occurred on January 15, 2022, at 4:00 (UTC) was an extremely large eruption. It has already been reported that TEC variations associated with the Tonga eruption propagated globally (Lin et al., 2022; Saito 2022; Themens et al., 2022). One of the characteristics of the ionospheric variations associated with the Tonga eruption is that the variations also occurred at conjugate points. In Japan, pressure variations of about 2 hPa, which arrived directly from the eruption, were observed from 11:00 UT to 12:00 UT, about 7 hours after the eruption. TEC variations were also observed earlier than the arrival of the pressure variation. It is thought that the TEC variations were caused by pressure changes propagated to Australia, which is the conjugate point of Japan, and that the variations propagated over Japan through magnetic field lines. In fact, TEC variations were observed in Australia about one and a half hours after the eruption, which is consistent with the TEC variations that occurred over Japan.

With the occurrence of ionospheric variations over Japan, Doppler frequency variations have also been observed in HF Doppler observations. Ionospheric fluctuations were observed at most of the stations. In addition, at Sarobetsu station, a characteristic periodic Doppler frequency variation was observed at 5006 kHz transmitted from Chofu. The period of this variation was about 4 minutes and showed the wavy fluctuation seen like the occurrence of traveling ionospheric disturbances (TIDs), characterized by the simultaneous observation of three frequencies at a certain time. From the TEC observations, the ionospheric disturbance propagated east-west, and the wavefront followed a north-south direction. Chofu-Sarobetsu has a north-south propagation path and is parallel to the wavefront. In this situation, it is possible to satisfy the radio wave reflection condition at three points on the ionosphere in the radio wave propagation between Chofu and Sarobetsu. The propagation paths of Chofu-Okinawa and Chofu-Awaji were also relatively long-distance propagation like Sarobetsu, but such variations were not observed in these propagation paths. This is because the reflection condition was not satisfied as in Chofu-Sarobetsu because the propagation path was perpendicular to the wavefront of the ionospheric disturbances.

In this eruption, it has been reported that Lamb waves propagated far away from the volcano and that atmospheric gravity waves were generated and followed the Lamb wave. In the simulation results, it is found that the atmospheric gravity waves were trapped in the region between the ground and the lower ionosphere and their period was about 4 minutes (Nakajima, 2022). Ionospheric disturbance generated by these gravity waves propagated to the opposite hemisphere, which caused fluctuations around Japan.

2022 年 1 月 15 日 4 時（世界標準時）に発生したトンガ海底火山噴火は，その規模が VEI6 であることからもわかるように極めて大規模な噴火であった。トンガ噴火に伴う TEC 変動が全地球的に伝搬したことが既に報告されている（Lin et al., 2022; Saito 2022; Themens et al., 2022）。今回のトンガ噴火に伴う電離圏変動の特徴として，変動の共役性が挙げられる。日本では，噴火から約 7 時間後の 11:00UT-12:00UT にかけて噴火から直接到達してきた気圧変化が観測された。それと同時に TEC 変動も観測されているが，この空振の到来よりも早い時間にも TEC 変動が観測されている。これは日本の共役点であるオーストラリアに伝搬した気圧変化により TEC 変動が発生し，磁力線を通じて，日本上空で変動が発生したと考えられる。事実，噴火から約 1 時間半後にオーストラリアで TEC 変動が観測されており，日本上空で発生した変動と一致しており，また，磁気共役点に変動を射影すると，その分布が一致することからもわかる。

日本上空での電離圏変動の発生に伴い，HF ドップラー観測においてドップラー周波数変動も観測されている。電離圏変動自体はほとんどの観測点で観測されたが，調布ーサロベツ間の 5006 kHz の観測では，特徴的な周期的変動が観測された。周期は約 4 分で，TID 発生時に見られる波状の変動を示しており，ある時刻に同時に 3 つの周波数が観測されていることが特徴である。電離圏電子密度構造が波状になることで，同時に 3 つの反射点が存在するために観測されたものと考えられる。TEC 観測から，今回の電離圏擾乱は，日本上空においてほぼ東西に伝搬しており，波面は南北に沿っている。調布ーサロベツはほぼ南北に伝搬経路を持ち，波面に平行となることから，このような受信が可能になったと考えられる。調布ー沖縄，調布ー淡路もサロベツ同様に比較的長距離の伝搬であるが，このような変動は観測されなかった。伝搬経路が波面に垂直なため，調布ーサロベツのような反射条件を満たさなかったと考えられる。

今回の噴火では，ラム波による大気波動が遠方まで伝搬したことが報告されているが，その後に大気重力波も継続して発生しており，伝搬していることが報告されている。大気重力波は，地上と下部電離圏で捕捉された波動で約 4 分周期であり（Nakajima, 2022），これが反対半球に伝搬することで日本付近にも約 4 分周期の変動が生じたと考えられる。

R005-12
B 会場 ：11/4　PM2 （15:45-18:15）
17:00〜17:15

Equatorial plasma bubbles observed over longitude 100ºE sector after Hunga Tonga-Hunga Ha'apai eruption on January 15, 2022

#Hozumi Kornyanat[1)],Supnithi Pornchai[2)],Tongkasem Napat[2)],Seechai Khanitin[2)],Sophan Somkit[2)],Jamjareegulgarn Punyawi[2)], 大塚　雄一[3)], 斎藤　享[4)], 西岡　未知[1)], 津川　卓也[1)], 山本　衛[5)]
(1 情報通信研究機構,(2KMITL, Thailand,(3 名大・宇地研,(4 電子航法研,(5 京大・生存圏研

Equatorial plasma bubbles observed over longitude 100ºE sector after Hunga Tonga-Hunga Ha'apai eruption on January 15, 2022

#Kornyanat Hozumi[1)], Pornchai Supnithi[2)], Napat Tongkasem[2)], Khanitin Seechai[2)], Somkit Sophan[2)], Punyawi Jamjareegulgarn[2)], Yuichi Otsuka[3)], Susumu Saito[4)], Michi Nishioka[1)], Takuya Tsugawa[1)], Mamoru Yamamoto[5)]
(1NICT, Japan,(2KMITL, Thailand,(3ISEE, Nagoya Univ., Japan,(4ENRI, MPAT, Japan,(5RISH, Kyoto University, Japan

There have been some reports on the plasma bubble detection at mid and low latitudes after the huge eruption of the Hunga Tonga-Hunga Ha'apai submarine volcano in the South Pacific on January 15, 2022, at 04:14 UT. The eruption released enormous energy into the atmosphere, and the pressure wave went around globally. The coupling from the upper atmosphere could trigger the electron density fluctuation in the ionosphere. Pre-reversal enhancement (PRE) causes uplift of the bottom side ionosphere and is considered one of the conditions for EPB seeding. The moderate magnetic storm commenced on 14 January 2022 followed by its recovery phase on January 15, 2022. An enhanced electric field due to the magnetic storm could also enhance the ExB drift and amplify the PRE around the sunset terminator causing a favorable condition for the EPB seeding.

Chumphon is considered a magnetic equator station as it locates at geographic 10.72 degrees N, 99.37 degrees E, where is at geomagnetic 1.33 degrees N, 172.19 degrees E based on IGRF-13. The new VHF radar is operated at the frequency of 30.65 MHz. This study reports strong Equatorial Plasma Bubbles (EPBs) observed by the new VHF radar over Chumphon, Thailand on January 15, 2022. The overhead radar beam detected the EPB as high as 750 km altitude. TEC enhancement in the Equatorial Ionization Anomaly (EIA) region is also detected by the GNSS network in Thailand on January 15, 2022. GNU Radio Beacon Receiver (GRBR) in Bangkok, Thailand also detects the enhanced S4 index. We will also report positioning error information regarding the event. Though the cause of the detected plasma bubble is still unclear, we report the preliminary results and seek a fruitful discussion.

There have been some reports on the plasma bubble detection at mid and low latitudes after the huge eruption of the Hunga Tonga-Hunga Ha'apai submarine volcano in the South Pacific on January 15, 2022, at 04:14 UT. The eruption released enormous energy into the atmosphere, and the pressure wave went around globally. The coupling from the upper atmosphere could trigger the electron density fluctuation in the ionosphere. Pre-reversal enhancement (PRE) causes uplift of the bottom side ionosphere and is considered one of the conditions for EPB seeding. The moderate magnetic storm commenced on 14 January 2022 followed by its recovery phase on January 15, 2022. An enhanced electric field due to the magnetic storm could also enhance the ExB drift and amplify the PRE around the sunset terminator causing a favorable condition for the EPB seeding.

Chumphon is considered a magnetic equator station as it locates at geographic 10.72 degrees N, 99.37 degrees E, where is at geomagnetic 1.33 degrees N, 172.19 degrees E based on IGRF-13. The new VHF radar is operated at the frequency of 30.65 MHz. This study reports strong Equatorial Plasma Bubbles (EPBs) observed by the new VHF radar over Chumphon, Thailand on January 15, 2022. The overhead radar beam detected the EPB as high as 750 km altitude. TEC enhancement in the Equatorial Ionization Anomaly (EIA) region is also detected by the GNSS network in Thailand on January 15, 2022. GNU Radio Beacon Receiver (GRBR) in Bangkok, Thailand also detects the enhanced S4 index. We will also report positioning error information regarding the event. Though the cause of the detected plasma bubble is still unclear, we report the preliminary results and seek a fruitful discussion.

R005-13
B 会場 ：11/4　PM2 （15:45-18:15）
17:15〜17:30

GNSS-TEC と SuperDARN 北海道レーダー観測データを用いた 2022 年 1 月 15 日のトンガ火山噴火後に見られた電離圏擾乱の特徴について

#新堀　淳樹 [1)], 大塚　雄一 [2)], 惣宇利　卓弥 [3)], 西岡　未知 [4)],PERWITASARI　SEPTI[5)], 津田　卓雄 [6)], 西谷　望 [7)]
[(1] 名古屋大学宇宙地球環境研究所,[(2] 名大・宇地研,[(3] 名大　ISEE,[(4] 情報通信研究機構,[(5]NICT,[(6] 電通大,[(7] 名大 ISEE

Characteristics of ionospheric disturbances after the Tonga volcanic eruption using GNSS-TEC and SuperDARN radar data

#Atsuki Shinbori[1)], Yuichi Otsuka[2)], Takuya Sori[3)], Michi Nishioka[4)], SEPTI PERWITASARI[5)], Takuo Tsuda[6)], Nozomu Nishitani[7)]
[(1]ISEE, Nagoya Univ.,[(2]ISEE, Nagoya Univ.,[(3]ISEE, Nagoya Univ.,[(4]NICT,[(5]NICT,[(6]UEC,[(7]ISEE, Nagoya Univ.

To elucidate the characteristics of electromagnetic conjugacy of traveling ionospheric disturbances just after the 15 January 2022 Hunga Tonga-Hunga Ha'apai volcanic eruption and their generation mechanism, we analyze global navigation satellite system (GNSS)-total electron content (TEC) data and ionospheric plasma velocity data obtained from the Super Dual Auroral Radar Network (SuperDARN) Hokkaido pair of radars. Further, we use thermal infrared grid data with high spatial resolution observed by the Himawari 8 satellite to identify surface air pressure waves propagating in the troposphere as a Lamb mode. After 07:30 UT on 15 January 2022, two distinct traveling ionospheric disturbances propagating in the westward direction appeared over Japan with the same structure as those at magnetically conjugate points in the Southern Hemisphere. These ionospheric disturbances were observed approximately 3 hours before the initial arrival of the surface air pressure waves. Corresponding to these traveling ionospheric disturbances with their large amplitude of 0.5-1.1x10^16 el/m^2 observed in the Southern Hemisphere, the plasma flow direction in the F region of the ionosphere changed from southward to northward. At this time, the magnetically conjugate points in the Southern Hemisphere were located in the sunlit region at a height of 105 km. The amplitude and period of the plasma flow perturbation are ~100-110 m/s and ~36-38 min, respectively. From the plasma flow signature, we estimated the magnitude of a zonal electric field as ~2.8-3.1 mV/m. Further, there is a significant phase difference of ~10-12 min between the total electron content and plasma flow perturbations. This result implies that an external electric field variation generates the traveling ionospheric disturbances observed in both Southern and Northern Hemispheres. Considering that the magnetically conjugate points in the Southern Hemisphere correspond to a sunlit region, we can interpret that the origin of the external electric field is an E region dynamo driven by the neutral wind oscillation associated with atmospheric acoustic waves and gravity waves. Finally, the electric field propagates to the F region and magnetically conjugate ionosphere along magnetic field lines with the local Alfven speed, which is much faster than that of Lamb mode waves. From these observational facts, it can be concluded that the E region dynamo electric field produced in the sunlit Southern Hemisphere is a main cause of the two distinct traveling ionospheric disturbances appearing over Japan before the arrival of the air pressure disturbances. Therefore, we can obtain important information of surface air pressure waves and relate tsunami from such ionospheric disturbances as seen in GNSS-TEC observation data.

R005-14
B 会場 ：11/4　PM2 （15:45-18:15）
17:30〜17:45

2013 年 3 月 1 日に発生した磁気嵐における中緯度域まで拡大するプラズマバブルの磁気共役性

#惣宇利　卓弥 [1)], 大塚　雄一 [2)], 新堀　淳樹 [3)], 西岡　未知 [4)],PERWITASARI　SEPTI[5)]
[(1] 名大　ISEE,[(2] 名大・宇地研,[(3] 名古屋大学宇宙地球環境研究所,[(4] 情報通信研究機構,[(5]NICT

Geomagnetic conjugacy of plasma bubbles extending to mid-latitudes during a geomagnetic storm on March 1, 2013

#Takuya Sori[1)], Yuichi Otsuka[2)], Atsuki Shinbori[3)], Michi Nishioka[4)], SEPTI PERWITASARI[5)]
[(1]ISEE, Nagoya Univ.,[(2]ISEE, Nagoya Univ.,[(3]ISEE, Nagoya Univ.,[(4]NICT,[(5]NICT

After sunset, a plasma density depletion (plasma bubble) often occurs at the bottom of the F region over the equator. It is widely accepted that plasma bubbles are caused by the Rayleigh-Taylor instability mechanism. It is well known that plasma bubbles have been generated by eastward electric fields after sunset during the main phase of geomagnetic storms. Since plasma bubbles are formed along magnetic field lines and extend to higher altitudes and latitudes, they have been observed in both hemispheres at geomagnetic conjugate points. On the other hand, conjugate observation of storm-time plasma bubbles extending to mid-latitudes has not yet been performed although storm-time plasma bubbles often extend to mid-latitudes. In this study, we report the geomagnetically conjugate structure of a plasma bubble extending to the mid-latitudes and the asymmetrical structure of the decay of the plasma bubble during a geomagnetic storm. We investigated the temporal and spatial variations of plasma bubbles in the Asian sector during a geomagnetic storm on March 1, 2013, using global navigation satellite system (GNSS)-total electron content (TEC) data with high spatiotemporal resolutions. The first important point of our data analysis results is that the plasma bubble extended from the equator to the mid-latitudes with geomagnetic conjugacy along the magnetic field lines. The TEC data showed that the plasma bubbles appeared in the equatorial regions near 150o E after sunset during the main phase of the geomagnetic storm. From ionosonde data (h'F: virtual height) over both Japan and Australia, they suggest that a large eastward electric field existed in the Asian sector. Finally, the plasma bubbles extended up to the mid-latitudes (~43o geomagnetic latitude) in both hemispheres, maintaining geomagnetic conjugacy. The second point is that the mid-latitude plasma bubble disappeared 1 – 2 hours earlier in the northern hemisphere than in the southern hemisphere at close to midnight. In the northern hemisphere, the ionospheric virtual height decreased near midnight, followed by a rapid decrease in the total electron content and a rapid increase in the ionospheric virtual height. These results imply that the mid-latitude plasma bubble disappeared as the background plasma density decreased after midnight due to the recombination resulting from the descent of the F layer. Therefore, we can conclude that mid-latitude plasma bubbles can be asymmetric between the northern and southern hemispheres because of the rapid decay of plasma bubbles in one of the hemispheres.

R005-15
B 会場 ：11/4　PM2 （15:45-18:15）
17:45〜18:00

短波ドップラー観測と全天大気光観測を組み合わせたプラズマバブルの研究

#瀬島　広海 [1)], 細川　敬祐 [1)],Chum　Jaroslav[2,6)],Lin　Jia-Ting[3)],Lin　Charles[3)], 中田　裕之 [4)], 坂井　純 [1)], 斎藤　享 [5)]
(1 電通大,(2 なし,(3 なし,(4 千葉大・工,(5 電子航法研,(6 なし

Simultaneous observations of plasma bubbles with HF Doppler sounding system and all-sky airglow imager in Taiwan

#Hiromi Sejima[1)], Keisuke Hosokawa[1)], Jaroslav Chum[2,6)], Jia-Ting Lin[3)], Charles Lin[3)], Hiroyuki Nakata[4)], Jun Sakai[1)], Susumu Saito[5)]
(1UEC,(2ASCR,(3NCKU,(4Grad. School of Eng., Chiba Univ.,(5ENRI, MPAT,(6ASCR

Plasma bubbles are regions of electron density depletion in the equatorial ionosphere appearing at altitudes above 200 km. Plasma bubbles, that develop to higher altitudes near the magnetic equator, are observed at low latitude regions 10-20 degrees away from the magnetic equator. Plasma bubbles are known to cause disruptions of global navigation satellite systems and/or degradations of their positioning accuracy. For this reason, various studies have been conducted on plasma bubbles. Chum et al. (2016) conducted a statistical study of Doppler spectrograms obtained from HF Doppler sounding systems in Taiwan, and suggested that plasma bubbles can be detected as oblique spreading structures in the Doppler spectrograms. However, it is not known what properties of plasma bubbles reflect the microstructure (striated structure) of the disturbances that are caused by the plasma bubbles (the oblique spread structures) in the Doppler spectrogram.

The purpose of this study was to analyze striated structure of the oblique spread structures in the Doppler spectrogram by simultaneous observations with an all-sky airglow imager in Tainan, Taiwan and an HF Doppler sounding system in Taiwan.

As a result, it was confirmed that branch structures of the plasma bubble have striated structures corresponding to the time when the branches reach the intermediate reflection point and that the number of branch structures and the number of striated structures coincide approximately with each other. This suggests that striated structures of the oblique spread structures in the Doppler spectrogram corresponds to the branch structures of the plasma bubbles.

On the other hand, four of the six branches reached the latitude of the intermediate reflection point, which did not match the six branches of the striated structure. This is inconsistent with the fact that the Doppler spectrogram reflects only data from reflections at intermediate reflection points. This suggests that the Doppler spectrogram does not reflect only the reflection data at the intermediate reflection point, but also the scattering data from other scattering points. Therefore, I analyze not only the intermediate reflection points but also the scattered points to determine whether the oblique spread structures in the Doppler spectrogram reflects reflection or scattering.

The change in Doppler shift due to the change in the position of the plasma bubble was determined to determine if it was reflection or scattering. The calculation method was based on the velocity and position of the plasma bubbles calculated from the keogram, and the Doppler shift was calculated from the change in radio propagation distance. In addition, the reflection altitude was estimated by comparing the calculated Doppler shift with the measured Doppler shift. By comparing the estimated reflection point with the scattered point, I intend to confirm whether the scattered data is reflected in the Doppler spectrogram.

R005-16
B 会場 ：11/5　AM1 （9:00-10:30）
09:00〜09:15

#チャクラボルティ　芝地 [1)], 西谷　望 [2)],Baker　Joseph. B.H.[3)],Ruohoniemi　John M.[4)]
[(1] バージニア工科大学,[(2] 名大 ISEE,[(3]Space@VT,[(4] バージニア工科大

Solar Flare effects on the High Latitude Electrodynamics

#Shibaji Chakraborty[1)], Nozomu Nishitani[2)], Joseph B.H. Baker[3)], John M. Ruohoniemi[4)]
[(1]Virginia Tech,[(2]ISEE, Nagoya Univ.,[(3]Space@VT,[(4]ECE, Virginia Tech,

A solar flare is a space weather event that causes a transient in the ionospheric system at sub-auroral, middle, and lower latitudes, commonly known as the solar flare effect (SFE). However, flare peaking beyond X-class or higher can impact current systems at auroral and polar latitudes. Using ground-based radars and magnetometers located in high latitude North American sectors, we conducted an event study on the X9.3 flare on 6 September 2017. We found: (i) SuperDARN radar located at Saskatoon (auroral latitude, dawn sector) observed a sudden appearance of ionospheric scatter following the flare; (ii) SuperDARN Inuvik radar, located at polar latitude, recorded a sudden reduction in plasma flow velocity; (iii) significant enhancement in geomagnetic field intensity observed by ground magnetometers, which lasted about 3-hours; (iv) several SuperDARN radars located at the nightside also recorded a change in plasma convection. Apparently, the sudden appearance of ionospheric irregularity structures near auroral latitudes-dawn sector and the change in nightside ionospheric plasma flow at auroral latitudes are related to a change in the ionospheric Hall/Pederson conductivity and current system. In addition, the longer lasting intense geomagnetic field variations detected by the magnetometer stations suggest a change in the day-night ionospheric current system. Finally, the reduction in plasma flow velocity observed by a polar latitude radar is predominantly driven by the reduction in efficiency of mechanical energy conversion in the dayside solar wind-magnetosphere-ionosphere (SW-M-I) interaction. This work demonstrates flare effects on auroral currents, nightside effects, and a reconfiguration of MI coupling morphology.

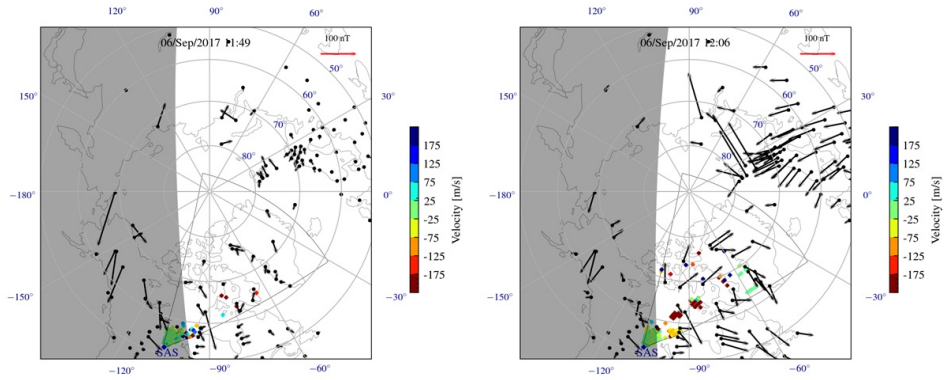

R005-17
B 会場 ：11/5　AM1 （9:00-10:30）
09:15〜09:30

SuperDARN レーダーデータによる磁気嵐発生時の中緯度電離圏対流の解析

#大森　康平 [1)], 西谷　望 [1)], 堀　智昭 [1)]
([1] 名大 ISEE

Study of mid-latitude ionospheric convection during geomagnetic storms using the SuperDARN radar data

#Kohei Omori[1)], Nozomu Nishitani[1)], Tomoaki Hori[1)]
([1]ISEE, Nagoya Univ.

Geomagnetic storm is a phenomenon in which the geomagnetic field decreases in the mid- and low-latitudes of the Earth due to the influence of the enhanced ring current in the magnetosphere. During geomagnetic storms, the plasma convection pattern changes in the mid-latitude ionosphere due to a variety of factors such as auroral oval expansion, subauroral polarization stream (SAPS), penetration and overshielding electric fields, and disturbance dynamo. To investigate the characteristics of mid-latitude ionospheric convection during geomagnetic storms, we performed a superposed epoch analysis of plasma velocities observed by Super Dual Auroral Radar Network (SuperDARN) by referring to the onset time of geomagnetic storms as the reference epoch. In this study, we have analyzed about 200 geomagnetic storms that occurred between December 2006 and December 2018, using data from the Hokkaido East and West radars. Just after the onset of geomagnetic storms, there was an equatorward expansion of high-latitude convection around 60 degrees magnetic latitude and an intensification in westward flow at slightly lower latitudes, which appeared to be SAPS. Approximately 20 hours after the storm onset, there was a continuous increase in westward flow around 40 degrees to 50 degrees magnetic latitude, presumably due to the disturbance dynamo. In the presentation, we discuss the results of an analysis using more radars.

磁気嵐は、太陽風変動の影響によって赤道環電流が増大することにより、地球の中低緯度域において地上磁場が減少する現象である。磁気嵐が発生した際、中緯度電離圏では、オーロラオーバルの拡大、SAPS、侵入電場、過遮蔽電場、Disturbance dynamo といった様々な要因によってプラズマのドリフトが発生する。我々は、磁気嵐発生時の中緯度電離圏対流の特性を調査するため、SuperDARN (Super Dual Auroral Radar Network) レーダーで得られたプラズマの速度に関して、磁気嵐の発生時刻を基準とした Superposed Epoch Analysis を行った。現時点で我々は、北海道-陸別第一・第二レーダーのデータを用い、2006 年 12 月から 2018 年 12 月までの期間に発生した約 200 個の磁気嵐について解析を行った。磁気嵐発生直後には、磁気緯度 60 度付近では高緯度対流の拡大が見られ、さらに低緯度側では SAPS と思われる西向きフローの増大が見られた。また、発生から約 20 時間後には、磁気緯度 40 度から 50 度付近において、Disturbance dynamo の影響と思われる継続的な西向きフローの増大が見られた。講演では、データを使用するレーダー数を増やし、その解析結果について議論する予定である。

R005-18
B 会場 ：11/5　AM1 （9:00-10:30）
09:30〜09:45

フィンランド・ニロラの 630nm 大気光イメージャによって観測された極域型の中規模伝搬性電離圏擾乱を特徴づける波動パラメータの統計解析

#佐藤　雅紀 [1)], 塩川　和夫 [1)], 大山　伸一郎 [1,3,4)], 大塚　雄一 [1)],Oksanen　Arto[2)]
([1] 名古屋大学宇宙地球環境研究所,[2]Jyväskylän Sirius ry, Jyväskylä, Finland,[3] 国立極地研究所,[4] オウル大学,[5] 国立極地研究所,[6] オウル大学

Statistical analysis of wave parameters of polar-type MSTIDs observed by a 630-nm airglow imager at Nyrola, Finland

#Masaki Sato[1)], Kazuo Shiokawa[1)], Shin ichiro Oyama[1,3,4)], Yuichi Otsuka[1)], Arto Oksanen[2)]
([1]ISEE, Nagoya Univ.,[2]Jyvaskylan Sirius ry, Jyvaskyla, Finland,[3]National Institute of Polar Research, Tokyo, Japan,[4]University of Oulu, Oulu, Finland,[5]National Institute of Polar Research, Tokyo, Japan,[6]University of Oulu, Oulu, Finland

Medium-scale traveling ionospheric disturbances (MSTIDs) are one of the ionospheric plasma density structures and are observable through 630-nm airglow images. Shiokawa et al. (2012; 2013) and Yadav et al. (2020) reported polar-type MSTIDs whose propagation direction changes with auroral brightening and magnetic field disturbances, based on airglow imaging observation at Tromso (69.6 ^{o}N, 19.2^o E; magnetic latitude: 66.7^{o}N), Norway. One report, MSTID observed at Shigaraki, Japan (34.8^{o}N, 136.1^{o}E; magnetic latitude: 25.4^{o}N), which is located at mid-latitude, shows no similar propagation direction change (Shiokawa et al., 2003). However, there has been little statistical analysis of the wave parameters of MSTIDs occurring between the polar regions and middle latitudes. In this study, we statistically analyzed the wave parameters of MSTID observed by an airglow imager from the PWING project at Nyrola (62.3^{o}N, 25.5^{o}E; magnetic latitude: 59.4^{o}N), Finland, which is located south of Tromso. The period analyzed was from January 23, 2017, to September 30, 2021. We found 11 cases of MSTIDs during this period, the majority of which were found to be of the polar type, whose motion changes associated with auroral brightening and magnetic field disturbances. By analyzing these 11 MSTID cases, we found that the low-latitude boundary of the polar-type MSTID is 61^o $\pm$ 2^{o}N for geographic latitude and 58^o $\pm$ 2^{o}N for magnetic latitude. In addition, the occurrence probability, velocity, wavelength, oscillation period, wave front directions and propagation direction of these MSTIDs were derived and compared with the Tromso and Shigaraki results. The results showed that the occurrence probability of MSTIDs at Nyrola is 1.9%, which is lower than that at Tromso (more than 50%) and Shigaraki (~ 30%). More than half of the wavelengths were less than 100 km, which tends to be smaller than in the mid-latitudes. In the presentation, we will discuss the differences in the causes of MSTIDs occurring in the mid-latitudes and those occurring in the polar regions based on these comparisons.

References:
Shiokawa et al. (2003), https://doi.org/10.1029/2002JA009491
Shiokawa et al. (2012), https://doi.org/10.1029/2012JA017928
Shiokawa et al. (2013), https://doi.org/10.1016/j.jastp.2013.03.024
Yadav et al. (2020), https://doi.org/10.1029/2019JA027598

電離圏のプラズマ密度の変動の一種である中規模伝搬性電離圏擾乱（MSTID）は、波長 630nm の大気光撮像を通して観測することができる。Shiokawa et al. (2012; 2013) と Yadav et al.(2020) は、オーロラ帯の緯度に位置するノルウェーの Tromsø (69.6° N, 19.2° E; 磁気緯度：66.7° N) で、MSTID 発生領域の極側で発生したオーロラの増光や地磁気変動に伴って伝搬方向が変化する極域型 MSTID の観測例を報告している。一報、中緯度に位置する日本の信楽 (34.8° N, 136.1° E; 磁気緯度：25.4° N) で観測された MSTID には同様な伝搬方向の変化は見られない（Shiokawa et al., 2003）。しかし、極域と中緯度の中間で発生する MSTID の波動パラメータの統計解析はこれまであまり行われていない。そこで今回は、Tromsøの南に位置するフィンランドの Nyrölä（62.3° N, 25.5° E；磁気緯度：59.4° N）で、PWING プロジェクトによる大気光イメージャによって観測された MSTID の波動パラメータを統計的に解析した。解析した期間は、2017 年 1 月 23 日から 2021 年 9 月 30 日までである。この期間に 11 例の MSTID を発見し、その大部分はオーロラ増光や地磁気変動に伴って動きが変化する極域型であることがわかった。この 11 例の MSTID を解析することにより、極域型 MSTID の低緯度側の境界が地理緯度：61° ± 2° N, 磁気緯度：58° ± 2° N 付近であることが分かった。さらに、これらの MSTID の発生確率・速度・波長・周期・波面の方向・伝搬方向を導出し、Tromsøや信楽の結果と比較した。その結果、Nyrölä では MSTID の発生確率が 1.9 %であり、Tromsø（50% 以上）や信楽（約 30%）に比べて低いことが分かった。また、波長は 100km 未満のものが半分以上あり、中緯度に比べて波長が小さくなる傾向があることが分かった。講演では、これらの比較から、中緯度で発生する MSTID と極域で発生する MSTID の発生原因の違いについて考察を行う。

References:

Shiokawa et al. (2003), https://doi.org/10.1029/2002JA009491
Shiokawa et al. (2012), https://doi.org/10.1029/2012JA017928
Shiokawa et al. (2013), https://doi.org/10.1016/j.jastp.2013.03.024
Yadav et al. (2020), https://doi.org/10.1029/2019JA027598

R005-19
B 会場 ：11/5　AM1 （9:00-10:30）
09:45〜10:00

あらせ衛星，地上全天カメラ，EISCAT レーダーによる磁気共役同時観測を用いた脈動オーロラ電子のエネルギー特性に関する研究

#伊藤　ゆり [1)], 細川　敬祐 [1)], 小川　泰信 [2)], 三好　由純 [3)], 村瀬　清華 [2)], 吹澤　瑞貴 [2)], 大山　伸一郎 [3)], 中村　紗都子 [3)], 笠原　禎也 [4)], 松田　昇也 [4)], 笠原　慧 [5)], 風間　洋一 [6)], 堀　智昭 [3)], 横田　勝一郎 [7)], 桂華　邦裕 [5)],Wang Shiang-Yu[6)],Tam　Sunny W. Y.[8)], 篠原　育 [9)]
([1 電通大,([2 極地研,([3 名古屋大学 ISEE,([4 金沢大学,([5 東京大学,([6Academia Sinica,([7 大阪大学,([8 国立成功大学 ISAPS,([9 宇宙研, 宇宙機構

Simultaneous conjugate observations of energy of pulsating auroral electrons by Arase satellite, all-sky imagers and EISCAT radar

#Yuri Ito[1)], Keisuke Hosokawa[1)], Yasunobu Ogawa[2)], Yoshizumi Miyoshi[3)], Kiyoka Murase[2)], Mizuki Fukizawa[2)], Shin ichiro Oyama[3)], Satoko Nakamura[3)], Yoshiya Kasahara[4)], Shoya Matsuda[4)], Satoshi Kasahara[5)], Yoichi Kazama[6)], Tomoaki Hori[3)], Shoichiro Yokota[7)], Kunihiro Keika[5)], Shiang-Yu Wang[6)], Sunny W. Y. Tam[8)], Iku Shinohara[9)]
([1UEC,([2NIPR,([3ISEE, Nagoya Univ.,([4Kanazawa Univ.,([5Univ. of Tokyo,([6Academia Sinica,([7Osaka Univ.,([8ISAPS, NCKU,([9ISAS, JAXA

Auroras are classified into two broad categories: discrete auroras, which have a distinct arc-like shape, and diffuse auroras, which have an indistinct patchy shape. Most of the diffuse auroras are known to show a quasi-periodic luminosity modulation called pulsating auroras (PsA). Magnetospheric electrons are scattered through wave-particle interactions with chorus waves and precipitate into the ionosphere, being referred to as “PsA electrons”. Recent studies demonstrated that sub-relativistic electrons originating from the radiation belt precipitate into the ionosphere during intervals of PsA. It was also pointed out that the energy of PsA electrons tends to be higher when the shape of the optical structure is patchy. These facts suggest that the loss process of such highly energetic electrons in the magnetosphere can be visualized by observing the shape/distribution of PsA and the energy of PsA electrons. In order to test and further validate this visualization method, it is crucial to understand what factors control the morphology of PsA and the energy of PsA electrons, although past studies have not sufficiently examined PsA and electron precipitation in this regard.

In this study, the Arase satellite, ground-based all-sky imagers, and the European Incoherent SCATter (EISCAT) UHF radar were used in combination to carry out simultaneous observations of PsA. We investigated the relationship between the morphology of PsA and the energy of PsA electrons by using the data set. First, the energy spectra of PsA electrons were estimated from the ionization profile obtained by EISCAT with an inversion technique, a modified version of CARD originally developed by Brekke et al. (1989). The estimated spectra were compared with those of energetic electrons observed by LEP-e and MEP-e onboard Arase. As a result, it was confirmed that when the footprint of the satellite was close to the sensing area of EISCAT, the energy spectra of precipitating PsA electrons and their temporal variation were in good agreement with those of magnetospheric electrons within the loss cone at the satellite location. In addition, the energy of PsA electrons tended to change in accordance with the transition of the morphology of PsA. Specifically, when the boundary of the patch structure is distinct, the energy of the corresponding PsA electron exceeded 10 keV. Based on these observational results, we hypothesize that both the morphology of PsA and the change in the energy of PsA electrons are controlled by the existence of ”ducts,” which are tube-like regions where the electron density is lower or higher than the surrounding area. Those duct structures guide chorus waves along the magnetic field to propagate to higher latitudes. In order to test this hypothesis, now we are analyzing PWE data obtained by Arase to infer the spatial structure of electron density in the source region of PsA. In this presentation, we introduce the observational results and discuss the factors controlling the morphology of PsA and energy of PsA electrons by showing the electron density estimates.

オーロラは，明るいアーク状の構造を持つ「ディスクリートオーロラ」と，パッチ状のぼんやりとした形状を示す「ディフューズオーロラ」の 2 つに大別される．ディフューズオーロラの多くは，数秒から数十秒の周期で明滅を繰り返しており，この明滅が脈を打つ様に見えることから脈動オーロラ（Pulsating Aurora: PsA）と呼ばれている．近年の研究によって，PsA の発生時に，放射線帯を起源とする準相対論的高エネルギー電子が同時に降下していることが示唆されている．また，脈動オーロラの形態がパッチ状になるほど，降下電子（PsA 電子）のエネルギーが高くなることも指摘されている．これらの結果は，PsA の形態を地上からモニターすることによって，放射線帯電子を含む磁気圏の高エネルギー電子の消失過程を 2 次元的に可視化できる可能性を示している．しかし，これまでの研究では，PsA の形態と降下電子エネルギーがどのような関係にあり，PsA 電子のエネルギーがどのような物理過程によって決定されているのかを，磁気圏における衛星観測を参照しながら議論することが行われてこなかった．

本研究では，あらせ衛星，地上全天カメラ，EISCAT レーダーを用いて，PsA の形態と PsA 電子のエネルギー特性の間の関係を調べた．特に，コーラス波動，磁気圏電子，PsA，電子密度の高度分布 (電離分布) の衛星・地上同時観測が成立し，かつ PsA の形態遷移が顕著に識別できる 2021 年 1 月 12 日 02:10:00 – 04:35:00 UT のイベントについて解析を行った．まず，EISCAT レーダーによる電離分布に対して CARD 法と呼ばれる逆問題解析手法を適用し，PsA 電子の

エネルギースペクトルを導出した．得られたエネルギースペクトルを，あらせ衛星の LEP-e, MEP-e による電子計測と比較したところ，衛星のフットプリントが EISCAT レーダーの観測領域の近くに位置している場合には，ロスコーン内に分布する電子のエネルギースペクトル，およびその時間変化が EISCAT から求められたものと良く一致していることが明らかになった．さらに，これらのエネルギースペクトルと PsA の画像データから，PsA の形態に伴って PsA 電子のエネルギーが変化する傾向も見て取ることができた．具体的には，PsA の空間構造が明瞭である場合（輪郭がはっきりとしている場合）に，10 keV を超えるような高いエネルギーを持った電子の降下が見られることが明らかになった．この観測事実に基づき，磁気圏においてダクトが形成されているときは，コーラスがダクト内のみを伝搬することで PsA の輪郭が明瞭になり，ダクトによってコーラスの高緯度伝搬が可能になるために PsA 電子のエネルギーが高くなる，という仮説を立てた．現在，磁気圏におけるダクトの存在を確認し，上記の仮説を実証することを目的として，あらせ衛星の PWE による観測から磁気圏の電子密度の空間構造を明らかにすることに取り組んでいる．発表では，解析事例を紹介し，PsA の形態と降下電子エネルギーを制御しているメカニズムを，ダクトによるコーラスの高緯度伝搬を考慮して議論する予定である．

R005-20
B 会場 ：11/5　AM1 （9:00-10:30）
10:00〜10:15

#陳　治宇 [1)], 大塚　雄一 [1)], 新堀　淳樹 [1)], 惣宇利　卓弥 [1)], 塩川　和夫 [1)],PERWITASARI　SEPTI[2)], 西岡　未知 [2)], 土屋　史紀 [3)], 熊本　篤志 [4)], 笠原　禎也 [5)], 三好　由純 [1)], 北原　理弘 [4)], 中村　紗都子 [1,6)], 松岡　彩子 [7)], 篠原　育 [8)]
([1] 名古屋大学宇宙地球環境研究所,[2] 情報通信研究機構,[3] 東北大・理・惑星プラズマ大気,[4] 東北大・理・地球物理,[5] 金沢大,[6] 名古屋大学高等研究院,[7] 京都大学,[8] 宇宙研／宇宙機構

A Study of Variations of Plasmaspheric Total Electron Content during Magnetic Storms by Using the GPS Total Electron Content Data

#ZHIYU CHEN[1)], Yuichi Otsuka[1)], Atsuki Shinbori[1)], Takuya Sori[1)], Kazuo Shiokawa[1)], SEPTI PERWITASARI[2)], Michi Nishioka[2)], Fuminori Tsuchiya[3)], Atsushi Kumamoto[4)], Yoshiya Kasahara[5)], Yoshizumi Miyoshi[1)], Masahiro Kitahara[4)], Satoko Nakamura[1,6)], Ayako Matsuoka[7)], Iku Shinohara[8)]
([1]ISEE, Nagoya Univ.,[2]NICT,[3]Planet. Plasma Atmos. Res. Cent., Tohoku Univ.,[4]Dept. Geophys., Grad. Sch. Sci., Tohoku Univ.,[5]Kanazawa Univ.,[6]IAR,[7]Kyoto University,[8]ISAS/JAXA

Total electron content (TEC) is an integration of the electron density along a ray path from satellite to receiver, which can be measured by dual-frequency Global Positioning System (GPS). However, the measured TEC contains inter-frequency biases inherent with satellites and receivers, which cannot be ignored in original TEC. Previous study has developed a method to separate ionospheric TEC from the inter-frequency biases by using the least square fitting procedure.[1] In this method, plasmaspheric TEC (PTEC) is not considered. However, it is known that the PTEC can be 10-50% of the ionospheric TEC. Considering the satellite zenith angle dependence on slant factor which converts the slant TEC to vertical TEC, PTEC could be included in the estimated inter-frequency bias. Therefore, we have analyzed the inter-frequency bias data obtained from approximately 9,000 receivers over the world. Storm events on September 2017 have been investigated to compare with Arase satellite observation data. In the first event, the Dst index reached a minimum of -122 nT at 2 UT on September 8, PTEC decreases by 2.85 TECU on September 8 by using GPS-TEC data and decreases by 1.10 TECU at around 17 UT on September 8 by using Arase satellite data, then recovers. In the second event, the Dst index reached a minimum of -54 nT at 10 UT on September 28, PTEC decreases by 0.59 TECU on September 28 by using GPS-TEC data and decreases by 0.63 TECU at around 21 UT on September 28 by using Arase satellite data, then recovers. The result shows the variation of PTEC deviation obtained from GPS-TEC data and Arase satellite observation data commonly shows that PTEC decreases after the onset of magnetic storm and recovers gradually. PTEC with high spatial and temporal resolutions during geomagnetic storms on March 2013, November 2017 and August 2018 is also investigated. It is shown that the bias at middle and low latitudes decreases during main phase of the three magnetic storms and bias decrease tends to be large at the longitudinal sector which is located in the nightside when the main phase starts. This result indicates occurrence of erosion process in the plasmasphere during the main phase of magnetic storms. Therefore, this study indicates the validity of GPS data on measuring PTEC variations.

R005-21
B 会場 ：11/5　AM2 （10:45-12:30）
10:45〜11:00

#LIU　SHUO[1,2],YU　TAO[1)]
(1 中国地質大学,(2 なごやだいがく

Study of the ionospheric spatial correlation

#Shuo LIU[1,2], TAO YU[1)]
(1China University of Geosciences,(2Nagoya University

In this study, we make a study for the Ionospheric spatial correlation scale. Firstly, the ionospheric horizontal spatial correlation study was conducted to collect global TECmap data from TEC Production that provided by the Jet Propulsion Laboratory (JPL). We use the monthly-averaged TEC over the world to calculate the deviation of the TEC and then the spatial correlation coefficient matrix of the deviation is also derived. According to the definition of correlation distance in statistics, the spatial characteristic scale is retrieved in the Zonal and meridian directions, and their variation of solar activity levels, geomagnetic field configuration conditions and seasonal conditions are investigated in details. Then, we using COSMIC occultation data, ion concentration profile data interpolation to establish electronic density three-dimensional grid data, the error covariance matrix of each level, and the error of the ion concentration in the vertical direction help poor matrix, analysis and study its time and space distribution at different heights, and its distribution in the vertical direction, The correlation scale model in the vertical direction of the ionosphere is constructed.

R005-22
B 会場 ：11/5　AM2 （10:45-12:30）
11:00〜11:15

ISS-IMAP/EUVI データから再構成した夜側電離圏 O+ 密度分布

#中野　慎也[1,2)], 穂積　裕太[3)], 齊藤　昭則[4)], 吉川　一朗[5)], 山崎　敦[6)], 吉岡　和夫[5)], 村上　豪[6)]
([1] 統計数理研究所,[2] データサイエンス共同利用基盤施設データ同化研究支援センター,[3] 情報通信研究機構,[4] 京都大・理・地球物理,[5] 東京大・新領域,[6]JAXA/宇宙研

O+ distribution in the nightside ionosphere reconstructed from ISS-IMAP/EUVI data

#Shin'ya Nakano[1,2)], Yuta Hozumi[3)], Akinori Saito[4)], Ichiro Yoshikawa[5)], Atsushi Yamazaki[6)], Kazuo Yoshioka[5)], Go Murakami[6)]
([1]The Institute of Statistical Mathematics,[2]Center for Data Assimilation Research and Applicatios,[3]NICT,[4]Graduate School of Science, Kyoto University,[5]Graduate School of Frontier Sciences, The University of Tokyo,[6]JAXA/ISAS

The International Space Station-Ionosphere-Mesosphere-Atmosphere Plasmasphere cameras (ISS-IMAP) mission operated a suite of imagers on board the International Space Station (ISS). One of the imagers, EUVI-B, was designed to observe extreme ultraviolet (EUV) emissions at 83.4 nm scattered by O+ ions. However, our previous study (Nakano et al., 2021) has concluded that EUVI-B mostly observed 91.1 nm emission due to recombination between O+ ions and electrons. This means that the EUV intensity observed from EUVI-B is approximately proportional to the line-of-sight integral of the square of O+ density. The EUVI-B data are thus useful for tomographic reconstruction of O+ distribution in the nightside ionosphere where EUVI-B was operated.

In this study, we have reconstructed O+ distribution in the nightside ionosphere from the EUVI-B data. We integrate multiple images acquired in each ISS orbit to obtain the three-dimensional O+ distribution in the vicinity of the orbit. Combining the reconstruction results for multiple ISS orbits, we obtain the temporal evolution of the ionospheric structure such as the equatorial anomaly. We will demonstrate some results of the reconstruction and discuss their scientific implications.

R005-23
B 会場 ：11/5　AM2 （10:45-12:30）
11:15〜11:30

#安藤　慧 [1)], 齊藤　昭則 [1)], 品川　裕之 [2)]
([1] 京大理,[2] 情報通信研究機構

Generation mechanism for the intra-seasonal enhancements of wintertime sporadic E layers

#Satoshi Andoh[1)], Akinori Saito[1)], Hiroyuki Shinagawa[2)]
([1]Graduate School of Science, Kyoto Univ.,[2]NICT

Present simulation provides a mechanism for intra-seasonal enhancements of wintertime sporadic E layers (WiEsLs). EsLs are highly dense plasma layers appearing in the ionospheric E region. During the wintertime, EsL intensity shows its minimum, which is partially because wind shears are weak in winter. Nevertheless, it has been reported that the intra-seasonal intensity enhancements of EsLs occur during the wintertime. One possible mechanism is considered to be major meteor showers such as the Geminid meteor shower. However, the intra-seasonal intensity enhancements of WiEsLs can occur not accompanied with the major meteor showers. Their cause has remained unclear. In this study, WiEsL simulation were performed by our ionospheric model coupled with neutral winds of a whole atmospheric model. The model succeeded generally in reproducing the intra-seasonal intensity enhancements of WiEsLs observed by an ionosonde at Kokubunji. We found that, in the simulation, zonal wind shears intensified at around 6 LT and 18 LT between 100 and 120 km altitude, and caused the intra-seasonal intensity enhancements of WiEsLs. In the observation, WiEsL intensity showed enhancements at the same local time. Thus, it was concluded that zonal wind shear intensification can drive the intra-seasonal intensity enhancements of WiEsLs. In this presentation, we will discuss causes of the wind shear intensification.

電離圏数値モデルを用いて、冬季におけるスポラディック E 層 (Es 層) の季節内強度上昇の物理機構を調査した。Es 層は、水平風の鉛直シアによって電離圏 E 領域に発生する、高密度プラズマ層である。冬季において Es 層強度は低く、その一因として風のシアが冬季において平均的に弱いことが考えられている。しかし、冬季において Es 層強度が数 10 日間にわたって上昇するという、Es 層強度の季節内変動がイオノゾンデ観測により報告されてきた。冬季 Es 層の季節内強度上昇の生成機構として、大規模な流星群 (例えば、双子座流星群) による金属イオンの供給量の増大が挙げられてきたが、大規模な流星群を伴わない時期にも冬季 Es 層の季節内強度上昇が発生することが報告されている。この場合の冬季 Es 層の季節内強度上昇に関する物理機構はいまだに解明されていない。本発表では、全球大気モデルの中性風を入力とした電離圏数値モデルを用い、2009 – 2011 年の 1 – 2 月において Es 層シミュレーションを実施した。1 – 2 月において国分寺で行われたイオノゾンデ観測では、2009 年に約 30 日間にわたる Es 層強度の季節内上昇を観測し、2010 年と 2011 年には観測していなかった。本発表のシミュレーションは、この 2009 – 2011 年の Es 層強度の季節内変動を再現することに成功した。モデルに入力した中性風を解析した結果、2010 年と 2011 年に比べて、2009 年において 6 LT と 18 LT 付近に強い東西風シアが高度 100 – 120 km 間に発生しており、この強い東西風シアが Es 層強度の季節内上昇を発生させていた。実際のイオノゾンデ観測でも、2010 年と 2011 年に比べて、2009 年の 6 LT と 18 LT 付近に Es 層強度が上昇していることを確認した。これらの結果から、平均的に弱いと考えられてきた冬季の風のシアが季節内変動を示し、強くなった風のシアが冬季 Es 層強度の季節内上昇を発生させていると結論づけた。本発表では冬季に東西風シアが強くなった原因についても議論する予定である。

R005-24
B 会場 ：11/5　AM2 （10:45-12:30）
11:30〜11:45

#傅　維正 [1)], 横山　竜宏 [2)],Ssessanga　Nicholas[3)], 馬　冠一 [4)], 山本　衛 [5)]
([1 京大・生存研,([2 京大生存研,([3 オスロ大学,([4 中国国家天文台,([5 京大・生存圏研

Study of nighttime midlatitude E-F coupling in geomagnetic conjugate regions using multi-source data

#Weizheng Fu[1)], Tatsuhiro Yokoyama[2)], Nicholas Ssessanga[3)], Guanyi Ma[4)], Mamoru Yamamoto[5)]
([1RISH, Kyoto Univ.,([2RISH, Kyoto Univ.,([34DSpace, Department of Physics, University of Oslo,([4NAO, Chinese Acad. Sci.,([5RISH, Kyoto Univ.

Nighttime midlatitude medium-scale traveling ionospheric disturbances (MSTIDs) are frequently observed in geomagnetic conjugate regions simultaneously. Previous observation results and theoretical analysis have underscored the importance of E-F coupling in MSTID generation and the postulation of hemisphere couple ionosphere. In this paper, the conjugate MSTIDs are studied to elucidate the causes and effects of E-F coupling in the interhemispheric coupled ionosphere. The hemisphere-coupled electrodynamics over Japan and Australia are observed and analyzed by using total electron content (TEC) measurements, supplemented with multi-source observations in ionogram, electron density, ion drift, neutral wind, and magnetic field. For the first time, observation results support the evidence that F-region geomagnetic conjugate irregularities in both hemispheres are mainly driven by the Es layers in the summer hemisphere. The Es layer is only observed in the summer hemisphere, subsequently triggers local E-F coupling and interhemispheric coupling. In the winter hemisphere, Es layers show dissipation during the interhemispheric coupling process. The thermospheric winds play an important role in the generation and development of MSTIDs, and the amplitude of MSTIDs is observed to vary with the meridional wind direction in respective hemisphere. Further, the observed interhemispheric field-aligned currents suggest non-equipotential magnetic field line, which may lead to the amplitude asymmetries in the conjugate MSTIDs. The magnitude of interhemispheric field-aligned currents, related with the Es-layer intensity, may explain the later formation of conjugate irregularities in the winter hemisphere.

R005-25
B 会場 ：11/5　AM2 （10:45-12:30）
11:45〜12:00

航空航法用 ILS 長距離伝搬波を用いた Es 下部構造の観測

#田淵　駿平 [1)], 細川　敬祐 [2)], 斎藤　享 [3)], 坂井　純 [2)], 冨澤　一郎 [4)], 高橋　透 [5)], 中田　裕之 [6)]
([1] 電通大,[2] 電通大,[3] 電子航法研,[4] 電通大・宇宙電磁環境,[5]ENRI,[6] 千葉大・工

Substructure of sporadic E layer as viewed by long-range propagation of aeronautical navigation signal

#Shumpei Tabuchi[1)], Keisuke Hosokawa[2)], Susumu Saito[3)], Jun Sakai[2)], Ichiro Tomizawa[4)], Toru Takahashi[5)], Hiroyuki Nakata[6)]
([1]UEC,[2]UEC,[3]ENRI, MPAT,[4]SSRE, Univ. Electro-Comm.,[5]ENRI, MPAT,[6]Grad. School of Eng., Chiba Univ.

The sporadic E (Es) layer is a phenomenon in which the electron density increases locally at an altitude of about 100 km in the ionosphere. The radio waves reflected by the Es layer can propagate anomalously for a long distance; thus, Es layer has a potential to cause interference to radio systems such as aeronautical navigation systems.

The aeronautical navigation uses the frequency band of 108-118 MHz to provide navigation information to aircrafts. The Instrument Landing System Localizer (ILS LOC), which is the focus of this study, transmits radio waves in 108-112 MHz frequency range with amplitude modulation at 90 Hz on the left side and 150 Hz on the right side as seen from the aircraft. Then, ILS provides information about the approach course based on the difference in the intensity of these two modulations (Difference in Depth of Modulation: DDM). Since the output radio wave has strong directivity, it may cause anomalous propagation over a long distance due to reflection by the Es layer. Recently, it has been reported that a 110.3 MHz radio wave, which seems to have been transmitted from the Localizer Type Directional Aid (LDA) at the Hualien Airport in Taiwan, was received in Kure, Hiroshima, Japan, using a software receiver. However, the source of the signal has not yet been confirmed and it is still unclear how the DDM data can be used for inferring the spatial structure of the Es layer. To overcome these problems, in this study, we have newly installed an ILS LOC receiver in Kure, which was actually used in the aircraft, and the direction of arrival of the radio wave was measured continuously.

During an anomalous propagation event on May 17, 2021, the ILS LOC receiver also received the 110.3 MHz radio signal. From the analysis of the received Morse code, it was confirmed that the radio signal actually arrived from Hualien. The difference between the direction of Kure as viewed from Hualien and the beam direction of the Hualien LDA is -0.68 deg. However, the most frequent DDM angle obtained during four months from May to August 2021 was slightly different (the mode of DDM values was -0.48 deg) from the direction of Hualien (-0.68 deg). This may be because the beam direction of the ILS LOC at the Hualien Airport changes due to the propagation direction and the spatial structure of the Es layer.

We have also investigated the deviation index (ROTI) of total electron content from GPS receivers during the intervals of anomalous propagation. The midpoint between Kure and Hualien, which is considered to be the reflection point of the Es layer, is located in sea areas. Therefore, in the case of a weak Es layer, it may not be possible to confirm the occurrence and propagation direction of Es layer only by using ROTI. However, in the three cases on May 27, June 8, and June 30, 2021, when anomalous propagation by Es was detected, Es signature in ROTI map was observed to move in the southwesterly direction from Honshu to southern Kyushu. The variation of the angle-of-arrival calculated from the DDM values shows that the angles are not always constant during the anomalous propagation, and there is sometimes a systematic decreasing trend. In particular, on June 30, 2021, there was a characteristic change in the angle, which continuously decreased by about 1.5 degrees in about 30 minutes. Based on the direction of motion of Es layer inferred from the ROTI mapping and the change in the angle-of-arrival on June 30, 2021, it can be suggested that Es layer has a wedge-like shape in its bottom part, which may explain the peak of the difference in the angle-of-arrival. This means that the motion and spatial of Es layer can be inferred from the change in the angle calculated from DDM of the ILS LOC receiver.

In the presentation, we show the statistics of the occurrence of anomalous propagation from Hualien in the two summer seasons in 2021 and 2022. We also discuss the characteristic change of the DDM values during the anomalous propagation as an indicator of the spatial structure and the motion of the Es layer.

スポラディック E (Es) 層は, 電離圏の高度約 100 km において局所的に電子密度が増大する現象である. 電子密度の増大に伴い, 通常電離圏 E 層において反射されることがない 100 MHz を超える VHF 帯の電波も Es 層により反射されることがある. Es 層によって反射された電波は, 長距離にわたって異常伝搬し, 航空航法システムなどの無線システムに電波干渉を引き起こす可能性がある.

航空航法用電波は, 108-118 MHz の周波数帯を使用して航空機への情報提供を行うために用いられている. 本研究で着目する計器着陸装置 ローカライザー (Instrument Landing System Localizer: ILS LOC) は, 108-112 MHz の電波を航空機から見て左側に 90 Hz, 右側に 150 Hz で振幅変調した電波を送信し, 変調度の差 (Difference in Depth of Modulation: DDM) により, 進入コースに関する情報を提供している. 出力される電波は, 強い指向性を持つため, Es による反射で長距離にわたる異常伝搬が生じる可能性がある. 著者らのグループの最近の研究によって, ソフトウェア受信機を使用して, 日本の広島県呉市において台湾の花蓮空港の ILS LOC 型の方向指示器 (Localizer Type Directional Aid: LDA) から送信

されたと考えられる 110.3 MHz の電波の受信事例が報告されている. 本研究では, ソフトウェア受信機に加えて航空機搭載用 ILS LOC 受信機を広島県呉市に設置し, 電波の到来方向を連続的に計測した．これにより，異常伝搬の送信元を明らかにするとともに，ILS の DDM の値から Es の空間構造に関する情報を抽出することが可能かを検証した.

2021 年 5 月 17 日に発生した Es 層による異常伝搬イベントでは, ILS LOC 受信機においても 110.3 MHz の電波が受信された. DDM から算出される観測点の ILS ビーム方向との偏位の角度や音声のモールス信号から, 電波が花蓮より到来したことが確認された. しかし, 2021 年 5 月から 8 月の期間に ILS LOC 受信機によって得られた 受信電波のビーム中心からの偏位の角度を統計的に解析した結果, 呉から見た実際の花蓮の方位角と電波のビーム中心の方位角の差 (-0.68 度) とは異なる値を多く示していたことが分かった. この原因として, Es 層の伝搬方向や空間構造によって, 花蓮空港 LDA の電波の伝搬に変化が起こっている事が考えられる.

上記の解析に加えて, 異常伝搬発生時の Es の空間構造を把握するために, GPS 受信機によって得られた電離圏全電子数の変動成分 (ROTI) との比較も行った. 異常伝搬波の反射点であると考えられている呉市と花蓮の中間点は海上にある. そのため, 小規模な Es の場合は, ROTI によってその Es の発生や伝搬方向が確認できない事がある. しかし, Es による異常伝搬が確認された 2021 年 5 月 27 日, 6 月 8 日, 6 月 30 日の 3 例においては, Es が本州から九州の南部に向かって南西方向に移動している様子が確認された. これは, これらの異常伝搬事例が Es による反射によって起こっていることを示す結果である.

また, DDM の値から算出した偏位角の変動について着目すると, 異常伝搬が発生したときに, 偏位角は常に一定の値を示しているわけではなく, 系統的な値の変動が見られる. 特に 2021 年 6 月 30 日の異常伝搬事例においては, 約 30 分にわたって偏位角が約 1.5 度にわたって連続的に減少するという特徴的な変化が観測された. ROTI のマッピングから考えられる Es の移動方向と偏位角の変化から, くさび形の Es が反射点を横切って移動したときに, このような偏位角の連続的な変化を説明できる. このような Es の空間構造が, 偏位角の分布に広がりを持たせた可能性がある. これらの結果は, ILS LOC 受信機の DDM の値から算出した偏位角の変化によって, Es の動きや空間構造を推測することができることを示唆する. 今後は, 2022 年夏季に得られた事例も含めて，偏位角の変化の仕方によって分類を行うことで, それぞれの変化に対応する Es の空間構造やその伝搬方向を検討する予定である．また，2021 年，2022 年のデータを用いた Es 異常伝搬の発生頻度に関する統計解析結果も示す予定である.

R005-26
B 会場 ：11/5　AM2 （10:45-12:30）
12:00〜12:15

スポラディック E 層の自動検出手法の改良とそれを用いた統計的性質の研究

#髙陽　直弘 [1)], 細川　敬祐 [1)], 斎藤　享 [2)], 坂井　純 [1)]
([1] 電通大,[2] 電子航法研

Improvement of an automated detection method and study of statistical characteristics of the sporadic E layer using the method

#Masahiro Takahi[1)], Keisuke Hosokawa[1)], Susumu Saito[2)], Jun Sakai[1)]
([1]UEC,[2]ENRI, MPAT

The Sporadic E (Es) layer is an ionospheric phenomenon having extremely increased electron density that frequently occurs at altitudes around 100 km in mid-latitude regions during summer. The enhanced electron density increases the critical frequency, causing radio waves in VHF frequency band, that normally penetrates through the ionosphere, to be reflected, resulting in anomalous propagation over long distances. As one of the fundamental features of the Es layers, it has often been reported that many of them have a two-dimensional frontal structure.

Radio waves for aeronautical navigation operative in VHF frequency band are reflected by the Es layer. In order to establish automated detection methods, it is required to evaluate the impact of anomalous long-range propagation on aircraft onboard equipment. In addition, the use of automated detection methods facilitates statistical studies using large amounts of data and is expected to be useful in predicting the occurrence of the Es layer in the future. However, no automated detection method has been established to date.

Therefore, we developed a method that employs the Hough transform and automatically detects frontal structures of the Es layer as a line-segment using a computer by inputting a ROTI map. The detection period was set to 00:00-06:00 UT on 120-240 days of year in 2019-2022. If two line-segments which have similar orientations were detected within 15 minutes, the velocity was also calculated using the displacement in the normal direction.

The results of the detection showed that inputting data within the divided areas led to output more consistent with visual detection than inputting data from the entire region (i.e., all Japan area). However, in some cases where multiple Es layers appeared in the area targeted for detection, the visual judgment and the detection results did not match. In the velocity calculations, north-south propagation was calculated more frequently than east-west propagation.

The detection within the divided areas made it possible to detect each of the two Es layers occurred in the entire Japan at the same time, and thus the detection results were close to visual judgment. On the other hand, since the method proposed in this study detects the Es layers as a single line-segment, it is still difficult to deal with the occurrence of multiple Es layers at one part within the divided areas. To solve this problem, it is necessary to select areas that does not contain multiple Es layers, but since the phenomenon is sporadic, manual selection of areas should have limitations. As for the velocity results, the distribution of ROTI data points in some areas are extended more in the east-west direction, and the line-segments tended to elongate more in the east-west direction, resulting in an increase in the number of calculated velocities in the north-south direction, which is the normal direction of the line-segment. In the area around Okinawa, movements of GPS satellites should have a huge impact on the calculation due to the small number of ROTI data points. In the presentation, we compare the motional characteristics of the Es layer in comparison with similar statistics based on manual estimation of the velocity.

スポラディック E 層 (Es) は、夏季の中緯度地域における高度 100km 付近で頻繁に発生する電子密度が急増する現象である。電子密度の上昇により、臨界周波数が上昇し、通常は電離圏を突き抜ける周波数帯の電波が反射され、長距離にわたって異常伝搬する。また、多くの Es が、前線状の二次元構造を持つことが明らかにされつつある。

Es により反射される電波として航空航法用無線電波があり、航空機搭載機器への影響を評価・監視するために Es の自動検出が求められている。また、自動検出手法を活用することで、大量のデータを扱った統計研究が容易になり、将来の Es の発生予測に役立てることが期待できる。しかし、現在までに自動的な検出手法は確立されていない。

そこで、本研究では Hough 変換を応用した手法を考案し、Es の二次元構造を可視化する手法の 1 つである ROTI マップを入力することで、前線状の Es を線分として計算機で自動的に検出した。検出期間は、2019-2022 年の通し日 120-240 における 00:00-06:00 UT とした。また、15 分以内に傾きの差が 2deg 以下の線分が検出された場合に、法線方向の移動距離と移動時間を用いて速度の算出も行った。

検出の結果、 日本全体を対象とした検出に比べ、分割したエリアでの検出の方が目視に近い検出結果となる傾向が強かった。ただし、検出対象とした範囲内で複数の Es が発生したとみられる例では、目視の判断と検出結果の一致が見られない場合があった。速度計算では、南北方向の伝搬が東西方向の伝搬と比較して多数算出された。

検出においては、エリアを分割することで日本全体において同時に 2 つの Es が発生した場合であってもそれぞれを検出することが可能となり、検出結果を目視の判断に近づけることが出来た。一方、本研究で提案した手法は 1 本の線分で検出を行うものであるため、1 つのエリアにおける複数の Es の発生に対処するのは依然として困難であった。これを解決するためには、複数の Es を含まないようにエリアを選択する必要があるが、現象が突発的であるため、手動では限界があることが予想される。速度の結果については、検出対象のエリアにおける ROTI データ点の分布が東西方向に広い

場合が多く、検出される線分が東西方向となり、結果としてその法線方向である南北方向の伝搬の算出数が増加した。また、沖縄付近のエリアでは、ROTI データ点の少なさゆえに、GPS 衛星の移動のみが速度計算に反映されてしまう例が頻繁にあり、速度の方位角分布に偏りができたと考えられる。発表では、Es の移動速度の統計結果を、これまでに目視で行われた同様の統計的研究と比較し、夏季の昼間における Es の移動特性を議論する。

R005-27
B 会場 ：11/5　PM1 （13:45-15:30）
13:45〜14:00

#野﨑　佑磨 [1)], 大矢　浩代 [2)], 土屋　史紀 [3)], 野崎　憲朗 [4)], 中田　裕之 [5)], 塩川　和夫 [6)]
([1] 千葉大・工,[2] 千葉大・工・電気,[3] 東北大・理・惑星プラズマ大気,[4] 電通大,[5] 千葉大・工,[6] 名大宇地研

Local time and seasonal variability of the D-region Ionosphere using OCTAVE observations

#Yuma Nozaki[1)], Hiroyo Ohya[2)], Fuminori Tsuchiya[3)], Kenro Nozaki[4)], Hiroyuki Nakata[5)], Kazuo Shiokawa[6)]
([1]Graduate School of Science and Engineering, Chiba University,[2]Engineering, Chiba Univ.,[3]Planet. Plasma Atmos. Res. Cent., Tohoku Univ.,[4]UEC,[5]Grad. School of Eng., Chiba Univ.,[6]ISEE, Nagoya Univ.

Daytime electron density in the D-region ionosphere varies depending on the solar zenith angle, which is a function of local time (LT) and season. In addition to the regular variation, D-region variations associated with various factors have been reported, for example, solar flares, geomagnetic storms, earthquakes, volcanic eruptions, and sudden stratospheric warming (SSW) [Lastovicka, 2006; Pal et al., 2017]. The detailed investigation of these factors is required to understand the D-region characteristics. In this study, we investigate seasonal and LT dependences of the D-region ionosphere using low frequency (LF) transmitter signals. The transmitter and receiver were JJY (60kHz, 33.47N, 130.18E) and RKB (Rikubetsu, Hokkaido, 43.45N, 143.77E), respectively. For removing effects of geomagnetic storms, we used international 5 quietest days (Q-days) for each month based on Kp index determined by GeoForschungsZentrum (GFZ) Potsdam. The daytime (or nighttime) mean value of amplitude and phase for each day (A_{mean} and P_{mean}) was subtracted from instantaneous values (A_i and P_i) to determine the perturbations in amplitude (Δ A) and phase (Δ P), i.e., Δ A=A_i-A_{mean} and Δ P=P_i-P_{mean}. In daytime, both Δ A and Δ P were large during 09:00-15:00 LT. Variations in Δ A and Δ P were large in January. Δ A was large in summer and winter, while Δ P was large in spring and fall. Calculated Δ A based on wave-hop method was larger during sunrise and sunset than that around 09:00-15:00 LT, which is opposite to the observation. The change in Δ P between observed and calculated results was opposite during sunrise/sunset. The calculation results showed that the Δ P was large in summer. In observations, both Δ A and Δ P were larger in January than those in other months, although only Δ A was large in calculation. The increases in the Δ A and Δ P in January 2017 could be associated with sudden stratospheric warming. Mean temperature at 10 hPa in the region where the latitude and longitude were $>$60N and 110E-170E, respectively, based on JRA-55 dataset, and the LF amplitude had two similar periods of 5 and 21 days. In this presentation, we will discuss the differences between the observed and calculated Δ A and Δ P, and cause of disturbances on the observed results for January 2017.

R005-28
B 会場 ：11/5　PM1 （13:45-15:30）
14:00〜14:15

X クラス太陽フレア発生時の OCTANE ネットワークによる空間不均一性の観測

#中山　雅晴[1)], 大矢　浩代[2)], 土屋　史紀[3)], 塩川　和夫[4)], 野崎　憲朗[6)], 中田　裕之[5)]
([1] 千葉大学,[2] 千葉大・工・電気,[3] 東北大・理・惑星プラズマ大気,[4] 名大宇地研,[5] 千葉大・工,[6] 電通大

Horizontal inhomogeneity detected by OCTAVE VLF/LF observations during a X-class solar flare

#Masaharu Nakayama[1)], Hiroyo Ohya[2)], Fuminori Tsuchiya[3)], Kazuo Shiokawa[4)], Kenro Nozaki[6)], Hiroyuki Nakata[5)]
([1]Chiba Univ.,[2]Engineering, Chiba Univ.,[3]Planet. Plasma Atmos. Res. Cent., Tohoku Univ.,[4]ISEE, Nagoya Univ.,[5]Grad. School of Eng., Chiba Univ.,[6]UEC

When solar flares occur, electron density in the ionosphere (60-100 km altitudes) increases because of intense X-rays. So far, relationship between VLF (3-30 kHz) and X-ray flux has been reported (Paulin et al., 2010), although there are few reports for horizontal inhomogeneity of the reflection height in the D-region ionopshere. The purpose of this study is to reveal horizontal homogeneity of electron density in the D-region ionosphere during a X-class solar flare using multi-path VLF/LF (30-300 kHz) transmitter signals of “Observation of CondiTion of ionized Atmosphere by VLF Experiment (OCTAVE)” network. When solar flares occur, VLF/LF amplitude and phase vary with decreasing the reflection height. The transmitters used in this study were NWC (21.817S, 114.167E, 19.8 kHz), JJI (32.05N, 130.82E, 22.2 kHz), JJY (37.37N, 140.85E, 40.0 kHz; 33.47N, 130.18E, 60.0 kHz), and BPC (34.63N, 115.83E, 68.5 kHz). The receivers were located at KAG (Tarumizu, Kagoshima, Japan, 31.59N, 130.55E), PKR (USA, 65.125N, 147.488W), and RKB (Rikubetsu, Hokkaido, 43.45N, 143.77E), which are part of OCTAVE network. A X2.2-class solar flare occurred at 08:57 UT on 6 September, 2017. During the solar flare, amplitudes of variations in the VLF/LF amplitude (Δ A) and phase (Δ P) were 2.65-14.73 dB and 31.0-150.25 degrees, respectively. Using wave-hop method, we estimated reduction in reflection height (Δ h) from the observed Δ A and Δ P. When the reference height was assumed to be 78.08-84.99 km, the Δ h were estimated to be 1.0-4.8 km for BPC-KAG, BPC-RKB, JJY40-KAG, JJY60-RKB and JJY40-RKB paths. The difference in the Δ h for each path would be caused by distance between the sub-solar point and each path, and sunset effects. In this presentation, we will discuss the horizontal inhomogeneity of the reflection height during the solar flare in detail.

太陽フレアが発生すると、強力な X 線により電離圏（高度 60-100km）の電子密度が上昇する。これまで、VLF（3-30kHz）と X 線フラックスの関係は報告されているが（Paulin et al.、2010）、電離圏 D 領域における反射高度の水平方向の不均一性についての報告はほとんどされていない。本研究の目的は、”Observation of CondiTion of ionized Atmosphere by VLF Experiment (OCTAVE)” ネットワークのマルチパス VLF/LF (30-300 kHz) 送信信号を用いて、X クラス太陽フレア時の電離圏 D 領域における電子密度の水平方向の不均一性を明らかにすることである。太陽フレアが発生すると、VLF/LF の振幅と位相は反射高度の低下に伴って変化する。送信局は NWC（21.817S, 114.167E, 19.8kHz）, JJI（32.05N, 130.82E, 22.2kHz）, JJY（37.37N, 140.85E, 40.0kHz; 33.47N, 130.18E, 60.0kHz） and BPC（34.63N, 115.83E, 68.5kHz）を使用した。受信局は、OCTAVE ネットワークの一部である KAG（鹿児島県垂水市、31.59N、130.55E）、PKR（米国、65.125N、147.488W）、RKB（北海道陸別市、43.45N、 143.77E）を使用した。2017 年 9 月 6 日 08 時 57 分（UT）に X2.2 クラスの太陽フレアが発生した。この太陽フレアの際、VLF/LF の振幅（Δ A）と位相（Δ P）の変動量はそれぞれ 2.65〜14.73dB、31.0〜150.25 度であった。wave-hop 法を用いて、観測されたΔ A およびΔ P から反射高度の低下量Δ h を推定した。基準高度を 78.08-84.99km とした場合、BPC-KAG, BPC-RKB, JJY40-KAG, JJY60-RKB, JJY40-RKB パスでは、Δ h は 1.0-4.8km と推定された。各パスのΔ h の違いは、太陽直下点と各パスとの距離、および日没の影響によるものである。本発表では、太陽フレア時の反射高度の水平方向の不均一性について詳しく説明する。

R005-29
B 会場 ：11/5　PM1 （13:45-15:30）
14:15〜14:30

酸素原子のイオン-中性衝突断面積：電離圏温度での関数フィット

#家田　章正 [1)]
(1 名大宇宙地球研

Fit of Atomic Oxygen Ion-Neutral Collision Cross Section at Ionospheric Temperatures

#Akimasa Ieda[1)]
(1ISEE, Nagoya Univ.

Atomic oxygen and its ion are major species in the ionosphere of Earth, Venus, and Mars. Collision between them controls the structure of ionosphere, and is expressed by collision cross section or frequency models. Recently, it is insisted that the textbook high-energy type model should be replaced by wide-energy type models. However, there are three wide-energy type models and it is not clear which of the three models is the most appropriate for ionospheric studies. In particular, the valid temperature range of their fits was unclear, although it was probably approximately between 300 and 2000 K, which is typically sufficient only for quiet-time Earth's F-region ionosphere.

The present study clarifies differences between the three models and proposes a new fit by including the curved-trajectory effect in the fitting basis function. As consequence, the valid temperature range is improved to be 75-9000 K, which is practically sufficient for the whole ionosphere of Earth, Venus, and Mars, including rare occasions.

酸素原子とそのイオンは、地球・金星・火星の電離圏を構成する主要な粒子種である。両粒子間の衝突は、衝突断面積や衝突周波数モデルとして表現される。最近 (Ieda, 2021)、教科書的な high-energy タイプのモデルでなく、教科書にはなぜか載らない wide-energy タイプのモデルが正しいことが示された。この wide-energy タイプには 3 つのモデルがあり、温度 1000 K ではその差は 6% と小さい。しかしこれまで、これらのモデルが有効な温度範囲は明らかでなかった。なお、電離圏の典型的な温度は、地球は 1000 K、金星と火星は 200 K である。

本研究では、電離圏研究に最適な、衝突断面積モデルの関数フィットを確定する。まず、過去の 3 つのモデルのうち、物理的に最適なモデルでは、本来の有効温度範囲が 300-2000 K であり、静穏時の地球の F 層の研究には十分であることを明らかにした。他の 2 つのモデルに、電離圏研究における長所は無い。本研究ではさらに、カーブ軌道効果 (Ieda, 2022) を考慮することにより、関数フィットの基底関数を改良した。この改良により、有効温度範囲は 75-9000 K と広がった。従って、結果の関数フィットは、E 層や擾乱時を含めて、地球・金星・火星の電離圏に適用することができる。

Ieda (JGR, 2021), https://doi.org/10.1029/2020ja028441
Ieda (JGR, 2022), https://doi.org/10.1029/2021ja029612

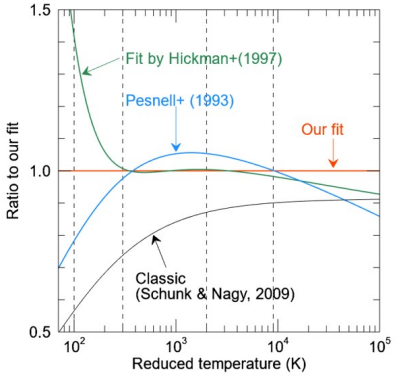

Figure 1.
O^+-O collision frequency or momentum-transfer cross section.
Our concluding fit is shown by the red line. Various models are shown as the ratio to our concluding fit.

Below 300 K, only our fit is accurate because low temperatures were not concerned in previous fits.
The collision frequency is underestimated in the classic model by 16% at 1000 K and by 35% at 200 K.

R005-30
B 会場 ：11/5　PM1 （13:45-15:30）
14:30〜14:45

HF ドップラー観測による流星エコーの解析

#齋藤　広樹 [1)], 中田　裕之 [2)], 大矢　浩代 [3)], 細川　敬祐 [4)]
[(1] 千葉大学,[(2] 千葉大・工,[(3] 千葉大・工・電気,[(4] 電通大

Examination of meteor echos observed by HF Doppler sounding

#hiroki saito[1)], Hiroyuki Nakata[2)], Hiroyo Ohya[3)], Keisuke Hosokawa[4)]
[(1]Chiba University,[(2]Grad. School of Eng., Chiba Univ.,[(3]Engineering, Chiba Univ.,[(4]UEC,

It is known that ionospheric disturbances occur at an altitude of 80 ˜120 km when meteors enter the Earth's atmosphere. The plasma associated with meteors entering is called a meteor trail and reflects radio waves in the HF and VHF bands due to its plasma density. Since most of the meteor radio observations have been performed using VHF band radio waves, meteor radio waves were observed using radio waves in the HF band in this study. Meteor echoes are classified into Underdense echoes and Overdense echoes by the scattering mechanism. The signal intensity at Underdense echo is exponentially attenuated. Om the other hand, the signal intensity at Overdense echo is remains constant for a while, and then it is rapidly attenuated. In addition, there are differences in the observed Doppler shifts between Overdense and Underdense echoes. While the Undedense echo reflects the movement of the meteor trail due to the neutral wind, the Overdense echo reflects the radial spread speed of the meteor trail. We have examined meteor echos observed by the HF Doppler sounding system utilized by the University of Electro-Communications and four other institutions. The transmitter of this system is located the Chofu Campus of the University of Electro-Communications. Since meteor trails are located at altitudes of 80 to 120 km, radio waves are reflected at these altitudes, which is lower than the usual reflections. We used Doppler data received at the Fujisawa, Sugito, Kakioka, Orai, and Kashima stations using 8 MHz radio waves transmitted from the Chofu campus. The event examined in this study occurred at 20: 30: 27 JST on October 25, 2014. In the meteor echo, radio waves are reflected under the condition that the incident angle is equal to the reflection angle. We found the reflection points that satisfies this condition. From the signal intensity of the observed meteor echo, it was clear that the observed meteor echos are the Overdense echo because the temporal variations of signal intensities have same features as the Overdense echoes. The duration of the meteor echo was much longer than that obtained by VHF radar. This is because the lifetime of the echo is proportional to the square of the wavelength. Because the meteor echo in this event is categorized as the Overdense echo, the Doppler shift is related to the speed of the radial diffusion of the meteor trail. Therefore, assuming that the trail is diffused, and the reflection point of the echo moves vertically downward, the speed of radial diffusion of the meteor trail can be estimated by the temporal variation of the Doppler shift at the time of meteor occurrence. Then, we also estimated it using the relation equations from the previous statistical results (Fish and Barkey, 1998). As a result, the speed of radial diffusion almost coincided in Kakioka, Oarai, and Kashima. Assuming that wind speed was the same at the reflection points and the meteor trail has moved in a certain direction, we estimated the speed and direction of the neutral wind from the Doppler shift and compared it with the neutral wind model. As a result, the wind speed almost coincided with the model, but the wind directions were almost inconsistent.

流星が高度 80〜120 km の地球大気に突入して、大気分子と激しく衝突した時に電離圏に擾乱が発生することが知られている．この時擾乱として生じるプラズマは流星飛跡と呼ばれ，電子密度の増加により HF，VHF 帯の電波を反射する性質をもつ．これまで流星電波観測の多くは，VHF 帯の電波を使用して行われてきた．そこで本研究では，HF 帯の電波を使用して，流星に伴うエコーの解析を行った．流星エコーは散乱機構によってアンダーデンスエコーとオーバーデンスエコーに分類される。それぞれのエコーの受信強度には違いがあり、アンダーデンスエコーの受信強度は指数関数的に減衰、オーバーデンスエコーは受信強度の強い時間が続き、やがて急速に減衰する特徴を示す。更に、観測されるドップラーシフトにも違いがあり、アンダーデンスエコーは中性風による流星飛跡の移動、オーバーデンスエコーは流星飛跡が半径方向に広がっていく速さを反映したものとなる。本研究では 電気通信大学を中心とした 5 機関で運用されている HF ドップラー観測システムにより取得された流星エコーを使用した．本来，HF ドップラー観測では、電波は送信点と受信点の中点直上の電離圏にて反射されるが、流星飛跡は高度 80˜120 km に生じるので、本来反射される高度より低い高度で反射される。解析には電気通信大学調布キャンパスより送信された 8 MHz の電波を藤沢，杉戸，柿岡，大洗，鹿島の各観測点で受信した際のドップラーデータを使用した．解析対象は 2014/10/25/20:30:27 JST に発生した流星である．流星エコーは、流星飛跡に対して入射角と反射角が等しくなるように反射される．各観測点に対して，この条件を満たす位置を反射点として求めた。観測された流星エコーの受信強度の時間変化から観測された流星エコーはオーバーデンスエコーであることが明らかとなった。エコーの継続時間は約 15 分とかなり長くなったが，本研究では HF 帯電波にて観測を行い，流星エコーの継続時間は送信周波数の波長に比例するため，これまでの VHF 観測によるものと比べ長くなったと考えられる．また，今回得られた流星エコーはオーバーデンスエコーであることから，ドップラーシフトは，流星飛跡の拡散速度を反映していると考えられる．そこで，飛跡の拡散により，エコーの反射点が鉛直下方向に移動したと仮定して，流星発生時刻からドップラーシフトが変化するまでのドップラーシフトの差から流星飛跡の半径方向への広がりの速さを求めた．統計的な結果から得られた関係式 (Fish and Barkey, 1998) を使用して求めた飛跡の広がりの速さと比較したところ，ほぼ一致した値が得られた．また，ドップラー周波数には中性風による飛跡の移動も含まれていると考え

られることから，流星飛跡が形状を保ったままある方角に移動したと仮定して、観測されたドップラーシフトから中性風の風速と風向を推測した．その結果を HWM モデルにより導出した風分布と比較したところ，風速の値はほぼ一致したが、風向はあまり一致しなかった．流星の飛跡がその形状を保ったまま中性風により移動すると仮定することはあまり適当でないと考えられ，より現実的な導出法を考える必要がある．

R005-31
B 会場 ：11/5　PM1 （13:45-15:30）
14:45〜15:00

#中村　卓司 [1)], 木暮　優 [2)],PERWITASARI　SEPTI[3)], 江尻　省 [1)], 冨川　喜弘 [1)], 堤　雅基 [1)], 塩川　和夫 [4)]
([1] 極地研,[2] 九大・理・地惑,[3]NICT,[4] 名大宇地研

Gravity wave and TID analysis using horizontal phase velocity spectrum: advantage of M-transform and tips for better performance

#Takuji Nakamura[1)], Masaru Kogure[2)], SEPTI PERWITASARI[3)], Mitsumu K Ejiri[1)], Yoshihiro Tomikawa[1)], Masaki Tsutsumi[1)], Kazuo Shiokawa[4)]
([1]NIPR,[2]Kyushu University,[3]NICT,[4]ISEE, Nagoya Univ.,

Phase velocity spectrum of the airglow images obtained by 3-D Fourier transform, i.e. M-transform, introduced by Matsuda et al. (2014) is the power spectrum of airglow intensity perturbation in horizontal phase velocity domain. This method quantitatively displays the wave energy of transient wave packets of the gravity waves, and clearly shows the wind filtering effects, direction of momentum, and possible source of the gravity waves. M-transform can also be used to analyze TID (Traveling Ionospheric Disturbance) characteristics observed in the GPS/TEC maps (Perwitasari et al., 2022). It has further been applied to the horizontal mapping of Doppler velocity observed by SuperDARN HF radar (Hazeyama et al., 2022). The software package of M-transform is delivered as an open software on the web site of National Institute of Polar Research. This presentation reviews the M-transform analysis applied to various dataset with different sampling in time and horizontal space, and discusses the advantage of M-transform analysis. Further discussed will be the tips for better performance of the M-transform when used to various new datasets, that could help a wider usage of the M-transform.

R005-32
B 会場 ：11/5　PM1 （13:45-15:30）
15:00〜15:15

南極観測船「しらせ」搭載全天イメージャーによる大気光とオーロラ観測

#山科　佐紀 [1)], 齊藤　昭則 [1)], 坂野井　健 [2)], 津田　卓雄 [3)], 青木　猛 [3)], 江尻　省 [4)], 西山　尚典 [4)], 穂積　裕太 [5)], 直井　隆浩 [5)], 永原　政人 [5)]
[(1] 京都大・理・地球物理,[(2] 東北大・理・PPARC,[(3] 電通大,[(4] 極地研,[(5] 情報通信研究機構

Airglow and aurora observation by all-sky imagers onboard Antarctic research vessel “Shirase”

#Saki Yamashina[1)], Akinori Saito[1)], Takeshi Sakanoi[2)], Takuo Tsuda[3)], Takeshi Aoki[3)], Mitsumu K Ejiri[4)], Takanori Nishiyama[4)], Yuta Hozumi[5)], Takahiro Naoi[5)], Masato Nagahara[5)]
[(1]Dept. of Geophysics, Kyoto Univ.,[(2]PPARC, Grad. School of Science, Tohoku Univ.,[(3]UEC,[(4]NIPR,[(5]NICT

Satellites are widely used to observe the ionospheric structures [1]. However, low orbit satellites have the disadvantage that it is difficult to separate temporal and spatial changes because their positions of the observations are variable, and geo-stationary satellites have the disadvantage of low spatial resolutions and limited observational areas. Wide-area observations have been conducted with grand-based all-sky imagers networks which can measure horizontal two-dimensional structures. Although the number of ground-based observational stations with imagers is increasing, they are limited to land, and the ionosphere over the ocean has not been sufficiently observed. In order to fill these observational gaps, we developed vessel-borne all-sky imagers that cancel the vibration of the vessel, and mounted them on the Antarctic research vessel ”Shirase” to conduct ionospheric observations on its routes between Japan and Antarctica. The small imagers (ZWO: ASI 183 mm Pro, approx. 410 g) were mounted on a 3-axis attitude-stabilized gimbal, and observations were conducted on three round trips between Tokyo and Syowa station over three years. A short wavelength observation (630.0 nm) was conducted with an exposure time of 19 seconds in the first year, a multi-wavelength observation (630.0 nm and 670.0 nm) with an exposure time of 8 seconds in the second year, and a multi-wavelength observation (630.0 nm and 760.0 nm) with an exposure time of 18 seconds in the third year. 630.0 nm emission corresponds to atomic oxygen airglow and F-region aurora, while both 670.0 nm and 760.0 nm emissions correspond to OH airglow and E-region aurora. Since the positions and directions of observations by the vessel-borne imagers differ from image to image, these were determined from the Shirase’ position/attitude data and the Shirase’s structures captured in the images. To identify the observed phenomena, emission altitudes were assumed (250 km for 630.0 nm emission and 100 km for 670.0 nm and 760.0 nm emissions), images were calibrated and converted into geographical images. During the three years of observations, OI 630.0nm airglow, OH airglow and aurora were successfully observed, and then we will report the results of these observations in this presentation. The observed phenomena will also be compared with data of total electron content observed by the GNSS receiver, which was installed on “Shirase” in the second and third year cruises, and with other spacecraft-borne and ground-based observation data.

References

[1] Immel, T. J., Mende, S.B., Frey, H.U., Peticolas, L.M., & Sagawa, E. (2003). Determination of low latitude plasma drift speeds from FUV images. Geophys Res Lett, 30, 1945. https://doi.org/10.1029/2003GL017573

[2] Shiokawa, K., et al. (1999). Development of Optical Mesosphere Thermosphere Imagers (OMTI). Earth Planets Space, 51, 887 – 896.

電離圏の時間変化・空間変化を観測するために人工衛星が広く用いられている [1]。しかし低軌道衛星では観測位置が変わり続けるため、時間変化・空間変化の分離が困難であり、静止衛星では空間分解能が低く、かつ観測領域が限られる等の欠点がある。地上からの電離圏観測としては、水平 2 次元構造の測定が可能な全天イメージャーを用いて広域観測が行われている [2]。地上のイメージャー観測点は増加しているが陸上に限られているため、海上に存在する電離圏は十分に観測されていない。このような観測空白領域を解消するため、私達は船舶の揺動を打ち消す船舶搭載型全天イメージャーを開発し、南極観測船「しらせ」に搭載して航路上で電離圏観測を行った。小型イメージャー（ZWO：ASI 183mm Pro、約 410g）は 3 軸姿勢安定ジンバルに搭載され、日本と昭和基地を 3 年間で 3 往復する航海において観測を行った。1 年目は露出時間 19 秒で単波長観測 (630.0nm)、2 年目は露出時間 8 秒で多波長観測 (630.0nm と 670.0nm)、３年目は露出時間 18 秒で多波長観測 (3 年目は 630.0nm と 760.0nm）を行った。630.0nm 発光は原子状酸素大気光・F 領域オーロラに対応し、670.0nm 発光と 760.0nm 発光はどちらも OH 大気光・E 領域オーロラに対応する。船舶搭載型イメージャーでは撮影位置、撮影方向が画像ごとに異なるため、これらをしらせの位置・姿勢データと画像内に写り込んだしらせの構造物を用いて決定した。観測された現象を特定するために、発光高度（630.0nm 発光は 250km、670.0nm 発光と 760.0nm 発光は 100km）を仮定し、画像を校正して地理画像に変換した。3 年間の観測で OI 630.0nm 大気光と OH 大気光及びオーロラの観測に成功し、本発表ではこれらの現象の観測結果について報告する。また観測した現象について、2 年目から本システムに導入した GNSS 受信機による全電子数観測データや、他衛星観測・地上観測データとの比較も行う。

References

[1] Immel, T. J., Mende, S.B., Frey, H.U., Peticolas, L.M., & Sagawa, E. (2003). Determination of low latitude plasma drift speeds from FUV images. Geophys Res Lett, 30, 1945. https://doi.org/10.1029/2003GL017573

[2] Shiokawa, K., et al. (1999). Development of Optical Mesosphere Thermosphere Imagers (OMTI). Earth Planets Space, 51, 887 – 896.

R005-33
B 会場 ：11/5　PM2 （15:45-18:15）
15:45〜16:00

インフラサウンドセンサ搭載 MOMO7 観測ロケットを用いた中層・高層大気中における低周波音計測

#水野　和樹 [1)], 山本　真行 [2)], 西川　泰弘 [3)], 田中　智泉 [4)]
([1] 高知工科大学大学院工学研究科,[2] 高知工科大学システム工学群,[3] 高知工科大学システム工学群,[4] 東北大学大学院工学研究科

Low-frequency sound measurements using the MOMO7 sounding rocket equipped with infrasound sensors

#Kazuki Mizuno[1)], Masayuki Yamamoto[2)], Yasuhiro Nishikawa[3)], Tomomi Tanaka[4)]
([1]Graduate school of Engineering, Kochi University of Technology,[2]School of Systems Engineering, Kochi University of Technology,[3]School of Systems Engineering, Kochi University of Technology,[4]Graduate School of Engineering, Tohoku University,

Introduction

Sound propagation in the Earth's atmosphere is closely related to parameters such as temperature, wind, and air density.

In the stratosphere, the mesosphere, and the thermosphere, which are considered to be the most difficult areas for in-situ observation sounding rockets are the best methods to measure the sound at altitudes of 30 km or more. In this study, infrasound sensors and buzzers were installed in the sounding rocket "MOMO" operated by a private company. We measured the propagation of the buzzer sound at each altitude, and also observed impulsive sound generated with fireworks launched from a near site of the rocket launcher. In addition, the shock wave emitted when the rocket itself reached the speed of sound was observed by using 9 sensors deployed on the ground and sensors abroad the rocket.

Purpose of the rocket experiment

The first purpose is to measure the signal strength of the buzzer sound inside the rocket at each altitude to investigate the propagation of sound at each altitude. The second one is to measure the sound generated with the fireworks on the ground by using the sensors abroad the rocket.

The third one is to observe the shock wave generated when the rocket descends with exceeding the sound speed , both on the ground and in the sky, to investigate how the shock wave propagates.

Observation Results

The sounding rocket MOMO7 developed by Interstellar Technologies Inc. was launched at 17:45 JST on July 3, 2021 in Taiki, Hokkaido, Japan.

Data of the infrasound sensor aboard the MOMO7 was acquired up to a maximum altitude of approximately 98 km during a time period of T+433 seconds after the launch(T) when to communications ground station were established.

The infrasound wave form data observed with the payload sensors shown in figure1.

Until T+120 seconds as noisy sound of the rocket engine combustion was observed, so the sound pressure values fluctuated violently. From there, the engine completed combustion at T+120 seconds, and the buzzing sound waveform could be observed up to around the highest altitude. However, no firework sound was observed and the buzzer sound did not show much variation than expected in attenuation at each altitude between 60 km˜98 km. From the data obtained with the payload, a large amplitude signal was observed at T+ approximately 240 seconds. All ground-based sensors observed a shock wave that may have been generated during the rocket's descent.

Discussion and Conclusion

The lack of change in the attenuation of the buzzer at each altitude is thought to be due to the fact that the vibration of the buzzer entered the sensor through the base.

As for the fact that the sound of the fireworks could not be observed in the sky, the fireworks were No. 4 fireworks under the restriction of the town of Taiki, and they were launched at a distance of about 14 km from the launch site of the rocket. It is thought that the sound was attenuated and did not reach the target due to the distance and insufficient power. As a measure for improvement, it would be better to increase the number of fireworks and launch them along the coast as close as possible to the rocket launch site.

The large signal observed at T+240 seconds was generated at an altitude of 98 km while the rocket body was accelerating at 286 m/s. This signal may have been generated immediately after the shock wave was generated. If so, it can be interpreted that the speed of sound is 286 m/s at an altitude of 98 km.

In this study, we were able to observe the buzzing sound up to an altitude of 98 km, and concluded that it is effective in predicting the propagation of sound at different altitudes. In the next experiment, it is necessary to replace the buzzer with a

device that expels air instantaneously to mitigate the resonance with the base. Since shock waves were observed at all of the ground sensors, we would like to use grid search to identify the source of the shock waves from the ground sensor side and investigate how the shock waves propagate.

はじめに

地球大気中の音の伝わり方は温度、風、大気密度などのパラメータに密接に関わっており、それらの高度プロファイル及び時間変動の理解が進められてきた。その中でも計測が困難とされる、成層圏～熱圏の高度 30 km 以上の場所では観測ロケットがほぼ唯一の計測手段である。本研究では民間会社が運用する観測ロケット MOMO 内にインフラサウンドセンサとブザーを搭載した。そして、高度毎のブザー音の伝わり方を計測するとともに、車上の近隣地域から打ち上げた花火による爆発音の上空での観測を試みた。また、ロケット自身が音速に達したときに発生する衝撃波を地上 9 か所のセンサとロケット内センサを使って観測した。

ロケット実験の目的

目的は 3 つあり、1 つ目はロケット内で鳴らしたブザーの信号強度を高度毎に計測し、高度毎での音の伝わり方を調査すること、2 つ目は地上で打ち上げた花火による音響を上空にいるロケット内のセンサで計測し、地上から高高度への音の伝わり方を調査すること、3 つ目はロケットが下降時に発生する衝撃波を地上と上空で観測し、高高度から地上への音の伝わり方を調査することである。

観測結果

インターステラテクノロジーズ株式会社が開発した観測ロケット MOMO7 号機が 2021 年 7 月 3 日 17:45:00 JST に北海道大樹町にて打ち上げられた。

MOMO7 搭載のインフラサウンドセンサのデータは地上局との通信が成立した打ち上げ (T) から T ＋ 433 秒までの時間帯、最高高度約 99 km までのデータを取得した。ペイロード内で計測されたインフラサウンド波形データを図 1 に示す。ペイロードデータの T+120 秒まではロケットエンジンの燃焼音が観測されており、音圧の値は激しく変動している。そこからエンジンが T ＋ 120 秒で燃焼終了し、ブザー音の波形が最高高度付近まで観測することができた。しかし、花火音の信号は一切見られなかったことと、ブザー音は 60 km~98 km 間の高度毎の減衰の変化が予想ほど見られなかった。ペイロード内での計測データより、T + 約 240 秒に大振幅の信号を観測した。さらに全 9 地点の地上設置センサがロケット下降時に発生したと思われる衝撃波を約 9 分 40 秒後にそれぞれ観測した

考察および結論

高度毎の減衰の変化があまり見られなかった点に関しては、ブザーの振動が回路基板を通じてセンサに入ってしまった可能性が考えられる。

花火音が上空で観測できなかった点に関しては、花火は協力いただいた大樹町との取り決めにより 3 号玉と 4 号玉のみを使用しており、ロケット打ち上げ場所から約 14 km 離れた場所でしか打ち上げられなかった。距離が遠かったことと威力が十分でないことから音が減衰してしまい届かなかったと思われる。改善策としては花火の号数を上げ、ロケット射場に限りなく近い海岸沿いで打ち上げられれば良いと考える。

T + 約 240 秒に観測した大きな信号に関しては、高度 98 km、ロケット機体が下降に向かい 286 m/s で加速しているときに発生した信号であり、衝撃波の発生直後を捉えた可能性がある。正しければ、このとき高度 98 ㎞では音速が 286 m/s だったと解釈できる。

本研究では高度 98 ㎞までブザー音を観測することができ、高度毎の音の伝わり方の予測に有効だと結論付けた。次に実験する際には、空気を瞬間的に吐き出す装置をブザーの代わりに取り付け、基盤との共板を緩和させる必要性がある。また地上センサ 9 地点のすべてにおいて衝撃波が観測されたので、グリッドサーチおよび音波レイ・トレーシングを使って地上センサ側から衝撃波発生源を特定して高層大気中での衝撃波の伝わり方を調査していきたい

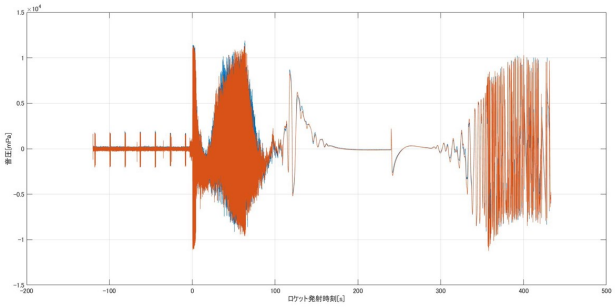

R005-34
B 会場 ：11/5　PM2 （15:45-18:15）
16:00〜16:15

トロムソ Na ライダーデータによる北極域 MLT 領域 8 時間と 6 時間大気波動の研究

#野澤　悟徳 [1)], 森川　千秋 [1)], 津田　卓雄 [2)], 川原　琢也 [3)], 斎藤　徳人 [4)], 和田　智之 [4)], 川端　哲也 [1)]
([1] 名大・宇地研,[2] 電通大,[3] 信州大学,[4] 理化学研究所

A study of 8 hr and 6 hr atmospheric waves in the polar MLT region above Tromsoe

#Satonori Nozawa[1)], Chiaki Morikawa[1)], Takuo Tsuda[2)], Takuya Kawahara[3)], Norihito Saito[4)], Satoshi Wada[4)], Tetsuya Kawabata[1)]
([1]ISEE, Nagoya Univ.,[2]UEC,[3]Shinshu Univ.,[4]RIKEN,

We have investigated characteristics of 8 hr and 6 hr atmospheric waves in the polar upper mesosphere and lower thermosphere (MLT) from 80 to 110 km above Tromsoe, Norway (69.6 deg N, 19.2 deg E). Aims of this study are to reveal (1) relative importance of 8 hr and 6 hr waves to a 12 hr wave (probably, semidiurnal tide) in the wind dynamics and the thermal structure, (2) vertical structures (wavelengths) of the 8 hr and 6 hr waves, and (3) importance of the 8 hr and 6 hr waves on the convective and dynamic instabilities in the polar MLT region.

Short periodic tidal waves are less known than diurnal and semidiurnal tidal waves even though an amplitude of the 8 hr tide sometimes becomes comparable to that of diurnal tidal wave in the polar MLT region [Thayaparan, 1997; Younger et al., 2002]. Solar heating, and nonlinear interactions between the diurnal and semidiurnal tides are thought to generate the 8 hour tide [Thayaparan, 1997; Akmaev, 2001; Younger et al., 2002; Moudden et al., 2013]. A modeling study by Smith [2001] showed the solar heating was a dominant source of generation of the 8 hr tide at high latitudes. Pancheva et al. [2021] using meteor radar wind data (1 hr/2 km resolutions) at Tromsoe reported that the vertical wavelength of the 8 hr tide in November shows the longest among months, and is larger than 100 km.

By using the Lomb-Scargle method, we have derived 12 hr, 8 hr, and 6 hr components using wind (110 nights) and temperature (192 nights) data obtained by the sodium LIDAR at Tromsoe. Data with their data length longer than 16 hours are used here, and only data whose normalized amplitudes being larger than 99% significance level are used. Maximum amplitudes of the 8 hr wave ranges from 14 (9) m/s to 128 (156) m/s with an average of 44 (47) m/s in the northward (eastward) wind data for 110 (110) nights, and ranges from 4 K to 33 K with an averaged of 12 K in the temperature data for 162 nights. The 6 hr component has amplitudes from 11 (12) m/s to 153 (93) m/s with an average of 43 (41) m/s in the norward (eastward) wind data for 104 (105) nights. In the temperature data, it ranges from 4 K to 29 K with an average of 13 K for 178 nights. It is found that both the 8 hr and 6 hr components have usually smaller amplitudes than the 12 hr component in the wind data, while they are comparable to those of 12 hr in the temperature data.

In the talk of Nozawa et al. in JpGU2022, we reported the relative importance of the 8 hr and 6 hr waves to the 12 hr wave, so this talk will focus on results of the latter two aims: we will report vertical structures (wavelength) of the 8 hr and 6 hr waves between 80 and 110 km, and their importance on the convective and dynamic instabilities in the polar MLT region.

Reference:
Akmaev, R. A., Seasonal variations of the terdiurnal tide in the mesosphere and lower thermosphere: A model study, GRL, 28, 3817-3820, https://doi.org/10.1029/2001GL013002, 2001.

Moudden, Y., and J. M. Forbes, A decade-long climatology of terdiurnal tides using TIMED/SABER observations, Journal of Geophysical Research: Space Physics, 118, 4534-4550, https://doi.org/10.1002/jgra.50273, 2013

Pancheva, D., P. Mukhtarov, C. Hall, A.K. Smith, M.Tsumi, Climatology of the short-period (8-h and 6-h) tides observed by meteor radars at Tromsoe and Svalbard, Journal of Atmospheric and Solar Terrestrial Physics, 212, 105513, https://doi.org/10.1016/j.jastp.2020.105513, 2021

Smith, A.K., and D. A. Ortland, Modelling and analysis of the structure and generation of the terdiurnal tide, Journal of the Atmosphere Sciences, 5, 3116-3134, 2001.

Thayaparan, T., The terdiurnal tide in the mesosphere and lower thermosphere over London, Canada (43 deg N,81 deg W), Journal of Geophysical Research, 102, 21,695-21,708, 1997.

Younger, P.T., D. Pancheva, D. Middleton, H. R., and Mitchell, N. J, The 8-hour tide in the Arctic mesosphere and lower thermosphere. Journal of Geophysical Research, 107(A12), 1420. https://doi.org/10.1029/2001JA005086, 2002.

R005-35
B 会場 ：11/5　PM2 （15:45-18:15）
16:15〜16:30

昭和基地における長期 OH 大気光観測データによる極域上部中間圏領域特有の変動解明

#石井　智士 [1)], 鈴木　秀彦 [1)], 田中　良昌 [2)], 堤　雅基 [3,4)], 田口　真 [5)], 江尻　省 [3,4)], 西山　尚典 [3,4)], 門倉　昭 [2)]
[(1] 明治大,[(2]ROIS-DS/国立極地研究所/総研大,[(3] 極地研,[(4] 総研大,[(5] 立教大・理・物理

Dynamics of the polar mesopause region inferred by the long-term OH airglow observation at Syowa Station, Antarctic

#Satoshi Ishii[1)], Hidehiko Suzuki[1)], Yoshimasa Tanaka[2)], Masaki Tsutsumi[3,4)], Makoto Taguchi[5)], Mitsumu K Ejiri[3,4)], Takanori Nishiyama[3,4)], Akira Kadokura[2)]
[(1]Meiji univ.,[(2]ROIS-DS/NIPR/SOKENDAI,[(3]NIPR,[(4]SOUKENDAI,[(5]Rikkyo Univ.

OH (8-4) airglow (emitting at an altitude of about 86 km) spectral observations with an OH spectrometer have been conducted at Syowa Station, Antarctic, during the winter season from February, 2008 until October, 2019. We selected data acquired under the clear sky condition without the influence of the moonlight by a sky condition judgment method (Ishii et al., SGEPSS2021) and derived the rotational line intensity of OH airglow (OH airglow intensity) and the rotational temperature for 12 years (from 2008 to 2019). We detected distinct intensity variations with various time scales; (1) a decadal scale that may be caused by the solar cycle, (2) seasonal intensity variations with a maximum around April and a minimum around the winter solstice, (3) relatively long-time scale events that lasted for several days and (4) relatively short-time scales of several tens of minutes to several hours. For the case (3), the rotational temperature also increased for several days. The case (4) is not like a wavy (sinusoidal) variation caused by atmospheric gravity waves often seen in the mid-latitude region, but asymmetric amplitudes of intensity variations were observed, with a sharp peak on the enhancement side.

The intensity of OH airglow is thought to be a fluctuation due to changes in atmospheric composition in the upper polar mesosphere associated with the energetic particle precipitation and the vertical transport of air masses with rich [O] from altitudes higher than the OH airglow layer. Therefore, we compared the peak altitude of the airglow layer, temperature distribution, and timing of the vertical transport enhancement with satellite data from TIMED/SABER, AURA/MLS. The results showed that the (1) ˜(3) variations can be generally understood by the supply of oxygen atoms associated with vertical transport to the OH layer. Regarding the variations (4), we focused on the relationship with auroral particles, which had been reported only once by Suzuki et al. (2009). We extracted energetic particle precipitation events from the cosmic noise absorption (CNA) data from the riometer observations at Syowa Station and conducted a superposed epoch analysis of OH airglow intensity for three hours before and after the events. As a result, the OH airglow intensity was observed to decay for about an hour after the events.

In this presentation, we will discuss the mechanisms of OH intensity variations detected over Syowa Station at various time scales and summarize the specific dynamics occurring in the upper polar mesosphere region.

南極昭和基地に設置された OH 大気光分光計は高度約 86 ㎞で発光する OH (8-4) バンドの観測により、直接観測が困難である極域上部中間圏領域の大気状態を 2008 年 2 月末より観測している。膨大な量の観測データの中から、雲や月の散乱光の影響を受けていない有効なデータのみを選別する手法（石井他, SGEPSS2021）により観測データを選別の上、約 12 年間（2008 年 2 月から 2019 年 10 月の夜間）の OH 分光データから OH 大気光の回転線強度（大気光強度）および、回転線強度比から算出される回転温度を導出した。その結果、（１）太陽活動に起因すると考えられる 10 年スケールの強度変動、（２）4 月ごろに極大、冬至ごろに極小をとる季節的な強度変動、（３）数日間増光が持続する比較的長い時間スケールのイベント、（４）数十分〜数時間程度の比較的短い時間スケールで OH 大気光強度が変動する特徴的なイベントをそれぞれ複数例検出した。（３）の数日スケールのイベントに関しては回転線強度が増加するとともに回転温度も数日間上昇していた。また、（４）の短時間スケールのイベントは中緯度帯でよく見られる大気重力波による波動的（正弦波的）な変動ではなく、強度変動の振幅が非対称であり、増光側に尖ったピークをもつ様子が観測されている。

OH 大気光の発光強度は高エネルギー粒子の降込みにともなう極域上部中間圏の大気組成変動や、OH 大気光層よりも高い高度から高い酸素原子濃度を有する空気塊が鉛直輸送されることによって変動すると考えられる。そこで、TIMED/SABER、AURA/MLS などの衛星データを用いて大気光層のピーク高度、温度分布、鉛直流強化のタイミングと比較した。その結果、上記変動のうち、（１）〜（３）の年々変動、季節変動、数日スケールの変動については、概ね鉛直下降流の強化による OH 層への酸素原子の供給により説明が可能であることが判明した。さらに、（４）の数十分スケールの OH 強度の変動は Suzuki et al. (2009) で 1 例のみ報告されていたオーロラ粒子降り込みとの関係に着目をした。昭和基地で実施されているリオメータ観測による銀河雑音吸収 (CNA) データから高エネルギー粒子降込みイベントを抽出し、その前後 3 時間の OH 大気光強度を積算・平均し、その変動を調査した。その結果、高エネルギー粒子の振り込みから数十分〜1 時間程度の間に OH 大気光が減光する様子が確認された。

本発表では、昭和基地上空で検出したこれら様々な時間スケールで発生する OH 大気光強度変動について、それぞれの発生メカニズムを考察し、極域上部中間圏領域で起こる特有のダイナミクスについて総括する。

R005-36
B 会場 ：11/5　PM2 （15:45-18:15）
16:30〜16:45

昭和基地 MF レーダーの流星エコー観測に基づく南極下部熱圏領域の大気重力波解析

#堤　雅基 [1)]
(1 極地研

Gravity wave analyses in the Antarctic lower thermosphere based on MF radar meteor observations at Syowa (69S)

#Masaki Tsutsumi[1)]
(1NIPR

MF (Middle Frequency) radars have long been used to measure wind velocity in mesosphere and lower thermosphere based on correlation analysis techniques [e.g., Reid, 2015]. The motion of atmosphere weakly ionized by solar insolation is measured in the technique. The ionized atmosphere is usually horizontally stratified, and radar echoes from such layered atmosphere are mostly obtained in the vertical direction. However, there also exist echoes coming back from large off-vertical angles. Meteor echoes are such type of echoes often detected at night (winter time in the polar region) mostly above 80 km. Because of the low radio frequency (2-3 MHz) the duration of MF radar meteor echoes is two orders longer than that of VHF meteor echoes. Thus, meteor echoes often dominate the MF radar echoes when the background atmospheric ionization is relatively low, and meteor winds can be estimated up to nearly 120 km altitude [Tsutsumi et al., 1999; 2001]. These meteor echoes have been used to compensate the known problem of MF radar correlation technique above about 90 km, and been applied to tidal wave and mean wind analyses at Syowa station (69S, 39E), Antarctic, since 1999 [Tsutsumi and Aso, 2005]. However, the time resolution of estimated winds has not necessarily been high enough for gravity wave studies, unfortunately.

We have recently redeveloped the MF radar meteor measurement technique and found that MF meteor winds are able to be estimated with time resolution of 1 hr or even much better resolution of 10 min under preferable ionosphere conditions. Combined with the conventional correlation analysis technique, we can now study gravity waves in a wide height range of 60-110 km. Seasonal and height variations of gravity wave energy are to be presented based on 20 years of reanalyzed meteor and correlation winds.

References

Tsutsumi, M., D. Holdsworth, T. Nakamura, and I. Reid (1999), Meteor observations with an MF radar, Earth Planets Space, 51, 691 – 699.

Tsutsumi, M., T. Aso, and M. Ejiri (2001), Initial results of Syowa MF radar observations in Antarctica, Adv. Polar Upper Atmos. Res., 15, 103 – 116.

Tsutsumi, M. and T. Aso (2005), MF radar observations of meteors and meteor-derived winds at Syowa (69_S, 39_E), Antarctica: A comparison with simultaneous spaced antenna winds, J. Geophys. Res., 110, doi:10.1029/2005JD005849

R005-37
B 会場 ：11/5　PM2 （15:45-18:15）
16:45〜17:00

#吉田　理人 [1)], 冨川　喜弘 [2)], 江尻　省 [2)], 高麗　正史 [3)], 佐藤　薫 [3)]
([1] 総研大・複合・極域,[2] 極地研,[3] 東大・理

Characteristics of inertia gravity waves over Syowa Station ~Comparison between the PANSY radar and the ERA5 reanalysis~

#Lihito Yoshida[1)], Yoshihiro Tomikawa[2)], Mitsumu K Ejiri[2)], Masashi Kohma[3)], Kaoru Sato[3)]
([1]Polar Science, SOKENDAI,[2]NIPR,[3]Graduate School of Science, Univ. of Tokyo

Gravity waves (GWs) are atmospheric waves whose restoring force is buoyancy. They are originated mainly from mountains, jet-front systems, and convection, and can modify a global wind structure through momentum transport and deposit. They do not only decelerate the upper part of the mesospheric jets, but also affect the horizontal winds in the lower stratosphere and contribute to driving the global meridional circulation. However, GW observations are not enough to verify their behaviour especially in the Antarctic, due to the harsh environment there. In addition, GWs have a wide range of horizontal wavelength (i.e., from several km to several thousand km) and period (i.e., from Brunt-Vaisala period (approximately 5 minutes) to inertial period (over 12 hours)), which makes it difficult to reproduce GWs in the entire frequency range even in the state-of-the-art atmospheric models in spite of the recent increase of the model resolution. In order to implement the effect of subgrid-scale phenomena into the models, which are not explicitly represented, GW parameterizations are introduced. In general, nonorographic GW parameterization assumes nearly constant wave sources and instantaneous upward propagation, but in reality, the wave sources are not constant and GWs propagate horizontally as well (Sato et al., 2009; Geller et al., 2013; Plougonven et al., 2020). Thus, it is required to constrain the GW effect in the models based on observations which cover the whole frequency range of GWs and estimate the GW momentum transport in the Antarctic.

Intermittency, a measure of how transient or intermittent a GW event is, has recently received much attention. Even if the total amount of momentum flux is the same, continuous, small amplitude events deposit momentum to higher altitudes, while sporadic and large amplitude events deposit momentum to lower altitudes. As a result, the structure and strength of the driven meridional circulation depend on the GW intermittency (Hertzog et al., 2008). In Antarctica, intermittency has been studied using super pressure balloons (Hertzog et al., 2012) and the Program of the Antarctic Syowa MST/IS radar (PANSY radar) at Syowa Station (Minamihara et al., 2020), suggesting differences in the characteristics of intermittency due to different wave generation mechanisms and wave filtering.

Our purpose of this study is to investigate the characteristics of sporadic and large amplitude GW events that can have a large impact on the overall momentum transport, and also to investigate how well the reanalysis data reproduces the GW events in the Antarctic. We used the PANSY radar for the observation data and the ERA5 reanalysis for the reanalysis data. The PANSY radar, which was installed at Syowa Station (69S,40E) in 2011, observes vertical profiles of three-dimensional winds in the troposphere and lower stratosphere with high accuracy and fine temporal and vertical resolution (Sato et al., 2014). It is the only instrument in the Antarctic that enables us to capture GWs in the almost entire frequency range. The ERA5 reanalysis is the latest meteorological reanalysis dataset provided by the European Centre for Medium-Range Weather Forecasts. The ERA5 data is distributed at 137 vertical levels from the surface to 0.01 hPa with a horizontal spacing of 0.25 degree every 1 hour.

We use three dimensional winds of the PANSY radar and the ERA5 reanalysis during the period of October 2015 to September 2016, in which the PANSY radar was continuously operated (Minamihara et al.,2018). The inertia-GWs are extracted by applying a bandpass filter with a cutoff period of 4-24 h and a cutoff vertical wavelength of 0.8-8 km. As a result, we found many similar wave-like structures between the PANSY radar and the ERA5 reanalysis. In order to examine the propagation characteristics of inertia-GWs, we use a hodograph analysis. It utilizes the feature that the hodograph (i.e., vertical change of the horizontal wind vector drawn in the zonal and meridional wind space) becomes an ellipse, in which the amplitude, intrinsic period, vertical wavelength, phase velocity, and group velocity of GWs can be estimated. Although the hodograph analysis generally has an ambiguity of horizontal propagation direction by 180, we exclude it by covariance of major axis amplitude $u_{jj}$and vertical wind w and vertical wave number m (Minamihara et al.,2018). Since the GWs are assumed to be quasi-monochromatic in the hodograph analysis, three dimensional winds are separated into components with upward and downward phase velocities by a two-dimensional Fourier transform. This procedure makes it possible to extract quasi-monochromatic GW events that were previously impossible to extract.

The results of the hodograph analysis show that the inertial period and the direction of the horizontal wavenumber vector are correlated. On the other hand, vertical and horizontal wavelengths were found to be overestimated by ERA5. We also plan to discuss altitude variations in the reproducibility of momentum fluxes.

R005-38
B 会場 ：11/5　PM2 （15:45-18:15）
17:00〜17:15

2018 年 12 月の成層圏突然昇温と準 4 日波の鉛直伝播について

#武田　大輝 [1)], 三好　勉信 [2)]
([1] 九大・理・地球惑星,[(2] 九大・理・地球惑星

Study of vertical propagation of quasi-four-day waves during the December 2018 SSW event

#Hiroki Takeda[1)], Yasunobu Miyoshi[2)]
([1]Dept. Earth & Planetary Sci, Kyushu Univ.,[(2]Dept. Earth & Planetary Sci, Kyushu Univ.

Sudden stratospheric warming (SSW) is a large scale meteorological event occurring mostly in the stratosphere during the northern hemisphere winter. During the SSW event in late December 2018, using meteor-radar in china and AURA/MLS satellite observations, Ma et al (2019) pointed out that the quasi 4-day wave (Q4DW), which is a westward moving wave with the zonal wavenumber 2 was excited in the 50-60 km height region, and propagated into the upper mesosphere However, it is not clear that the global structure of the Q4DW and its impact on the general circulation in the mesosphere and lower thermosphere (MLT). In this study, using an atmosphere-ionosphere coupled model (GAIA), we investigate the vertical and latitudinal propagations of the Q4DW during the 2018 SSW event. using a Fourier transform and band-pass filter with 3.0-5.0day window were applied to extract the Q4DW. Our results indicate that the Q4DW amplitude after the SSW event has maxima at 20N and 100km height (8 m/s) and at 20S and 110 km height (6 m/s). This means that the Q4DW propagates from the stratosphere in the Arctic region to the lower thermosphere in the southern hemisphere. Detailed analysis and discussions concerning traveling planetary waves during SSW events will be shown.

成層圏突然昇温（SSW）は冬季の成層圏において発生する大規模な気象現象である。2018 年 12 月下旬に発生した SSW では、Ma et al(2019) では、中国における流星レーダ観測および AURA/MLS による観測結果から、SSW の発生時に東西波数 2 の西向き準 4 日波が高度約 50〜60km で励起され上方へ伝播していることが指摘されている。観測結果だけでは限られた範囲の 4 日波の構造しか明らかにすることはできず、準 4 日波が地球の大気循環に与える影響やより上方の下部熱圏への伝播や低緯度域や反対半球への伝播は不明瞭である。そこで本研究では、全大気圏-電離圏結合モデル（GAIA）を用いることで、SSW 時の成層圏から中間圏・下部熱圏への準 4 日波の伝播について明らかにすることを目的とした。方法として、GAIA モデルのシミュレーション結果をもとにフーリエ変換やバンドパスフィルタを用いて東西波数 2 の 3-5 日周期成分を抽出した。その結果、SSW 発生時での準 4 日波の振幅は高度約５０ km の北緯 75 度付近で、極大（最大値 10m/s）となっており、準 4 日波を再現することができた。SSW 発生から数日経過すると準 4 日波の振幅は高度 100km 付近、北緯 20 度付近（最大値 8m/s）でもみられるようになった。また、南半球の下部熱圏領域でも、準 4 日波の振幅の極大（最大値 6m/s）がみられた。これらの結果より、準 4 日波の振幅の極大域が SSW の発生に伴って下部熱圏領域や低緯度側・反対半球側へと伝播していることが分かった。今後は、他の SSW 発生時に励起された惑星波の解析を行うことで、SSW 時における惑星波の励起や伝播ついての議論を深めていきたい。

R005-39
B 会場 ：11/5　PM2 （15:45-18:15）
17:15〜17:30

#Liu　Huixin[1)], 木暮　優 [2)], 陣　英克 [3)]
[(1] 九大・理・地惑,[(2] 九大・理・地惑,[(3] 情報通信研究機構

DW1 Tidal Enhancements in the Equatorial MLT During 2015 El Nino: The Relative Role of Tidal Heating and Propagation

#Huixin Liu[1)], Masaru Kogure[2)], Hidekatsu Jin[3)]
[(1]Kyushu Uni.,[(2]Kyushu University,[(3]NICT

Ground-based and satellite observations have shown that the tidal component DW1 in
the equatorial mesosphere and lower thermosphere (MLT) was enhanced in July − October 2015, which was an intense El Nino year. This enhancement is reproduced in the 21 years reanalysis-driven model simulation by the Ground-to-topside model of Atmosphere and Ionosphere for Aeronomy (GAIA). Our analysis shows the (1,1) Hough mode dominates this tidal enhancement, and its peak amplitude was 74% higher than that under neutral (non-ENSO) conditions at 90 km. The corresponding tidal heating was found to increase by 5%, which can explain 7% of the (1,1) enhancement. To explain the remaining enhancement, we quantitively examined the upward propagation condition by calculating the vertical wavenumber and the latitudinal shear of the zonal wind. The analysis reveals that the vertical wavenumber between 18 and 60 km was one standard deviation smaller than that under neutral conditions. The latitudinal zonal wind shear also decreased in 18 − 30 km. These results suggest smaller dissipation and damping of the (1,1) mode during its upward propagation, which dominantly contributed to the tidal enhancement at 90 km altitude. This decrease in the vertical wavenumber and the wind shear can be reasonably explained by the eastward phase of the quasi-biennial oscillation (QBO) in the lower stratosphere. This study suggests that the overlapping of the 2015 El Nino with the eastward phase of the QBO induced the large enhancement of the DW1.

R005-40
B 会場 ：11/5　PM2 （15:45-18:15）
17:30〜17:45

木暮　優 [1)],#Liu　Huixin[1)], 陣　英克 [2)]
[(1 九大・理・地惑,(2 情報通信研究機構

DW2 tide enhanced by equatorial tropospheric ozone variation due to El Nino.

#Masaru Kogure[1)], Huixin Liu[1)], Hidekatsu Jin[2)]
[(1Kyushu University,(2NICT

Thermal tides transport their energy and momentum vertically from the lower to the upper atmosphere. Thermal tides also drive a neutral wind in the E-region, causing the geomagnetic solar quiet variation. One of primary tidal sources is atmospheric heating (i.e., atmospheric absorption of solar radiative and latent heating) strongly affected by the meteorological phenomenon (Chapman & Lindzen, 1970). Water vapor and rainfall are primary sources of atmospheric heating in the equatorial region and are strongly modulated by El Nino. Some studies have shown the impacts of the El Nino modulation on tides via the water vapor and rainfall modulation (Lieberman et al., 2007; Liu et al., 2017; Pedatella and Liu, 2012; Kogure et al., 2021).

On the other hand, ozone also absorbs solar radiative heating and generates tides. While ozone is well known as a primary heat source and tidal source in the stratosphere(Chapman and Lindzen, 1970), tropospheric ozone is well known as one of the greenhouse gases, as well (IPCC, 2013; Cooper et al., 2014). El Nino modulates a longitudinal variation of tropospheric ozone over the equatorial region, which possibly influences tidal activity in the mesosphere and lower thermosphere (MLT).

To investigate the impact of the ozone variation on equatorial tides, we performed two simulations by using the GAIA model (Ground-to-topside Atmosphere Ionosphere model for Aeronomy)(Jin et al., 2012) from September 2006 to 2007 March (El Nino phase). An ozone variation in run1 is prescribed as zonally symmetric values while that in run2 is prescribed as an El Nino pattern (based on Omen et al., 2013), i.e., positive anomaly (26% at maximum) in 50-120degreeE and negative anomaly (11% at maximum) in 120-300degreeE between 7 and 17 km altitudes (its maximum at 12 km). Both zonal mean values are the same.

We compared both tidal amplitudes and found, in run2, an increase in DW2 (diurnal tide with wavenumber 2) up to ˜0.3 K (˜1 m/s) at 100 km altitude. We decomposed the DW2 temperature perturbation into Hough mode functions, and this DW2 enhancement is attributed to the first symmetric propagation mode. Also, the enhancement of the first symmetric mode was found between the troposphere and MLT, suggesting the enhancement of the DW2 in the troposphere propagates into the MLT. Therefore, our results suggest that the ozone El Nino pattern in the troposphere strengthens the DW2, which propagates into the MLT. This presentation will show those results and discuss a dynamical mechanism of the DW2 enhancement.

R005-P01
ポスター 3 ：11/6　AM1/AM2 （9:00-12:30）

複数波長のオーロラ画像を用いたオーロラコンピュータトモグラフィ解析手法の開発と評価

#吹澤　瑞貴 [1)], 田中　良昌 [2)], 小川　泰信 [2)], 細川　敬祐 [3)],Kauristie Kirsti[4)],Raita Tero[5)]
([1] 極地研,[2] 国立極地研究所/ROIS-DS/総研大,[3] 電通大,[4] フィンランド気象研究所,[5] オウル大学ソダンキラ地球物理観測所

Development and evaluation of Aurora Computer Tomography using multiple wavelength auroral images

#Mizuki Fukizawa[1)], Yoshimasa Tanaka[2)], Yasunobu Ogawa[2)], Keisuke Hosokawa[3)], Kirsti Kauristie[4)], Tero Raita[5)]
([1]NIPR,[2]NIPR/ROIS-DS/SOKENDAI,[3]UEC,[4]Finnish Meteorological Institute,[5]Sodankyla Geophysical Observatory, University of Oulu

Auroral computer tomography (ACT) is a method for reconstructing the three-dimensional structure of auroral emission intensity and the two-dimensional distribution of precipitating electrons from auroral images at a single wavelength observed by cameras installed at multiple locations on the ground. The method we have developed has used only auroral images of nitrogen molecular ion emission at 427.8 nm wavelength. Since the peak altitude of auroral emission varies with wavelength, the emission intensity ratio between different wavelengths contains information on the characteristic energy of the precipitating electron flux. Sharp structures will also be reconstructed using brighter auroral emission images. Therefore, ACT using auroral images at multiple wavelengths can provide more reliable reconstruction results.

In this study, auroral images of oxygen atom emission at wavelengths of 557.7 nm were incorporated into the ACT analysis method using the GLOW model. The auroral emission intensity at 557.7 nm is several times brighter than that at 427.8 nm. We used auroral images at 427.8 nm obtained from Abisko (geographic latitude (glat): 68.36, geographic longitude (glon): 18.82), Kilpisjarvi (glat: 69.05, glon: 20.78), and Skibotn (glat: 69.35, glon: 20.36) and those at 557.7 nm from Kilpisjarvi, Skibotn, and Tromso (glat: 69.58, glon: 19.23). The relative sensitivities between the six images were determined by the five-fold cross-validation method. The golden segmentation method was implemented to reduce the computational cost, whereas a trial-and-error method was previously used to narrow the search area by a grid search method. Using this newly developed ACT with multi-wavelength images, we plan to reconstruct the 3D distribution of emission intensity of discrete and pulsating auroras and show the dependence of the upper and lower limits and peak altitudes of auroral emission on auroral morphology and magnetic local time.

オーロラコンピュータトモグラフィ（ACT）は、地上多地点に設置されたカメラによって観測された単一波長のオーロラ画像からオーロラ発光強度の 3 次元構造や降下電子の 2 次元分布を再構成する手法である。これまで我々が開発してきた手法は、波長 427.8 nm の窒素分子イオン発光のオーロラ画像のみを使用してきた。オーロラ発光のピーク高度は波長によって異なるため、異なる波長間の発光強度比は降下電子フラックスの特性エネルギーの情報を含む。また、波長によって発光強度が異なるため、より明るい波長のオーロラ画像を使用することで、シャープな構造を再現できることが期待される。したがって、複数波長のオーロラ画像を用いて ACT を行うことで、より信頼性のある再構成結果を得ることができる。

本研究では、GLOW モデルを用いることで、波長 427.8 nm のオーロラ発光よりも数倍明るい発光強度を持つ波長 557.7 nm の酸素原子発光のオーロラ画像を ACT 解析手法に組み込んだ。427.8 nm の画像は Abisko (68.36° N、18.82° E)、Kilpisjarvi (69.05° N、20.78° E)、Skibotn (69.35° N、20.36° E)、557.7 nm の画像は Kilpisjärvi、Skibotn、Tsomsø (69.58° N、19.23° E) に設置された全天カメラで取得されたオーロラ画像を使用した。6 枚の画像間の相対感度を 5 分割の交差検証により決定した。これまではグリッドサーチにより探査範囲を随時狭めていくトライアンドエラー法を用いていたが、計算コストを下げるために黄金分割法を実装した。今後は、この新たに開発した多波長画像を使用した ACT を用いて、ディスクリートオーロラや脈動オーロラなどの発光強度 3 次元分布を再構成し、オーロラ発光の上限・下限・ピーク高度のオーロラ形態の依存性や磁気地方時依存性などを調査した結果を示す予定である。

R005-P02
ポスター 3 ：11/6　AM1/AM2 （9:00-12:30）

南極昭和基地大型大気レーダーによる電離圏沿磁力線不規則構造のイメージング観測

#香川　大輔 [1)], 橋本　大志 [2)], 齊藤　昭則 [3)], 西村　耕司 [4)], 堤　雅基 [2)], 佐藤　亨 [5)], 佐藤　薫 [6)]
([1] 京大・理,[2] 極地研,[3] 京都大・理・地球物理,[4] 京都大・生存圏研究所,[5] 京大・国際高等教育院,[6] 東大・理

Imaging Observation of Ionospheric Field Aligned Irregularities by the PANSY radar at Antarctic Syowa Station

#Daisuke Kagawa[1)], Taishi Hashimoto[2)], Akinori Saito[3)], Koji Nishimura[4)], Masaki Tsutsumi[2)], Toru Sato[5)], Kaoru Sato[6)]
([1]Kyoto univ.,[2]NIPR,[3]Dept. of Geophysics, Kyoto Univ.,[4]RISH, Kyoto Univ.,[5]ILAS, Kyoto Univ.,[6]Graduate School of Science, Univ. of Tokyo

Program of Antarctic Syowa MST/IS radar (PANSY radar) is the large atmospheric and VHF-band radar located at the Antarctic Syowa Station. This radar has the capability of observing plasma quantities at altitudes of 100-500km using the ionospheric incoherent scatter (IS). In 2015, the PANSY radar performed the first ionospheric IS observation in the Antarctica.This radar also has a frequency of 47MHz, so it can observe the echoes of field aligned irregularities (FAIs) in E-region. If FAIs have a space scale of half wavelength of radio waves, they are coherently backscattered, so the PANSY radar observes the coherent echoes from 3-meter-scale FAIs in E-region. In order to suppress contamination from the FAI echoes during the IS observation, Hashimoto et al.(2019) separated the FAI echoes from IS echoes by the multichannel signal processing technique using the antenna array for observing FAIs (”FAI array”). On the other hand, if we utilize this method to observe FAIs, we can resolve E-region FAIs in detail and measure their motion.

In this research, we conduct the experimental observation of E-region FAIs in 19th November 2021. In this experiment, we transmitted the radio waves using the FAI array and received the FAI echoes using the meteor array installed for observing the meteor. The FAI array has the degree of freedom only of azimuth angles, whereas the meteor array can observe FAIs three-dimensionally because the five antennas of the meteor array are positioned areally. First, FAI imaging was performed using the Capon method for FAIs observed in this experiment, but it was found that the Capon imaging cannot accurately measure the spatial structures caused by the antenna pattern. FAI echoes are generally observed if the conditions that radio waves are perpendicular to FAI are satisfied. The grating lobes, however, are generated because the distance of adjacent antenna are wide, so it was considered that the ”ghosts” were also mistakenly generated in the non-echoing region. Therefore, due to remove their effects and provide the accurate spatial structure, we conducted deconvolution based on the CLEAN algorithm. In this algorithm, we subtract the transmit pattern of the FAI array and receive pattern of the meteor array in each iteration. This algorithm makes smaller the responses of the non-mainlobe region, such as grating lobes and sidelobes, because the antenna pattern are subtracted, so we can suppress the ”ghosts” and conduct high-resolution FAI imaging observation.

In this presentation, we will introduce the result of application of imaging method based on the CLEAN algorithm which can remove the effects of the antenna pattern and conduct accurate and high-resolution FAI observation. Also, we try to find out physical processes of FAI generation and the spatial structure of FAIs.

南極昭和基地大型大気レーダー (PANSY レーダー) は、南極の昭和基地に設置されている大型 VHF 帯大気レーダーである。本レーダーは電離圏非干渉性散乱 (IS) を用いて地表 100km から 500km におけるプラズマ物理量を観測することが可能であり、2015 年には南極で初となる電離圏 IS 観測が開始された。また、47MHz の周波数を用いているため、E 領域における沿磁力線不規則構造 (Field Aligned Irregularity; FAI) エコーの観測も可能である。FAI がレーダー電波の半波長の空間スケールを持つとき、電波をコヒーレントに散乱するため、PANSY レーダーでは約 3m スケールの E 領域 FAI からのコヒーレント・エコーを観測できる。Hashimoto et al.(2019) では、この FAI エコーの混入による IS 観測への干渉を除去するため、PANSY レーダーに備えられた FAI 受信用アンテナアレイ（以下、FAI アレイ）を用いた多チャンネル信号処理技術により、異なる角度からの信号（IS エコーと FAI エコー）を分離した。一方、FAI の観測に主眼を置いて同様の手法を用いれば、E 領域 FAI を詳細に解像し、その運動を観測することが可能である。

そこで本研究では、2021 年 11 月 19 日に E 領域 FAI の観測実験を行った。本実験では FAI アレイを用いて電波の送信を行い、流星観測用に設置されている流星アレイを用いて FAI からの反射波の受信を行った。FAI アレイは直線状に配置されているため自由度は方位角方向にしか持たないのに対し、流星アレイは 5 本のアンテナが面的に配置されているため、流星アレイを用いることで FAI の立体的な位置情報を得ることができる。まず、本実験で観測された FAI に対し Capon 法を用いてイメージングを行ったところ、空間構造にアンテナパターンに起因する角度の不確定性が発生した。本来、FAI はレーダー電波と地磁気の磁力線が直交するところで観測されるはずである。しかし、流星アレイのアンテナ間隔が大きいためにグレーティングローブを生じ、これによってそれ以外の方位にも偽像が生じたと考えられた。そこで、その影響を除去し真の空間構造を推定するために、本観測では CLEAN アルゴリズムに基づいたデコンボリューショ

ン処理を行った。本アルゴリズムでは、毎回のイタレーション処理において、FAI アレイの送信パターンと流星アレイの受信パターンを組み合わせたパターンを差し引いている。これにより、グレーティングローブやサイドローブといったメインローブ以外の領域でもアンテナパターンが考慮されて自動的に応答値が小さくなるため、偽像を抑えつつ高分解能な FAI のイメージング観測が可能となる。

本発表では、アンテナの放射パターンの影響を除去し FAI の正確かつ高分解能に観測できる、CLEAN アルゴリズムに基づいたイメージング手法の適用結果を紹介する。また、これによって得られたイメージから、FAI 発生の物理過程および空間構造の解明を試みる。

R005-P03
ポスター 3 ：11/6　AM1/AM2 （9:00-12:30）

#行松　彰 [1)]
[(1] 国立極地研究所/総研大

SENSU SuperDARN - progress in Japanese Antarctic Research Project Phase X

#Akira Sessai Yukimatu[1)]
[(1]NIPR/SOKENDAI

A new phase-X 6-year Japanese Antarctic Research Expedition (JARE) project (2022-2028, JARE64-69) started this spring, including Prioritised Research Projects (PRPs) and long-term monitoring observation. SENSU SuperDARN Syowa radars observation operated by NIPR has become an essential long-term scientific monitoring observational research since this phase X JARE project for long-term stable contribution to broader coverage of magnetospheric, ionospheric and upper atmospheric research and applications, which can also contribute to the PRP particularly on space weather and space climate research - “Aurora Xcosmic” project proposed by Kataoka et al. Their proposal tries to reveal the impact of high energy particles on the Earth’s atmosphere with cosmic ray observations and new spectral riometers, etc. and also to understand the geospace environment quantitatively under a lower solar activity where polar cap region observation, such as optical imager network in Antarctica, is essential and important for understanding and predicting geospace under recently started lower solar activity condition after about a half-century long high solar activity period in collaboration with theoretical and simulation studies. In the proposal, SuperDARN is characterised as one of the important tools to provide the global ionospheric condition to contribute to the research. We will discuss mid- to long-range tangible and realistic scientific strategy of SENSU/SuperDARN research including the PRP on space weather/climate and required/desired technical improvement for more stable, near-maintenance-free and more flexible and advanced operation including upgrading antennae and transmitters and imaging capability during JARE phase X period and future, as well as progress so far for coming JARE 64 for 2023 observation.

R005-P04
ポスター 3 ：11/6　AM1/AM2 （9:00-12:30）

#浅村　和史[1)], 滑川　拓[2)], 横田　勝一郎[3)], 小嶋　浩嗣[4)], 栗田　怜[5)], 頭師　孝拓[6)], 石坂　圭吾[7)], 熊本　篤志[8)], 松岡　彩子[9)], 野村　麗子[10)], 齋藤　義文[11)]
([1 宇宙研,([2 東大・理・地惑,([3 大阪大,([4 京大・生存圏,([5 京都大学 生存研,([6 奈良高専,([7 富山県大・工,([8 東北大・理・惑星プラズマ大気,([9 京都大学,([10JAXA,([11 宇宙研

Supra-thermal ions observed by TSA/IMS onboard the SS520-3 sounding rocket

#Kazushi Asamura[1)], Taku Namekawa[2)], Shoichiro Yokota[3)], Hirotsugu Kojima[4)], Satoshi Kurita[5)], Takahiro Zushi[6)], Keigo Ishisaka[7)], Atsushi Kumamoto[8)], Ayako Matsuoka[9)], Reiko Nomura[10)], Yoshifumi Saito[11)]
([1ISAS/JAXA,([2Earth and Planetary Science, Tokyo Univ.,([3Osaka Univ.,([4RISH, Kyoto Univ.,([5RISH, Kyoto Univ.,([6National Institute of Technology , Nara Col,([7Toyama Pref. Univ.,([8Planet. Plasma Atmos. Res. Cent., Tohoku Univ.,([9Kyoto University,([10JAXA,([11ISAS

On November 4th, 2021, the SS520-3 sounding rocket was launched from Ny Alesund, Spitsbergen, Norway during a severe geomagnetic storm. The main objective of the SS520-3 mission is to reveal ion acceleration mechanisms as a source of ion outflow in the magnetospheric cusp region. It was confirmed that the rocket passed through the cusp region based on the observations of low-energy ions. Two ion energy-mass spectrometers were installed onboard SS520-3. One is Thermal and Supra-thermal ion energy-mass Analyzer (TSA), and the other is low-energy Ion energy-Mass Spectrometer (IMS). These two instruments jointly observe ions with energies from $<$1eV/q up to 20 keV/q with species identification, which covers higher-energy component of accelerated ions in the polar ionosphere. During the flight, TSA/IMS successfully observed cusp ion precipitations which are continuously detected. On the other hand, upgoing ion flux were minor, but weak flux enhancement was observed with energies from 1 to 10 keV/q in perpendicular direction throughout the flight. It might be an indication of the upflowing ions, since they are considered to be accelerated in the perpendicular direction by wave-particle interactions. We will report on the observations and the initial results regarding TSA/IMS.

R005-P05
ポスター 3 ：11/6　AM1/AM2 （9:00-12:30）

SS-520-3 号機観測ロケット搭載 LEP による極域カスプでのイオン電子の観測

#横田　勝一郎 [1)], 齋藤　義文 [2)], 浅村　和史 [3)], 松岡　彩子 [4)], 野村　麗子 [5)]
([1] 大阪大,[2] 宇宙研,[3] 宇宙研,[4] 京都大学,[5] 宇宙航空研究開発機構

Observation of low-energy electrons and ions by LEP on the SS520-3 sounding rocket

#Shoichiro Yokota[1)], Yoshifumi Saito[2)], Kazushi Asamura[3)], Ayako Matsuoka[4)], Reiko Nomura[5)]
([1]Osaka Univ.,[2]ISAS,[3]ISAS/JAXA,[4]Kyoto University,[5]JAXA

The phenomenon of accelerated upper-atmospheric outflow is universal not only for the Earth but also for other terrestrial planets. Elucidating the physical mechanisms is important for understanding and predicting the atmospheric evolution that leads to the diversity of planetary atmospheres, and its scientific significance is not limited to the planets of the solar system. Scientific observations to verify theoretical studies are essential to elucidate the acceleration and outflow mechanisms of the upper atmosphere, and the Earth's upper atmosphere is the most easily observable target.

The SS520-3 rocket was launched from Ny-Alesund on November 4, 2021 to observe the acceleration and heating of outflowing ions at the top of the ionosphere in the polar cusp region. The low-energy particle instrument (LEP) was installed along with magnetic and electric field sensors as observation equipment.

LEP contains a pair of sensors that analyze the energy of electrons and ions below 10 keV. The two sensors are completely identical, and both measure secondary electrons emitted from ultra-thin carbon foil when incident electrons and ions pass though it. Therefore, the uniqueness of LEP is that two sensors use detectors (MCPs) for electrons. This means that a single tophat-type electrostatic analyzer can be used for both ions and electrons if the polarity of the high-voltage power supply connected to the spherical electrode can be changed. An example of use is when resources are limited in deep space exploration where plasma observation is not the main purpose. For LEP, the SS520-3 rocket experiment was an opportunity not only to conduct scientific research through observation, but also to prove this new technology.

The SS-520-3 sounding rocket has observed the precipitation of accelerated electron and decelerated ion, which are considered to be the characteristics of polar cusp. We will report the LEP observation results.

超高層大気の加速・流出現象は, 地球に限らず地球型惑星にとって普遍的な現象である. その物理機構を解明することは惑星大気の多様性をもたらす大気進化を理解・予測する上で重要であり, その科学的意義は太陽系の惑星に留まらない。この超高層大気の加速・流出機構の解明には理論研究を検証する科学観測が必須であり, 地球の超高層大気が最も観測が容易な対象である.

地球カスプ上空電離層最上部における流出イオンの加速・加熱の現場を観測することを目的に、SS520-3 ロケットが 2021 年 11 月 4 日に Ny-Alesund から打ち上げられた。 観測装置として磁場・電場センサーと共に低エネルギー粒子計測器 (LEP) も搭載されている.

低エネルギー粒子計測器は 10 keV 以下のイオンと電子のエネルギー分析を行う一対の分析器である. 二つの分析器は完全に同一の形状であり、どちらも入射する電子とイオンを超薄膜カーボンに通過させて, そこから放出される二次電子を計測する。従って、検出器（MCP）は両者とも電子用のものが用いられているのが LEP の特徴である. この特徴は, 球殻電極に接続する高圧電源の極性を変更することが出来れば, たった一つの TOPHAT 型静電分析器がイオン用とも電子用ともなることを意味する. 利用例としては, プラズマ観測を主目的としない深宇宙探査においてリソースが限られる場合などが挙げられる. LEP にとっては、SS520-3 号機観測ロケット実験は観測による科学研究だけでなく, この新技術の立証の機会となった.

SS-520-3 号機観測ロケット実験によって、極域カスプの特徴とされる加速された電子降下や, 減速されたイオン降下などが観測されたので、ここに報告する.

R005-P06
ポスター 3 ：11/6　AM1/AM2 （9:00-12:30）

#熊本　篤志 [1)], 小嶋　浩嗣 [2)], 石坂　圭吾 [3)], 頭師　孝拓 [4)], 栗田　怜 [2)], 加藤　雄人 [1)], 阿部　琢美 [5)], 齋藤　義文 [5)]
([1] 東北大・理・地球物理,[2] 京大・生存圏,[3] 富山県大・工,[4] 奈良高専,[5] ＪＡＸＡ宇宙科学研究所,[6] 東北大・理・地球物理,[7] ＪＡＸＡ宇宙科学研究所,[8] 宇宙研

Lower hybrid resonance (LHR) frequency measurements in the ionosphere by SS-520-3 NEI/PWM

#Atsushi Kumamoto[1)], Hirotsugu Kojima[2)], Keigo Ishisaka[3)], Takahiro Zushi[4)], Satoshi Kurita[2)], Yuto Katoh[1)], Takumi Abe[5)], Yoshifumi Saito[5)]
([1]Dept. Geophys, Tohoku Univ.,[2]RISH, Kyoto Univ.,[3]Toyama Pref. Univ.,[4]National Institute of Technology , Nara Col,[5]ISAS/JAXA,[6]Dept. Geophys., Grad. Sch. Sci., Tohoku Univ.,[7]ISAS/JAXA,[8]ISAS

The lower hybrid resonance (LHR) frequency in the ionosphere has been measured by NEI/PWM (Number density of Electron measurement by Impedance probe/Plasma Wave Monitor) onboard the Sounding Rocket SS-520-3. SS-520-3 was launched from Svalbard on Nov. 4, 2021 to perform observations of the ion acceleration and heating processes in the cusp region. The NEI/PWM was successfully operated during the flight and background electron number density and plasma wave spectrogram along the rocket trajectory were obtained. In addition, NEI/PWM was designed to measure the probe capacitance Cp not only in a frequency range around upper hybrid resonance (UHR) frequency (0.1 to 20 MHz) but also in a frequency range around LHR frequency (5 to 11 kHz) in order to estimate ion composition in the ionosphere.

As shown by Balmain [1964], the impedance of short dipole antenna in a plasma around UHR frequency can be derived using the dielectric tensor with terms of electron. The probe impedance in a plasma around LHR frequency also can be derived using the dielectric tensor with terms of electron and ion. It is expected that a pair of minimum and maximum is once found around LHR frequency in each frequency sweep of the probe capacitance measurement. In the observation, such frequency profile was found only when the probe is in the wake. In addition, the frequency profile was found multiple times in one frequency sweep. They were beyond our expectations.

We consider that they are explained as follows: On the basis of the probe capacitance model mentioned above, the frequency profile of the probe capacitance at LHR becomes unclear when the electron collision frequency is higher than 300 Hz. The electron collision frequency depends on the electron temperature and ion number density [Nicolet, 1953]. If assuming that the electron temperature is 1500 K [Kitamura et al., 2011], and ion number density is $4x10^5$ /cc (from electron number density measured by NEI) around the apex of SS-520-3, the electron collision frequency is estimated as 350 Hz. In the wake, the electron temperature is higher and the ion number density is lower than those outside of the wake, and the frequency profile at LHR is unclear. If the ion number in the wake is $2x10^5$ /cc, the electron collision frequency is less than 170 Hz and the frequency profile at LHR becomes clear. Since the ion thermal velocity (~0.9 km/s) is less than the velocity of the rocket (3 km/s), it is considered that the ion wake with a length of 0.9 m is formed and fluttered. It would be why the frequency profile are found multiple times in one frequency sweep. If we can consider that they are frequency profiles around LHR frequency, the LHR frequency at an altitude around 700 km is estimated as 7 to 9 kHz, which suggests ion composition with O+ of 90% and H+ of 10 %.

R005-P07
ポスター 3 ：11/6　AM1/AM2 （9:00-12:30）

#栗田　怜[1)], 小嶋　浩嗣[1)], 頭師　孝拓[2)], 石坂　圭吾[3)], 熊本　篤志[5)], 浅村　和史[4)], 笠原　禎也[6)], 尾崎　光紀[6)], 松岡　彩子[7)], 野村　麗子[4)], 横田　勝一郎[8)], 阿部　琢美[4)], 細川　敬祐[9)], 小川　泰信[10)], 齋藤　義文[4)]
([1] 京大・生存圏,([2] 奈良高専,([3] 富山県大・工,([4] 宇宙研,([5] 東北大・理・地球物理,([6] 金沢大,([7] 京都大学,([8] 大阪大,([9] 電通大,([10] 極地研,([11] 極地研,([12],([13] 電通大,([14] 極地研,([15] 宇宙研

Broadband electric field fluctuations observed by LFAS/WFC onboard the SS-520-3 sounding rocket

#Satoshi Kurita[1)], Hirotsugu Kojima[1)], Takahiro Zushi[2)], Keigo Ishisaka[3)], Atsushi Kumamoto[5)], Kazushi Asamura[4)], Yoshiya Kasahara[6)], Mitsunori Ozaki[6)], Ayako Matsuoka[7)], Reiko Nomura[4)], Shoichiro Yokota[8)], Takumi Abe[4)], Keisuke Hosokawa[9)], Yasunobu Ogawa[10)], Yoshifumi Saito[4)]
([1]RISH, Kyoto Univ.,([2]National Institute of Technology , Nara Col,([3]Toyama Pref. Univ.,([4]ISAS/JAXA,([5]Dept. Geophys, Tohoku Univ.,([6]Kanazawa Univ.,([7]Kyoto University,([8]Osaka Univ.,([9]UEC,([10]NIPR,([11]NIPR,([12]I,([13]UEC,([14]NIPR,([15]ISAS

The SS-520-3 sounding rocket campaign is planned to investigate the escape of ionospheric ions from the cusp region. It has been suggested that the ion escape is originated from the ion acceleration/heating by plasma waves in the direction perpendicular to the ambient magnetic field. The broadband extremely-low-frequency (BBELF) waves have been proposed as a candidate to cause the ion acceleration/heating. The SS-520-3 sounding rocket is equipped with instruments to measure plasma and electromagnetic fields to reveal the mechanism for the ion acceleration/heating by plasma waves. Low-Frequency wave Analyzer System (LFAS) is developed to measure the BBELF waves during the flight of the sounding rocket. LFAS consists of two pairs of dipole electric field sensors in the rocket spin plane and two different receivers which cover the different frequency ranges. WaveForm Capture (WFC) measures electric fields in the frequency range from 10 Hz to 10 kHz with a sampling rate of 40 kHz. Because of the telemetry limitation, waveforms of two dipole sensors are available for 300 seconds. The data acquisition is programmed to start 330 seconds after the launch of the rocket so that the observation covers well near the apex height, where the BBELF waves are expected to be present.

The sounding rocket was launched at 10:09:25 UT on 4th November 2021 during a severe geomagnetic storm, reaching its apex height of 742 km at 489 seconds after the launch. Two electric field waveforms were successfully obtained by WFC for 300 seconds although the failure of the electric field sensor extension results in the orthogonal monopole sensor configuration. Analysis of the waveforms obtained by WFC shows that broadband electric field fluctuations are observed after the rocket reaches the apex height. The waveforms of the fluctuations are quite similar to those of BBELF previously reported [Wahlund+, 1998]. Utilizing the orthogonal monopole configuration, the interferometry technique can be applied to the waveforms to deduce the phase velocity and wavelength of the waves. In the presentation, we will show an overview of the WFC measurements and the initial results of the interferometry analysis.

R005-P08
ポスター３：11/6　AM1/AM2（9:00-12:30）

#榎本　結衣[1)], 石坂　圭吾[2)], 栗田　怜[3)], 小嶋　浩嗣[4)], 頭師　孝拓[5)], 熊本　篤志[6)], 齋藤　義文[7)], 阿部　琢美[8)]
([1)] 富山県大,[(2)] 富山県大・工,[(3)] 京都大学 生存研,[(4)] 京大,[(5)] 奈良高専,[(6)] 東北大・理・地球物理,[(7)] 宇宙研,[(8)] ＪＡＸＡ宇宙科学研究所

Analysis of DC electric field in the cusp region observed by SS-520-3 rocket

#Yui Enomoto[1)], Keigo Ishisaka[2)], Satoshi Kurita[3)], Hirotsugu Kojima[4)], Takahiro Zushi[5)], Atsushi Kumamoto[6)], Yoshifumi Saito[7)], Takumi Abe[8)]
([1)]Toyama Pref. Univ.,[(2)]Toyama Pref. Univ.,[(3)]RISH, Kyoto Univ.,[(4)]Kyoto Univ.,[(5)]National Institute of Technology , Nara Col,[(6)]Dept. Geophys, Tohoku Univ.,[(7)]ISAS,[(8)]ISAS/JAXA

The region called the cusp is near the surface where the lines of magnetic field close. Some physical phenomena are observed in the cusp region due to the downward flow of high-energy plasma particles from the solar wind or the magnetosphere. The SS-520-3 rocket was launched in November 2021 to observe ion heating and acceleration due to the interaction of atmospheric ions and waves over the Arctic region. The SS-520-3 sounding rocket payload is equipped with low frequency wave analysis system (LFAS) with two set of orthogonal double probes to measure both DC and AC electric fields in the spin plane of the payload by using the double probe method. The Electric Field Detector (EFD) is one of the instruments in the LFAS. The EFD observe the DC electric field and extreme low frequency components less than 400 Hz. The EFD electronics was normally operating but only two of the four antennas were normally extended. However, the two antennas extend on different axes. In the case of the S-520-27 sounding rocket, the electric field detector was outputted the potential difference measured by probes extended on different axes. We compared the electric field waveform measured by a normal double probe system with the electric field waveform by a probe extended on a different axis. As a result, both electric field waveforms were almost the same. Therefore, we obtained the electric field waveform using single probe data observed by two antennas extended on the different axis measure by the EFD onboard the SS-520-3 sounding rocket. In this presentation, we will describe the derivation of the DC electric field vector using the single probe data observed by the SS-520-3 sounding rocket.

R005-P09
ポスター 3 ：11/6　AM1/AM2 （9:00-12:30）

#野村　麗子[1)], 松岡　彩子[2)], 小嶋　浩嗣[4)], 齋藤　義文[5)], 阿部　琢美[6)], 池田　博一[3)]
([1] 宇宙航空研究開発機構,[2] 京都大学,[3] 京大・生存圏,[4] 宇宙研,[5] ＪＡＸＡ宇宙科学研究所,[6]JAXA・宇宙研

Geomagnetic field observed by DFG onboard the SS-520-3 sounding rocket

#Reiko Nomura[1)], Ayako Matsuoka[2)], Hirotsugu Kojima[4)], Yoshifumi Saito[5)], Takumi Abe[6)], Hirokazu Ikeda[3)]
([1]JAXA,[2]Kyoto University,[3]RISH, Kyoto Univ.,[4]ISAS,[5]ISAS/JAXA,[6]ISAS, JAXA

Digital-type FluxGate magnetometer (DFG) is installed in the SS-520-3 sounding rocket which is aimed to investigate the cusp region by in-situ observation. DFG includes ASIC-based circuit for an axis in the spin plane and is placed on the top deck of the rocket where is suitable for avoiding the noise from rocket systems itself. On 4th November 2021 at 11:09:25LT, the rocket was successfully launched from the Svalbard Rocket Range (78.55N, 11.51E) of Andoya space center in Norway and it reached to 756km. The AFG successfully operated and observed the geomagnetic field during its flight. We did the onboard calibration with the flight data and derived the attitude of the sounding rocket. Also, we will discuss the field-aligned current observed during its flight.

R005-P10
ポスター 3 ：11/6　AM1/AM2 （9:00-12:30）

ロケット GNSS-TEC に適した GNSS 受信器の開発

#上谷　仁亮 [1)], 芦原　佑樹 [2)]
([1] 奈良高専 専攻科,[2] 奈良高専

Development of GNSS receiver optimized for rocket GNSS-TEC observation

#Hitoaki Uetani[1)], Yuki Ashihara[2)]
([1]Faculty of Advanced Engineering, NIT Nara,[2]NIT Nara

Various disturbance phenomena occurring in the ionosphere are a major factor in the degradation of GNSS positioning accuracy.Since GNSS is becoming increasingly important as a social infrastructure, not only for automotive applications but also for agricultural equipment and drones. It is important to observe ionospheric disturbance phenomena and elucidate the mechanism of their occurrence.

Ready-made GNSS receiver can be mounted on sounding rocket, some problems are to be occurred, such as unstable reception and loss of accuracy are expected due to the high dynamics of rocket motion. However, since the motion of the observation rocket can be accurately predicted, the TEC accuracy can be improved if the Doppler shift predicted in advance can be reflected in the parameters of the GNSS internal receiver and positioning engine.

In this study, a software radio is configured using FPGA and ADC to enable the manipulation of parameters by in-house GNSS receiver. We have succeeded in receiving and demodulating GNSS signals and positioning, multi-channel reception and positioning with FPGA alone, and have also produced software for receiver control and monitoring that runs on a PC. Currently, we are optimizing the operation of the receiver for onboard use on a sounding rocket.

電離圏で発生する様々な擾乱現象は、GNSS の測位精度低下の大きな要因となる。GNSS は車載用途だけでなく農業機器やドローン等に応用範囲が広がっており、社会基盤として重要度が増している為、電離圏擾乱現象の観測と発生機構の解明は重要課題である。

観測ロケットに搭載する GNSS-TEC 受信器には既製の GNSS 受信器を用いることもできるが、ロケットが持つ高い運動ダイナミクスにより、受信が不安定になる、精度が低下する等の問題が予想される。この問題に対して、観測ロケットの運動は精度良く予想できるため、予め予想されるドップラーシフト量を GNSS 内部の受信・測位エンジンのパラメータに反映できれば TEC 精度の向上が期待できる。

本研究では、FPGA と ADC を用いてソフトウェアラジオを構成し、GNSS 受信器の内製化を行うことでパラメータの操作を可能とする。GNSS 信号の受信及び復調・測位、マルチチャネルの受信及び FPGA 単体での測位に成功し、PC 上で動作する受信器制御・モニタリング用ソフトウェアも製作した。現在はロケット搭載用に動作の最適化を進めている。

R005-P11
ポスター 3 ：11/6　AM1/AM2 （9:00-12:30）

電離圏擾乱時におけるリアルタイムキネマティック測量の精度解析、初期結果

#西岡　未知 [1)], 津川　卓也 [1)], 今給黎　哲郎 [2)]
[(1] 情報通信研究機構,[(2] 株式会社　ジェノバ

Preliminary evaluation of Real-Time Kinematic (RTK) positioning error during ionospheric disturbances periods

#Michi Nishioka[1)], Takuya Tsugawa[1)]
[(1]NICT,[(2]jenoba

“Council for the advancement of space weather forecast” was held in the first half of 2022 by the Ministry of Internal Affairs and Communications.
（https://www.soumu.go.jp/main_sosiki/kenkyu/space_weather/index.html）
In the council, “Working group on space weather alert criteria” was established and a new alert system was discussed. It is reported that there is no clear international space weather standard for positioning derived from user-side requirements and the threshold for issuing a warning should be quantitatively determined (https://www.soumu.go.jp/menu_news/s-news/01tsushin05_02000047.html).

In this study, we focused on real-time kinematic (RTK) positioning, which uses dual frequency for precise positioning. RTK positioning errors were analyzed with GEONET observation network data developed by the Geographical Survey Institute during ionospheric disturbance periods at the end of October 2021 (https://swc.nict.go.jp/report/topics/view.html?ids=202111291740).
It was found that fix rates of the positioning clearly decreased for stations with rover stations separated by about 10 km. In this presentation, we show initial result of the analysis as a start point of determining the threshold for a new alert system.

電離圏を通過する電波は、電離大気によって伝搬遅延を受ける。電離大気の空間勾配が特に大きい場合は、地上における受信強度が著しく低下する。そのため、GNSS 等を利用した衛星測位では、電離圏の時空間変動の影響を受けてその精度が劣化する場合がある。衛星測位が測位分野の主要な測位手法となる状況の下、2022 年 1 月より総務省にて開催された「宇宙天気予報の高度化の在り方に関する検討会」（https://www.soumu.go.jp/main_sosiki/kenkyu/space_weather/index.html）では、宇宙天気の影響を受ける社会インフラの一つとして測位分野が挙げられ、そのリスクに着目した予報・警報について議論された。その結果、電離圏現象に基づいた指数・基準は存在するが、測位への影響を明確にする予警報の基準が未設定のため、早急に設定する必要があると報告された。測位手法には様々あるが、最も予警報の基準策定の必要性が高いされた測位手法が二周波精密測位である (https://www.soumu.go.jp/menu_news/s-news/01tsushin05_02000047.html)。そこで本研究では、二周波精密測位であるリアルタイムキネマティック測量（RTK 測量）に着目し、国土地理院の展開する GEONET 観測網データを用いて、電離圏擾乱時の RTK 測位誤差について解析を行った。2021 年 10 月末に発生した宇宙天気現象（https://swc.nict.go.jp/report/topics/view.html?ids=202111291740）に伴う RTK 測位への影響を調べたところ、約 10km 隔てた仮想的な観測点とローバー局の間で fix 率が明らかに減少していることがわかった。本発表では、電離圏擾乱時における RTK 測位の精度劣化についての初期解析結果を示し、測位への影響を明確にする予警報の基準設定の足掛かりとする。

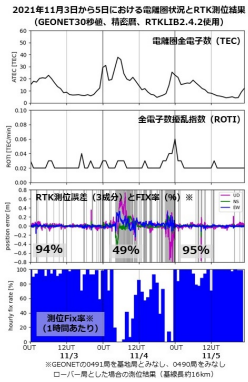

R005-P12
ポスター 3 ：11/6　AM1/AM2 （9:00-12:30）

赤道大気レーダーで観測された 150km エコーの太陽・地磁気活動依存性

#横山　竜宏 [1)], 高木　理絵子 [1,2)], 山本　衛 [1)]
([1] 京大生存研,[2]KDDI 株式会社

Solar and geomagnetic activity dependence of 150 - km echoes observed by the Equatorial Atmosphere Radar

#Tatsuhiro Yokoyama[1)], Rieko Takagi[1,2)], Mamoru Yamamoto[1)]
([1]RISH, Kyoto Univ.,[2]Now at KDDI Corporation

The occurrence characteristics of 150-km echoes in low-latitude regions arestudied using the Equatorial Atmosphere Radar (EAR) in Indonesia. The long-term observation of the 150-km echoes by the EAR enables us to study the occurrence characteristics of 150-km echoes statistically. It is shown that the occurrence rate of the 150-km echoes observed by the EAR shows a semiannual variation with two peaks in solstices and a negative correlation with both the EUV flux and Sigma Kp index, that is, the solar and the geomagnetic activity. Geomagnetic activity correlates with the occurrence rate of 150-km echoes observed one day after when the Sigma Kp was measured. However, the occurrence rate is always low during the high solar activity period regardless of the geomagnetic activity. While the seasonal variation and the solar activity dependence of the occurrence of 150-km echoes are consistent with previous studies, this is the first time a negative correlation with geomagnetic activity is reported.

電離圏で発生するプラズマ不規則構造は，電波のシンチレーションを引き起こし GPS 等による電子航法に深刻な障害を及ぼすものも多く，その発生機構の解明は重要な課題である．150km エコーと呼ばれる現象は電離圏 E 領域で発生するプラズマ不規則構造の一つだが，150km エコーの発生機構は未だに明らかにされていない部分が多い．2007 年から 2020 年までの EAR による 150km エコーの観測結果を用いた長期統計解析を実施した．長期統計解析によって，150km エコーの発生と太陽活動との間に明瞭な逆相関が見られることが確認された．さらに，地磁気擾乱との間にも逆相関があることが明らかとなった。1 日の Kp 指数を合計した値 (Sigma Kp) と発生傾向を比較した結果、Sigma Kp が高くなった日の 1 日後との相関が最も高く、太陽活動が高い時期は地磁気指数に関わらず発生頻度は非常に低いことが明らかとなった。150km エコーと地磁気活動との相関は本研究で初めて明らかとなった。

R005-P13
ポスター 3 ：11/6　AM1/AM2 （9:00-12:30）

タイ・チュンポンにおける下向きに移動する沿磁力線不規則構造の VHF レーダー観測

#大塚　雄一 [1)], 塩川　和夫 [2)],Hozumi　Kornyanat[3)], 西岡　未知 [4)], 津川　卓也 [4)], 斎藤　享 [5)],Supnithi Pornchai[6)],Jamjareegulgarn　Punyawi[6)], 山本　衛 [7)]
([1] 名大・宇地研,[2] 名大宇地研,[3]NICT,[4] 情報通信研究機構,[5] 電子航法研,[6]KMITL,[7] 京大・生存圏研

VHF radar observation of downward moving field-aligned irregularities in the F region over Chumphon, Thailand

#Yuichi Otsuka[1)], Kazuo Shiokawa[2)], Kornyanat Hozumi[3)], Michi Nishioka[4)], Takuya Tsugawa[4)], Susumu Saito[5)], Pornchai Supnithi[6)], Punyawi Jamjareegulgarn[6)], Mamoru Yamamoto[7)]
([1]ISEE, Nagoya Univ.,[2]ISEE, Nagoya Univ.,[3]NICT,[4]NICT,[5]ENRI, MPAT,[6]KMITL,[7]RISH, Kyoto Univ.

Plasma bubble is a localized plasma density depletion in the ionosphere. The plasma bubbles are generated at the magnetic equator through the Rayleigh-Taylor instability. The plasma density depletion moves to higher altitude by ExB drift due to the eastward polarization electric field generated in the plasma bubbles. On the other hand, Tulasi Ram et al. (2020) have reported downward development of field-aligned irregularities (FAIs) observed by the Equatorial Atmosphere Radar at Kototabang in Indonesia, which is located at low magnetic latitude (10 deg S dip latitude). The FAIs appeared at higher altitude at post-sunset, and extended to lower altitudes. In this study, by using a VHF radar at Chumphon in Thailand, located near magnetic equator, downward moving FAI echo regions were observed at the post-midnight on July 24, 2022. Around midnight (17 UT), FAI echo appeared around 300 km in altitude with narrow altitude range (less than 20 km). From 17:30 UT, the echo region extended to higher altitudes, and reached an altitude of 500 km. The downward extension of the echo region was also observed. The downward moving echo region was separated from the upward extending echo region. All-sky airglow imager install at the Chumphon radar site observed 630-nm airglow intensity depletion extending in the meridional direction. In order to compare the FAI echo region with the airglow structures, the FAI echo regions are mapped on the surface at the 630-nm airglow layer (250 km in altitude) along the magnetic field line. We found that the FAI regions moving upward and downward coincide with the airglow depletion, and that the airglow intensity was enhanced at the west of the airglow depletion. This result indicates that the plasma bubble in which FAI existed was embedded in the airglow enhanced region, where the F layer descent to lower altitudes increasing the airglow intensity. The downward motion of the FAI echo region may be caused by the downward motion of the F layer.

R005-P14
ポスター 3 ：11/6　AM1/AM2 （9:00-12:30）

新短波ドップラー観測システムにおける FM-CW 測距機能の実機シミュレーション

#並木　紀子 [1)], 細川　敬祐 [1)], 野崎　憲朗 [1)], 坂井　純 [1)], 冨澤　一郎 [1)], 有澤　豊志 [1)]
([1] 電通大

Experimental verification of FM-CW ranging capability in a new shortwave Doppler observation system

#Noriko Namiki[1)], Keisuke Hosokawa[1)], Kenro Nozaki[1)], Jun Sakai[1)], Ichiro Tomizawa[1)], Toyoshi Arisawa[1)]
([1]UEC

Our team of shortwave Doppler (HF Doppler: HFD) ionospheric disturbance observers launched our experimental station JG2XA for transmitting observation signals in 2001 on the premises of the University of Electro-Communications (UEC). It is constantly transmitting observation signals of 5006 kHz and 8006 kHz, 200 W each (Tomizawa et al., 2003). Ionospheric disturbances are studied using Doppler shift of HF continuous wave (CW) reflected from the ionosphere. It is characterized by receiving non-directional radio waves emitted from Chofu, where the university is located, over a wide area using antennas installed at 11 locations in the country. From multi-point observation data, it is possible to observe how the regions where reflection, scattering, and transmission in the ionosphere move in a three-dimensional space in the horizontal and vertical directions together with the directivity.

The outline of the HFD project and data is open to the public in ”http://gwave.cei.uec.ac.jp/˜hfd”.

We reported the additional ranging plan during HFD renovation in the previous JPGU meeting (Namiki et al., 2022). Receivers have been replaced by software radios since 2020 (Nakata et al., 2021). In this paper, we report the results of an indoor experiment in which the distance was measured simultaneously with the current HFD observation by combining a transmitter and a receiver.

The ranging function by Frequency Modulated Continuous Wave (FM-CW) is expected as follows:

・Determine the reflectance altitude quantitatively in units of 2-3 km, which has been determined by experience.
・Time resolution is improved by setting the sweep period to 50 ms.
・ Enhancement of interference rejection capability by sweeping.

The new observation system aims to ensure the continuity of the current observation results by superimposing FM-CW ranging signals between the identification codes while maintaining the continuous CW transmission without switching.

If the signal generation timing is matched for transmission and reception, the reflection distance of the ionosphere can be obtained from the relational expression $r = c\, f_b/2f'$ (r = distance, c = speed of light, f_b = beat frequency, f’ = rate of frequency change).

We constructed a prototype low-power radio transmitter and receiver pair closely installed in a laboratory. The transmitter and the receiver are synchronized to the reference signal. Although the actual range between the transmitting and receiving antennas is nearly zero, we confirmed pseudo range variation by differing frequency between transmitting and receiving sweep signals. We obtained negligible range error when the receiver is synchronized to the transmitter accurately.

As a result, it was confirmed that the conventional CW wave for Doppler observation and the new FMCW wave for ranging did not interfere with each other. Based on this result, we plan to add a distance measurement function to the existing new observation system.

我々短波ドップラー (HF Doppler:HFD) 法による電離圏擾乱観測チームは、電気通信大学敷地内に 2001 年から観測信号送信用の実験局 JG2XA を立ち上げ、5006kHz と 8006kHz それぞれ 200W の観測用信号を常時送信している (冨澤ほか, 2003) 。電離圏擾乱観測には連続波が用いられ、短波が電離圏で反射されるという性質を利用して、反射波のドップラーシフトを観測している。

大学のある調布から発せられた無指向性電波を日本国内 11 カ所に設置したアンテナで広域に受信することを特徴とし、多点観測データから、電離圏での反射や散乱が起こる領域が水平垂直方向の立体空間で移動している様子を、方向性と合わせて観測できる。

HFD プロジェクトの概要と測定データは”http://gwave.cei.uec.ac.jp/˜hfd”にて公開されている。

前回の JPGU では送信機に測距機能を追加する計画を報告した (Namiki et al., 2022)。受信機は 2020 年よりソフトウェアラジオへ置き換えが進められた（Nakata et al., 2021）。今回、送受信機を組み合わせて現行の HFD 観測と同時に距離測定を行った室内実験の結果を報告する。

周波数変調連続波（Frequency Modulated Continuous Wave：FM-CW）による測距機能では、次のことが期待される。

・従来経験的に判定していた反射高度を、2-3km 単位で定量的に確定する

・掃引周期 50ms として、時間分解能を向上する

・掃引による混信排除能力の強化

新観測システムでは、現行の切替無しの常時 CW 送信を維持しながら、識別符号の合間に FM-CW 測距信号を重畳し、現行の観測結果の継続性を担保することを想定している。信号の発生タイミングを送受信で一致させれば、$r=cf_b/2f'$（r=距離、c=光速度、f_b=ビート周波数、f'=周波数変化率）の関係式から、電離圏の反射距離が得られる。

これらを目標として、我々は新システムのプロトタイプを作成し、小電力無線の範囲で実験を行った。室内で極近接した送信機と受信機に、基準周波数を発生させる装置を組み合わせ、受信側に周波数オフセットをかけて一定時間経過した後での受信を模擬させた。

実験の結果、送受信信号のタイミング制御は観測対象に対して無視できるほどの誤差に抑えられ、従来の CW 波と新しい FMCW 波が互いに干渉しないことが確認できた。この結果をもって実際の新観測システムに、距離測定機能を追加する予定である。

R005-P15
ポスター 3 ：11/6　AM1/AM2 （9:00-12:30）

イオノゾンデ観測から見た、日本上空のスポラディック E 層の長期変動

#寺岡　宙惟 [1)],Liu　Huixin[2)], 西岡　未知 [3)], 木暮　優 [4)]
([1] 九州大学,[2] 九大・理・地惑,[3] 情報通信研究機構,[4] 九大・理・地惑

Long-term variations in the sporadic E layer over Japan from ionosonde observations.

#Sorai Teraoka[1)], Huixin Liu[2)], Michi Nishioka[3)], Masaru Kogure[4)]
([1]Kyushu University,[2]Kyushu Uni.,[3]NICT,[4]Kyushu University,

A sporadic E (Es) layer is one of the important ionospheric irregularities and disturbs wireless communications. In this study, we investigate how Es is modulated by increased CO2. We examine the long-term trend of Es by using long-term data of ionosonde observations at Japanese 4 stations, i.e., Wakkanai(45.16 north latitude, 141.75 east longitude, during 1948-2021), Kokubunji(35.71 north latitude, 139.49 east longitude, during 1957-2020), Yamagawa(31.20 north latitude, 130.62 east longitude, during 1965-2020), Okinawa(26.68 north latitude, 128.15 east longitude, during 1972-2021). To derive their long-term trend, we apply a multiple regression method with the ionosonde data. The presentation focuses on variabilities of its occurrence frequency and intensity, and latitudinal dependence. We also show trend correlations with the background ionospheric E and F layers.

スポラディック E(Es) 層は、無線通信に影響を与える重要な電離圏現象である。本研究は、CO2 増加により、Es はどのように変調されたかを調べる。日本の 4 つのイオノゾンデ観測点：稚内 (45.16° N, 141.75° E, 1948-2021 年)、国分寺 (35.71° N, 139.49° E, 1957-2020 年)、沖縄 (26.68° N, 128.15° E, 1972-2021 年、山川 (31.20° N, 130.62° E, 1965-2020 年) の長期間データを用いて、多重回帰法で Es の長期トレンドを調べる。特に、Es の発生頻度や強度、緯度依存性などの変動特性に注目して解析を行う。また、背景の電離圏 E 層と F 層のトレンドの相関性を明らかにする。

R005-P16
ポスター 3 ：11/6　AM1/AM2 （9:00-12:30）

#西山　祐樹 [1)], 中田　裕之 [1)], 大矢　浩代 [1)], 細川　敬祐 [2)], 西岡　未知 [3)],PERWITASARI　SEPTI[3)]
([1] 千葉大学大学院,[2] 電気通信大学大学院,[3] 情報通信研究機構

Three-dimensional propagation characteristics of MSTIDs obtained by HF Doppler sounding and GPS-TEC observations

#Yuki Nishiyama[1)], Hiroyuki Nakata[1)], Hiroyo Ohya[1)], Keisuke Hosokawa[2)], Michi Nishioka[3)], SEPTI PERWITASARI[3)]
([1]Graduate School of Chiba Univercity,[2]Graduate School of Informatics and Engineering, University of Electro-Communications,[3]National Institute of Information and Communications Technology

In Japan, MSTIDs frequently occur at nighttime in summer and daytime in winter. MSTIDs are caused by Perkins instability in summer and atmospheric gravity waves in winter (Otsuka et al.2021). Their period and velocities are 15 to 60 minutes and the velocity is 100 to 200 m/s respectively. However, the three-dimensional structures of MSTIDs are still unclear. Although there have been many studies about MSTIDs, most of them discuss horizontal characteristics. There are few studies about vertical characteristics. Therefore, the purpose of this study is to examine the three-dimensional structure of MSTIDs by HF Doppler sounding and GPS-TEC observations. HF Doppler sounding used in this study utilizes radio waves at different frequencies the vertical motions of the ionospheric plasma at different altitudes are obtained as Doppler shifts from the different reflected altitudes. It is also possible to calculate the horizontal propagation directions and propagation velocities of MSTIDs by comparing data from multiple receiving points. In this study, Doppler frequencies with a time resolution of 10 seconds observed at Sugadaira, Oarai, and Fujisawa by 5.006 MHz and 8.006 MHz radio waves were used .We also used GPS-TEC data for examining electron density variations at higher altitudes than HF Doppler sounding. The advantage of GPS-TEC data is that the disturbances occurred over wide area of Japan can be examined. In this study, GPS-TEC data with a time resolution of 30 seconds was obtained from 32 satellites and more than 1000 receiver combinations. The altitude of the ionospheric pierce points is assumed to be 300 km in this study. We analyzed the TEC fluctuations occurred on December 13, 2013 around the observation points Sugadaira, Oarai, and Fujisawa in the HF Doppler observations.

In the present event, the HF Doppler soundings observed the variations of Doppler frequencies of 5.006 MHz and 8.0006 MHz. Reflection height of these radio waves were 140 km for 5.006 MHz and 185 km for 8.006MHz. The directions of propagations at both altitudes were almost the same, but the propagation velocity was about 30 m/s faster at 185 km than at 140 km. Moreover, in the GPS-TEC observation, the direction of propagation was also in the southwest direction and the propagation velocity was over 200 m/s. These results indicate that the direction of propagation is the same regardless of altitude, but the propagation velocity increases with altitude.

R005-P17
ポスター 3 ：11/6　AM1/AM2 （9:00-12:30）

ダーウィン及び佐多で得られた大気光画像の 3 次元スペクトル解析に基づく中間圏大気重力波および電離圏 MSTID の水平位相速度分布の比較解析

#坪井　巧馬 [1)], 塩川　和夫 [1)], 大塚　雄一 [1)], 藤波　初木 [1)], 中村　卓司 [2)],Neudegg　David[3)]
([1] 名大 ISEE,[2] 極地研,[3] アデレード大学

Spectral Analysis of Mesospheric Gravity Waves and Traveling Ionospheric Disturbances in Airglow Images at Darwin and Sata

#Takuma Tsuboi[1)], Kazuo Shiokawa[1)], Yuichi Otsuka[1)], Hatsuki Fujinami[1)], Takuji Nakamura[2)], David Neudegg[3)]
([1]ISEE, Nagoya Univ.,[2]NIPR,[3]Adelaide Univ.

Atmospheric gravity waves (AGWs) and medium-scale traveling ionospheric disturbances (MSTIDs) in the upper atmosphere affect the atmospheric circulation and the radio-wave transmission including satellite positioning. These waves can be observed in nocturnal airglow images. Thus, spectral analysis of airglow images provides propagation direction and intensity of these waves. In this study, we calculated the horizontal phase velocity distribution of AGWs in the mesosphere-lower-thermosphere (MLT) at 90-100 km altitude, and MSTIDs in the F-region ionosphere at 200-300 km altitude by applying the 3-dimensional spectral analysis method of Matsuda et al. [JGR, 2014] to the airglow images obtained at Darwin (12.4^{o}S, 131.0^{o}E) in Australia from 2001 to 2019 and Sata (31.0^{o}N, 130.7^{o}E) in Japan from 2000 to 2020. Darwin and Sata are located nearly at geomagnetic conjugate points, but geographically Darwin is located at lower latitudes than Sata. The climate and surrounding topographic conditions are very different between Darin and Sata. In this presentation, we discuss the similarity and difference of airglow spectra between Darwin and Sata, considering the difference of the geographic and magnetic characteristics.

The spectra of AGWs in the MLT region show that the poleward power spectral density (PSD) is stronger in summer and weaker in winter at both stations. The ERA5 database provided by European Centre for Medium-Range Forecasts (ECMWF) show clear characteristics of seasonal variation of tropospheric convection, suggesting that the tropospheric convection is a possible source of AGWs in the MLT region.

The spectra of F-region MSTIDs show that the westward PSD is stronger in summer at both stations. The stronger PSD in summer in Darwin is different from previous and present observations of stronger PSD in summer over Japan, if we consider symmetry of MSTIDs between northern and southern hemispheres. A weak positive correlation was observed between PSDs of MLT region AGWs and higher F-region MSTIDs, suggesting partial connection between the AGWs and MSTIDs separated by over 100 km in altitude. In this presentation, we will discuss possible causes of this result by looking into spectral comparison of individual events.

Acknowledgement
The operation of the all-sky imager at Darwin has been carried out with support of the Space Weather Services (SWS) of the Bureau of Meteorology, Australia.

超高層大気中を伝搬する大気重力波や中規模伝搬性電離圏擾乱（MSTID）は、大気の大循環や短波通信に影響を与える。これらの波動現象は地上から大気光イメージャで撮像観測され、そのスペクトル解析から、これらの波動の伝搬方向やパワーを見積もることができる。本研究では南半球のオーストラリアのダーウィン観測点（12.4° S, 131.0° E）および北半球の日本の佐多観測点（31.0° N, 130.7° E）で得られた大気光画像に Matsuda et al. [JGR, 2014] の 3 次元スペクトル解析手法を適用し、ダーウィンでは 2001 年から 2007 年および 2011 年から 2019 年、佐多では 2000 年から 2020 年のデータを用いて、中間圏の大気重力波と電離圏の MSTID の解析を行った。ダーウィンと佐多は磁気的には互いに磁気共役な関係にあるものの、地理的には南半球の低緯度（12.4° S）と北半球の中緯度 (31.0° N) に位置しており、気候や周囲の地形的状況が大きく異なる。発表では両者の地理的特性や磁気的特性によるスペクトルの違いを考察する。

波長 557.7 nm の大気光画像に見られる中間圏大気重力波の水平位相速度スペクトルの解析から、両観測点で夏において極方向に伝搬する波動のスペクトルが大きくなっていることがわかった。対流圏の観測に基づく客観解析データである ERA5（https://doi.org/10.1002/qj.3803）のデータによると、対流圏の鉛直流にも特徴的な季節変動が見られることから、この鉛直流が大気重力波の波源となり、鉛直流と観測点の相対位置によって、中間圏大気重力波のスペクトルの方向依存性が左右されている可能性が考えられる。

波長 630.0 nm の大気光画像に見られる MSTID の水平位相速度スペクトルの解析から、両観測点ともに夏において、西方向に伝搬する MSTID のスペクトル強度が増大していることがわかった。この夏の強度増大は、先行研究で指摘されている MSTID が南北半球に同時に投影される結果と矛盾するように思われる。また、両観測点において、中間圏大気重力波と MSTID の強度の間に弱い相関が見られている。これらのことから、南北半球に投影される電場によらない MSTID の生成が示唆される。発表では両半球の同時観測イベントの個別比較も交えて考察する。

謝辞：ダーウィンにおける大気光イメージャの運用はオーストラリア気象局の宇宙天気サービスの支援を受けてい

ます。

R005-P18
ポスター 3 ：11/6　AM1/AM2 （9:00-12:30）

#大矢　浩代 [1)], 土屋　史紀 [2)], 鴨川　仁 [3)], 鈴木　智幸 [4)],Chum　Jaroslav[5)], 高村　民雄 [6)]
([1] 千葉大・工・電気,[2] 東北大・理・惑星プラズマ大気,[3] 東京学芸大・物理,[4] 学芸大・教育,[5] なし,[6] 千葉大・環境リモセン

Effects of the 2022 Tonga volcanic eruption on the D-region ionosphere based on observation of AVON VLF/LF transmitter signals

#Hiroyo Ohya[1)], Fuminori Tsuchiya[2)], Masashi Kamogawa[3)], Tomoyuki Suzuki[4)], Jaroslav Chum[5)], Tamio Takamura[6)]
([1]Engineering, Chiba Univ.,[2]Planet. Plasma Atmos. Res. Cent., Tohoku Univ.,[3]Dept. of Phys., Tokyo Gakugei Univ.,[4]Education, Gakugei Univ.,[5]ASCR,[6]CEReS, Chiba Univ.

The Hunga Tonga-Hunga Ha‘apai volcano in Tonga (in southern Pacific, 20.54S, 175.38W) explosively erupted during 04:10-04:30 UT on 15 January, 2022, and large pressure variations occurred from the volcano. Large and medium scale traveling ionospheric disturbances (LSTID and MSTID) due the eruptions were observed (Themens, 2022), which were caused by Lamb wave excited by the eruptions. Due to magnetic conjugate effect, the northern hemisphere TIDs appear three hours prior to the arrival of the Lamb wave (Lin et al., 2022). Both direct and conjugate TIDs match with the theoretical dispersion relation of the atmospheric Lamb and gravity modes. However, D-region behavior for the Tonga eruptions has not been revealed yet. In this study, we investigate variations in VLF/LF transmitter signals and atmospheric electric field (or potential gradient) associated with Tonga volcanic eruptions of 15 January, 2022 to understand D-region ionosphere and atmosphere coupling. The VLF/LF transmitters used in this study were JJY(60 kHz, Japan), JJI(22.2 kHz, Japan), and BPC(68.5 kHz, China). The receivers were Tainan (TNN, 23.07N, 120.12E) in Taiwan, where is one of Asia VLF observation network (AVON). We used 0.1-s sampling amplitude data. Unfortunately, there were no phase data for all paths on that day. The minimum distances of the JJI-TNN, JJY60kHz-TNN, and BPC-TNN propagation paths from the Tonga volcano were 8167.7 km, 8311.6 km, and 8499.9 km, respectively. The atmospheric electric field has been observed in Chiba University (CHB), (35.63N, 140.10E), Seikei High School (SHS, Tokyo, 35.72N, 139.57E), Japan, and Studenec (STU), Czech Republic (50.26N, 12.52E). The distances of CHB, SHS, and STU from the Tonga volcano were 7789.5 km, 7830.4 km, and16634.7 km, respectively. The first variations in pressure data were seen around 10:57 UT and 19:03 UT on 15 January in CHB and STU, respectively. The propagation velocity was 310-320 m/s, which is typically propagation velocity of atmospheric Lamb waves. The VLF/LF amplitudes for all three paths showed the similar period around the first arrival time of the Lamb waves. The common periods for multi-paths were 4-6, 8-10, 20, and 50 minutes. There were significant coherences (0.45-0.72) of more than 95-% confidence levels between atmospheric pressure at CHB and two LF amplitudes with a period of 14.4 minutes. On the other hand, after arrival time of the Lamb wave, the atmospheric electric field at CHB showed similar variations with the pressure data at CHB. The periods of the variations were 40-50 and 80-100 minutes. The amplitude of the variation in the atmospheric electric field at CHB and STU was similar after arrival time of the Lamb wave at each site. There were variations in atmospheric electric field with a period of 10-100 minutes at CHB at the first (direct) and second (rounding the Earth) arrival times of the Lamb waves. The conductivity in the atmosphere might change due to Lamb wave excited from the Tonga volcanic eruptions. In this presentation, we will report and discuss the phenomena in detail.

R005-P19
ポスター 3 ：11/6　AM1/AM2 （9:00-12:30）

#穂積　裕太 [1)], 齊藤　昭則 [2)],Yue　Jia[3)], 坂野井　健 [4)],Liu　Hanli[5)], 山崎　敦 [6)]
([1]NICT,[2] 京都大・理・地球物理,[3]NASA Goddard Space Flight Center,[4] 東北大・理・PPARC,[5]National Center For Atmospheric Research,[6]JAXA/宇宙研

Visualization of gravity wave hot spots at the upper mesosphere with airglow imaging observation by IMAP/VISI

#Yuta Hozumi[1)], Akinori Saito[2)], Jia Yue[3)], Takeshi Sakanoi[4)], Hanli Liu[5)], Atsushi Yamazaki[6)]
([1]NICT,[2]Dept. of Geophysics, Kyoto Univ.,[3]NASA Goddard Space Flight Center,[4]PPARC, Grad. School of Science, Tohoku Univ.,[5]National Center For Atmospheric Research,[6]JAXA/ISAS

A global characteristic of gravity wave activity at the upper mesosphere is derived with airglow image data set of IMAP/VISI. Nadir-viewing imaging from satellites provides an excellent opportunity to study gravity waves in the upper atmosphere on a global scale. Compared to limb and occultation experiments, nadir-viewing instruments have good horizontal resolution and sensitivity to gravity waves with short horizontal wavelengths. The Atmospheric Infrared Sounder (AIRS) aboard the Aqua satellite and The Cloud Imaging and Particle Size (CIPS) instrument on the AIM satellite have revealed stratospheric gravity wave activity characteristics. In the mesosphere, however, the global characteristic of gravity wave activity is less studied based on nadir-viewing instruments compared to the stratosphere. In this study, mesospheric gravity waves are studied with a 3-year data-set (from 2013 to 2015) by the Visible and Near-Infrared Spectral Imager of the Ionosphere, Mesosphere, upper Atmosphere and Plasmasphere mapping mission (IMAP/VISI). Gravity waves are detected based on the O2(0-0) atmospheric band (762 nm), the typical emission peak of which is around 95 km altitude. In the analysis, we focus on gravity wave peak events, in which the airglow variance exceeds a threshold. The occurrence frequency of the peak events is derived for each season, and the hotspots of gravity waves are located. The results show the hotspots of gravity waves over the Andes and North America, both are well-known hotspots reported by previous studies of stratospheric gravity waves.

R005-P20
ポスター 3 ：11/6　AM1/AM2 （9:00-12:30）

ISS-IMAP/VISI によって観測された赤道中間圏における高輝度大気光構造

#齊藤　昭則 [1)], 坂野井　健 [2)], 穂積　裕太 [3)]
([1] 京都大・理・地球物理,[2] 東北大・理・PPARC,[3]NICT

Bright airglow structures in the equatorial mesosphere observed by ISS-IMAP/VISI

#Akinori Saito[1)], Takeshi Sakanoi[2)], Yuta Hozumi[3)]
([1]Dept. of Geophysics, Kyoto Univ.,[2]PPARC, Grad. School of Science, Tohoku Univ.,[3]NICT

International Space Station-Ionosphere, Mesosphere, upper Atmosphere and Plasmasphere mapping (ISS-IMAP) mission frequently observed bright band-like structures of the mesospheric airglow in 762nm wavelength with Visible and near Infrared Spectral Imager (VISI) instrument. VISI's nadir-viewing observation captured two-dimensional structures of the airglow from the molecular oxygen between September 2012 and August 2015. The FOV width of VISI's 762nm observations was 600 km in the direction perpendicular to the ISS trajectory, and longer than 10,000km along the trajectory. Bright band-like structures that stretched in the zonal direction, and have higher emission than 3k Rayleigh In the equatorial region were one of the outstanding structures observed by VISI. Statistical analysis revealed that the occurrence of the bright band has the first maximum in March and the second maximum in August. It appeared in the pre-midnight local time sector and is located around the geographical equator. It tends to appear in the longitudinal sector from -100 degrees to +100 degrees. It has low occurrence rate in the longitudinal sector over the Pacific Ocean. The GAIA model indicates that the enhancement of the 762nm airglow is caused by the enhancement of the atomic oxygen in the mesosphere not only by the downward diurnal tidal wind but the convergence of the meridional neutral wind on the equator. The intensity of the bright band can be a proxy of these wind system in the mesosphere. The features of the bright band-like structures of the 762nm airglow, and their generation mechanism will be discussed in the presentation.

R005-P21
ポスター 3 ：11/6　AM1/AM2 （9:00-12:30）

#須川　天万 [1)], 田口　真 [1)]
[(1] 立教大・理・物理,[(2] 立教大・理・物理

Image analysis of the polar vortices of Venus observed by LIR

#Temma Sugawa[1)], Makoto Taguchi[1)]
[(1]Rikkyo Univ.,[(2]Rikkyo Univ.

Atmospheric temperature at the cloud tops of Venus around an altitude of 65 km decreases with latitude, but it is known that there are high-temperature regions near the poles and cooler regions around them. The high-temperature regions rotate around the poles, and called as the polar vortices, where zonal wavenumber 0, 1 and 2 shapes of the temperature distribution predominate [Garate-Lopez et al. 2013; Sato et al. 2014]. Previous studies have derived a rotation period of about -2.8 to -3.2 days and about -2.2 to -2.5 days for the northern and southern polar vortices, respectively, but the cause of the difference in the rotation periods of the northern and southern polar vortices is unknown [Schofield et al, 1983; Garate-Lopez et al, 2013]. In addition, no observational studies have yet investigated the relationship between Venusian atmospheric dynamics and the temperature structure in the polar regions.

The Venus orbiter Akatsuki has been orbiting around Venus in an almost equatorial plane since December 2015. Longwave Infrared Camera is one of the cameras onboard Akatsuki, still obtaining images of brightness temperature around the cloud-top altitudes every day. In this presentation, we report temporal variations of the rotational period and the center position of rotation of the polar vortices, and the comparison with atmospheric dynamics at mid- and low-latitudes, using brightness temperature data observed by LIR.

R005-P22
ポスター 3 ：11/6　AM1/AM2 （9:00-12:30）

#津田　卓雄[1)], 三好　勉信[2)], 穂積　裕太[3)], 安藤　芳晃[1)], 細川　敬祐[1)], 鈴木　秀彦[4)], 村田　健史[3)], 中村　卓司[5)],Yue　Jia[6)],Nielsen　Kim[7)]
([1] 電通大,[2] 九大・理・地球惑星,[3] 情報通信研究機構,[4] 明治大,[5] 極地研,[6]NASA Goddard Space Flight Center,[7]Utah Valley University,[8]Utah Valley University,[9]Utah Valley University

Variations in polar mesospheric clouds observed by Himawari-8/AHI

#Takuo Tsuda[1)], Yasunobu Miyoshi[2)], Yuta Hozumi[3)], Yoshiaki Ando[1)], Keisuke Hosokawa[1)], Hidehiko Suzuki[4)], Ken T. Murata[3)], Takuji Nakamura[5)], Jia Yue[6)], Kim Nielsen[7)]
([1]UEC,[2]Dept. Earth & Planetary Sci, Kyushu Univ.,[3]NICT,[4]Meiji univ.,[5]NIPR,[6]NASA Goddard Space Flight Center,[7]Utah Valley University,[8]Utah Valley University,[9]Utah Valley University

To advance polar mesospheric cloud (PMC) observations by Advanced Himawari Imager (AHI) onboard the Japanese geostationary-Earth-orbit (GEO) meteorological satellite Himawari-8, we have developed a PMC detection method for application to the Himawari-8/AHI full-disk images. The PMC detection method consists of two steps: detection in stronger PMC signals in the first step and detection in weaker PMC signals in the second step. By using this two-step detection, we eliminate false detections as much as possible and enhance detection sensitivity. As a result, the PMC detection sensitivity by Himawari-8/AHI is well comparable to that by Cloud Imaging and Particle Size (CIPS) onboard Aeronomy of Ice in the Mesosphere (AIM). By analyzing the detected PMC data, various PMC variations such as quasi 5-day waves and mid-latitude extensions can be revealed. Among the variations, we focus on interhemispheric coupling, specifically a relationship between PMC occurrence rates in the summer hemisphere and sudden stratospheric warmings in the winter hemisphere.

R005-P23
ポスター 3 ：11/6　AM1/AM2 （9:00-12:30）

北海道における 2020 年および 2021 年の夜光雲出現イベントの成因

#白　秉安 [1)], 鈴木　秀彦 [1)], 津田　卓雄 [2)], 穂積　裕太 [3)], 石井　智士 [1)], 中村　優里子 [1)]
([1] 明治大,[2] 電通大,[3]NICT

The causes of the 2020 and 2021 noctilucent cloud appearance events in Hokkaido, Japan.

#BENG AUN PEH[1)], Hidehiko Suzuki[1)], Takuo Tsuda[2)], Yuta Hozumi[3)], Satoshi Ishii[1)], Yuriko Nakamura[1)]
([1]Meiji univ.,[2]UEC,[3]NICT

Noctilucent Clouds (NLCs) are known to be seen at high latitudes during the twilight period in the summer hemisphere. However, in recent years, NLC appearance at lower latitudes is increasing. In Japan, NLCs were first sighted in Hokkaido in 2015. They were subsequently observed again in 2020 and 2021. Especially in the summer of 2020, 4 cases of NLC events were observed. This was the first time in which multiple cases were confirmed within one season in Japan. According to previous research, NLCs shown in the middle latitude regions are mainly due to the transportation of NLC particles from higher latitude (i.e colder) regions by a horizontal wind. If this hypothesis is correct, the detection of NLCs in the mid-latitudes would increase when plenty of NLC particles are generated at high latitudes and effectively transported by meridional wind. In this study, the atmospheric temperature distribution in the upper mesospheric region of the Northern Hemisphere mid-high latitudes in 2020 and 2021 was investigated by using data from NASA's polar-orbiting meteorological satellite Aura/Microwave Limb Sounder (MLS), and the intensity and phase of NLCs transportation from north to south was investigated by using geostationary Japanese meteorological satellite Himawari 8. Both data are then analyzed and compared with several methods. The lowest latitudes of the noctilucent clouds appearance around 70-80ºE and 150-160ºW are retrieved from processed Himawari 8 data, and their time-series variations and periods of variation were analyzed. Based on the results of these analyzes, we present a discussion on the causes of noctilucent cloud appearance events in Hokkaido in 2020 and 2021.

夜光雲 (Noctilucent Clouds, NLCs) は夏半球の中高緯度帯において、日の出前と日没後の時間帯で観測されやすいことが知られている。しかし、近年では NLCs が低緯度側で観測される事例が頻繁に確認されている。海外では、Logan, Utah (Taylor et al., 1999) など中緯度帯で観測された報告も多くあり、国内では 2015 年に初めて北海道において NLCs が確認された。北海道ではその後、2020 年、2021 年に再び観測された。特に 2020 年の夏には NLCs が 4 例も観測され、国内で 1 シーズンの中で複数の事例が確認されたのはこの年が初となる。また、2021 年のシーズンにも 1 例のみであるが夜光雲が確認され、国内で 2 年連続で夜光雲が観測された初のケースとなった。先行研究によれば、中高緯度帯において夜光雲が検出されるメカニズムとしては、より低温な高緯度帯で形成された夜光雲粒子が同高度の水平風によって低緯度側へ輸送されたという説がある。このメカニズムが正しければ、高緯度側で多数の夜光雲粒子が発生し、低緯度側へ速やかな輸送が起こるときに中緯度帯での夜光雲の検出が増えると考えられる。このことを検証するために、本研究では 2020 年および 2021 年における北半球中高緯度の上部中間圏領域における大気温度分布を NASA の極軌道気象衛星 Aura/Microwave Limb Sounder(MLS) のデータにより、夜光雲の南北の輸送の強度と位相を日本の気象観測衛星ひまわり 8 号の可視画像データ（Tsuda et al., 2018）より、それぞれ解析し比較した。ひまわり 8 号でのデータからは、東経 70-80 度および西経 150 度-160 度付近の夜光雲の南限緯度を抽出し、その時系列変動および変動周期を解析した。本発表では、これらの解析結果に基づき、北海道における 2020 年および 2021 年の夜光雲出現イベントの成因について考察した結果を報告する。

R005-P24
ポスター 3 ：11/6　AM1/AM2 （9:00-12:30）

航空機観測により撮像された中緯度夜光雲の発生メカニズム

#面　征宏 [1)], 鈴木　秀彦 [1)], 中村　優里子 [1)], 石井　智士 [1)], 松本　紋子 [2)]
([1] 明大,[2]ANA ホールディングス

Cause of noctilucent clouds appearance in middle latitude regions observed by airline jets

#Masahiro Omote[1)], Hidehiko Suzuki[1)], Yuriko Nakamura[1)], Satoshi Ishii[1)], Ayako Matsumoto[2)]
([1]Meiji Univ.,[2]ANA HOLDINGS INC.

Noctilucent clouds (NLCs) have been known as a phenomenon observed mainly from high latitudes. However, in recent years, they have been frequently observed in mid-latitudes as well. For example, NLCs were observed for the first time in Hokkaido, Japan in June 2015 [Suzuki et al. 2016]. The expansion of the NLCs area to lower latitudes is possibly caused by a global increase in the greenhouse effect leading the global warming. Therefore, accurate and continuous monitoring of the frequency of NLC appearance in the mid-latitudes is important to know the progress of global warming. To improve the observation opportunities of NLCs in the mid-latitudes, Suzuki et al. [2022] conducted aircraft observations on a trial basis from June 8 to July 12, 2019, and successively found NLCs in the mid-latitudes on 8 of 13 flights. In this study, the mechanism of NLC appearance in the middle-latitude area is discussed based on this data. According to the previous studies, NLC appearance in middle latitude areas is thought to be a result of the transportation of ice clouds by background winds from high latitudes. Since NLC particles would sublimate quickly if they pass through high-temperature regions during transportation, NLC particles detected in middle latitudes were considered to pass through only cold areas. Therefore, we traced back the history of advection from the detection location and compared it with the temperature distribution in the same altitude region by satellite data (AURA/MLS) to verify whether the transport mechanism is possible. The results indicate that in most cases the NLCs most likely encountered a high-temperature region during transport. However, since satellite data represent an averaged temperature in a wide area, the possibility remains that high and low-temperature regions are distributed in the area and the NLCs may have passed through low-temperature regions. Since aircraft observations can also capture the spatial structure of NLCs while flying in the longitude direction, the zonal structure of mid-latitude NLCs can also be derived. In some events, there is a remarkable wavy structure in the longitude direction with a horizontal wavelength of ˜300 km, which may reflect the non-uniformity of the temperature distribution described above. In this study, we analyzed several mid-latitude NLC events observed by the jet, satellite data, and wind velocity models to discuss the mechanism of mid-latitude NLC appearance.

夜光雲は、主に高緯度帯で観測される現象であると考えられていたが、近年中緯度帯でも頻繁に観測されている。日本でも 2015 年 6 月に北海道で初めて夜光雲が観測されている [Suzuki et al .2016]。夜光雲の出現領域が低緯度側へ拡大することは、地球温暖化をもたらす温室効果の全球的な増加が原因であると考えられている。そのため、夜光雲の出現頻度を中緯度帯においても正確に監視することは、地球温暖化の進行度を測る上で重要である。中緯度帯における夜光雲の観測機会を向上させるために、Suzuki et al . [2022] では 2019 年 6 月 8 日から同 7 月 12 日にかけて航空機観測を試験的に実施し 13 フライトのうち 8 フライトで中緯度帯に発生する夜光雲を検出した。本研究ではこのデータに基づき中高緯度帯における夜光雲発生メカニズムを考察した。先行研究による示唆によれば、夜光雲は背景の風に乗って高緯度から低緯度へ輸送されるが、その間に高温領域を通過すると速やかに昇華してしまうと考えられる。したがって、検出場所から移流の履歴を遡り、衛星データ（AURA/MLS）による同高度領域における温度分布と比較することで、観測された各イベントについて輸送メカニズムが成り立つかを検証した。その結果、ほとんどの事例において夜光雲は輸送途中で大域的な高温領域に遭遇している可能性が高いことが示された。しかし衛星データは広範囲の平均温度を示すものであるため、空間内に温度が非一様に分布しており、夜光雲が低温領域を通過してきた可能性も残る。航空機観測では経度方向に飛行しながら夜光雲の空間構造を捉えることもできるため、中緯度夜光雲の空間的分布も導出可能である。あるイベントにおいては、経度方向に顕著な波状構造（水平波長約 300 km）を示すものがあり、これらが上述の温度分布の非一様性を示している可能性もある。本研究では航空機観測でえられた中緯度帯における複数の夜光雲の観測事例を、衛星データ、風速モデルを用いて詳細に解析し、中緯度夜光雲出現のメカニズムを考察した。

R005-P25
ポスター 3 ：11/6　AM1/AM2 （9:00-12:30）

夜光雲観測のための係留気球開発システムの軽量化の検討と試験飛揚結果

#須原　廉 [1)], 高田　拓 [1)], 上田　真也 [2)], 石井　智士 [3)], 加藤　恵輔 [3)], 鈴木　秀彦 [3)]
([1] 産技高専,[2] 高知高専,[3] 明治大

Weight reduction of tethered balloon observation system for noctilucent cloud observation and results of test flights

#Ren Suhara[1)], Taku Takada[1)], Shinya Ueta[2)], Satoshi Ishii[3)], Keisuke Kato[3)], Hidehiko Suzuki[3)]
([1]TMCIT,[2]NIT, Kochi College,[3]Meiji univ.

Noctilucent clouds are icy clouds that form at the mesospheric interface at approximately 85 km altitude and reflect sunlight from below the horizon before sunrise and after sunset. Traditionally, this phenomenon has been observed around the summer solstice in the summer hemisphere, primarily at high latitudes (50-70 degrees latitude). However, in recent years it has been observed in mid-latitude locations, such as Hokkaido, Japan, expanding the area of occurrence. This expansion is thought to be attributable to environmental changes due to increasing greenhouse gases. We are aiming to conduct regular observations of noctilucent clouds as an indicator of the degree of global warming at very high altitudes.

In July 2021, we conducted a balloon test flight at Nayoro City Observatory in Hokkaido. In order to solve the problems encountered during the test flight, we studied ways to reduce the weight of the observational equipment mounted on the balloon and to reduce the blurring of the camera images obtained.

First, we reviewed the combination of on-board components and decided on a combination of a data transmitter, a GoPro camera, and a simple gimbal. A GPS sensor, temperature/humidity sensor, 9-axis sensor, and barometric pressure sensor were attached to the data transmitter, and Raspberry Pi was used as the microcontroller. The data transmitter was housed in a waterproof plastic case. The simple gimbal was constructed using a GoPro camera attachment and fixed to the plastic case for filming.

Next, we studied ways to suppress camera shake in the sky. In the July 2021 experiment, many of the still images taken in time-lapse mode showed the moon and city lights extending horizontally. This was attributed to the twisting of the string to which the camera was attached, which caused the camera to rotate during the exposure. To investigate the effect of camera shake on the captured images, we measured acceleration and angular velocity, which were calculated from image differences during video capture, by subjecting the camera to typical patterns of variation, such as rotational motion due to torsion, single pendulum motion, and conical pendulum motion. The acquired data showed that rotational motion by torsion and conical pendulum motion caused a significant change in the horizontal direction, which is the cause of image blurring, while the single pendulum motion had a limited effect.

In August 2022, a tethered balloon experiment is scheduled to be conducted in Oarai, Ibaraki Prefecture, and the results of the test flight and improvements will be reported.

夜光雲とは中間圏界面 (高度約 85 km) に形成される氷粒の雲が、日出前と日没後の時間帯に地平線下からの太陽光を反射して光る現象のことである。

従来は、夏半球の夏至頃に緯度 50˜70° の高緯度帯を中心に観測されていたが、近年、北海度などの中緯度帯で観測されることがあり、発生領域が中緯度側へ拡大している。

この発生領域拡大の原因として温室効果ガスの増加による環境変化が考えられており、超高層での地球温暖化の進行度合いを監視するために、夜光雲の定常的な観測を目指している。

夜光雲の定常的な観測のため、夏至頃に 1˜2 週間程度の連続観測を行うことを目標とした観測装置の開発を行っている。2021 年 7 月には北海道名名寄市立天文台で試験飛揚を行った。

試験飛揚での課題点を解決するため、気球に搭載する観測装置の軽量化とカメラ画像のぶれを抑える方法の検討を行った。

まず、観測装置の搭載部品の組み合わせを見直し、データ送信機、GoPro カメラ、簡易ジンバルの組み合わせとした。データ送信器には GPS センサ、温湿度センサ、9 軸センサ、気圧センサを取り付け、マイコンには Raspberry Pi を使用した。データ送信機は雲中での防水のためプラスチックケースに収めている。

簡易ジンバルには GoPro カメラ用の取り付け器具を使用し、プラスチックケースに固定して撮影を行う構造とした。

次に上空でのカメラのぶれを抑えるための検討を行った。

2021 年 7 月の飛揚実験では、タイムラプスモードで撮影した静止画像の多くで月や街明かりが水平方向に伸びていた。この原因としては、カメラを取り付けた紐のねじれにより、撮影中にカメラが回転していたことが考えられた。

カメラの揺れが撮影画像に与える影響を調べるために、カメラに典型的な変動（ねじれによる回転運動、単振り子運動、円錐振り子運動）パターンを与えて加速度と角速度（動画撮影時の画像差分から算出）を計測することにした。取得

したデータから、ねじれによる回転運動と円錐振り子運動では、画像のブレの原因となっている水平方向への変化が激しく、単振り子運動ではあまり影響がないことが分かった。

今回は、夜光雲観測のための係留気球装置に関して、装置の軽量化の方法とカメラぶれを抑える方法の 2 つについて検討を行った。2022 年 8 月には、茨城県の大洗で係留気球実験を実施するため、試験飛揚による結果や新たな改善点などについて報告する予定である。

R005-P26
ポスター 3 ：11/6　AM1/AM2 （9:00-12:30）

電離圏観測用中性大気質量分析器の開発

#米田　匡宏 [1)], 齊藤　昭則 [1)], 齋藤　義文 [2)]
[(1] 京都大学理学研究科,[(2] 宇宙科学研究所

Development of a Neutral Mass Spectrometer for Ionospheric Observations

#Masahiro Yoneda[1)], Akinori Saito[1)], Yoshifumi Saito[2)]
[(1]Graduate School of Science, Kyoto University,[(2]ISAS

We are currently developing a neutral mass spectrometer for ionospheric observations in preparation for the sounding rocket experiment scheduled for 2024. The neutral atmospheric composition in the ionosphere is an important parameter for understanding not only thermospheric variations but also ionospheric variations, because it affects the plasma density through ionization and recombination processes and contributes to electric field variations through the electric conductivity. However, in recent in-situ ionospheric observations by artificial satellites and sounding rockets, the atmospheric composition has rarely been measured, and empirical models such as MSIS have been used. Since the observational data which these empirical models are based on are limited and there are discrepancies between the actual spatial and temporal variations and the models, new in-situ observations of the atmospheric composition are desired. Therefore, we are developing a neutral mass spectrometer to measure the neutral atmospheric composition at the ionospheric altitudes onboard low earth orbit satellites and sounding rockets. The instrument being developed will be installed on S-310-46 sounding rocket targeting sporadic E layers in 2024. In the rocket experiment, the neutral atmospheric composition of O, O_2 and N_2, which are the major components in the lower part of the ionosphere up to an altitude of 130 km, will be mainly obtained to clarify the formation process of sporadic E layers. This neutral mass spectrometer is based on an instrument developed for lunar exploration by ISAS/JAXA, and adopts a time-of-flight system with triple reflections to provide sufficient resolution with its small size. The instrument needs to be downsized for the installation on the sounding rocket, and its design and performance evaluation were carried out by numerical simulations. In parallel, the development of an antechamber was also conducted. When the spectrometer is mounted on a flight vehicle, particles enter the instrument with relative velocity of the vehicle, which can result in some difficulties in measurements such as sensitivity degradation. Therefore, before particles enter the instrument, they are captured in a spherical antechamber attached in front of the particle intake and collided with the inner wall to slow them down to about their thermal velocity. In addition, the atmospheric density inside the antechamber is higher, which can increase the measurement sensitivity. These performances were estimated in the design phase. For the next step, we will manufacture the instrument, evaluate its performance and acquire its characteristics through tests, and then verify them in the sounding rocket experiment.

現在、2024 年に実施予定の観測ロケット実験に向けて、電離圏観測用中性大気質量分析器の開発を行っている。電離圏における中性大気組成は、電離・再結合過程によりプラズマ密度に影響し、さらに電気伝導度を介して電場変動に寄与するため、熱圏変動のみならず電離圏変動を捉える上でも重要な物理量である。しかし、近年の人工衛星や観測ロケットによる電離圏その場観測において、中性大気組成の測定例は少なく、MSIS などの経験モデルが用いられている。このような経験モデルの基となっている観測データは限定されており、実際の時空間変動とモデルのずれが指摘されているため、新たな中性大気組成のその場観測が望まれている。そこで、観測ロケットや低軌道衛星に搭載し、電離圏高度の中性大気組成を測定するために、中性大気質量分析器の開発を行っている。開発している装置は、2024 年に行われるスポラディック E 層を対象とした観測ロケット S-310-46 号機に搭載される予定である。このロケット実験ではスポラディック E 層の形成過程を明らかにするために、電離圏下部に当たる高度 130km までの主要な成分である酸素や酸素分子、窒素分子を中心とした中性大気組成を取得する。この中性大気質量分析器は JAXA 宇宙科学研究所において開発されていた装置を基にしており、小型ながらも十分な分解能を持たせるため、質量分析部に三回反射式の飛行時間型機構を採用している。観測ロケット搭載のためには装置の小型化が必要であり、そのための設計、及び性能評価を数値シミュレーションにより行った。また、並行して観測ロケット搭載のために必要となる前室部 (antechamber) の設計・性能評価も行った。飛翔体に搭載して中性大気計測を行う際、粒子は相対的にロケット速度を持ったまま装置に入射することとなり、感度低下などが生じる。そこで、装置に入射する前に粒子を球殻状の antechamber に取り込み、内壁に衝突させることで熱速度程度まで減速させる。また、antechamber 内では大気密度が高くなるため、測定感度を上げることができる。現在進めている設計ではこれらの特性の見積もりを行っている。今後は装置を製作し、試験を通して性能評価、特性取得を行った後、観測ロケット実験にて検証を行う。

R005-P27
ポスター 3 ：11/6　AM1/AM2 （9:00-12:30）

#川原　琢也 [1)], 斎藤　徳人 [2)], 津田　卓雄 [3)], 兵藤　初美 [3)], 野澤　悟徳 [4)], 川端　哲也 [4)], 和田　智之 [2)]
([1] 信州大・工,[2] 理化学研究所基幹研,[3] 電通大,[4] 名大・宇地研

Faraday filter transmission measurements with a narrowband 589 nm light source for the Na lidar observations at Tromsoe

#Takuya Kawahara[1)], Norihito Saito[2)], Takuo Tsuda[3)], Hatsumi Hyodo[3)], Satonori Nozawa[4)], Tetsuya Kawabata[4)], Satoshi Wada[2)]
([1]Faculty of Engineering, Shinshu University,[2]ASI, RIKEN,[3]UEC,[4]ISEE, Nagoya Univ.,

An Na lidar at Tromsoe is currently at a stage of upgrading the receiver system for the thin Na atom observations in the lower thermosphere (<200km). The Na atom density at this altitude region is expected to be only ~2-3 atms/cm3 compared with ~2,000 atoms/cm3 at the Na layer peak (~90 km). To achieve the high S/N ratio measurement, even at the nighttime, the ultra-narrow optical filter such as a Faraday filter is necessary to reject the background skylight. The Faraday filter consists of a heated Na cell placed in a strong magnetic field (i.e., ~200 mT) between two polarizers. Using the Faraday rotation and the Zeeman effect, ultra-narrow optical bandpass (~10GHz or ~0.01nm at 589 nm) can be achieved.

We assembled a transmission diagnosis system at 589 nm on the basis of two narrowband DFB lasers at RIKEN. The more robust system is already used for the lidar observations. The details of the DFB laser system and the measured Na-saturation spectrums for the absolute frequency reference are presented by Hyodo et al. at the SGEPSS fall meeting, 2022. Using the same light source, the transmission profile measurements of the Faraday filter can be conducted.

In this talk, the results of the transmission measurements are discussed, and the performance of a commercially available Na cell is evaluated. A newly developed Na cell is also presented.

R005-P28
ポスター 3 ：11/6　AM1/AM2 （9:00-12:30）

#兵藤　初美 [1)], 斎藤　徳人 [2)], 津田　卓雄 [1)], 渡部　蓮 [1)], 野澤　悟徳 [3)], 川端　哲也 [3)], 川原　琢也 [4)]
([1] 電通大,[2] 理化学研究所基幹研,[3] 名大・宇地研,[4] 信州大・工

Sodium saturation spectroscopy using distributed feedback lasers

#Hatsumi Hyodo[1)], Norihito Saito[2)], Takuo Tsuda[1)], Ren Watabe[1)], Satonori Nozawa[3)], Tetsuya Kawabata[3)], Takuya Kawahara[4)]
([1]UEC,[2]ASI, RIKEN,[3]ISEE, Nagoya Univ.,[4]Faculty of Engineering, Shinshu University,

Sodium (Na) resonance scattering lidar is a means of laser remote sensing capable of measuring temperature and wind velocity in the mesospheric and lower thermospheric (MLT) region (the altitude range from 80 to 110 km). To perform such lidar observation, it is important to tune the laser frequency to a resonance line of Na for accurate measurements of the Doppler broadening (related to the temperature) and Doppler shift (related to the wind velocity) in the Na resonance fluorescence spectrum. The Na saturation spectroscopy can produce fine structures ($<$10 MHz), called Lamb dips and crossover peaks, in the Na resonance fluorescence spectrum, and these structures can be used as the absolute frequency standards for accurate laser frequency control. Narrow linewidth distributed feedback (DFB) lasers have the potential for several applications, e.g., telecommunication and trace molecular gas detection. In addition, the DFB lasers have advantages as stable and compact laser systems. Generally, to obtain a Na D2 resonance light (589 nm) by use of DFB lasers, nonlinear frequency conversion, i.e., sum frequency generation (SFG) or second harmonic generation (SHG), is needed. As a result of this kind of wavelength conversion (with 20 mW DFB lasers), the obtained output power, however, becomes normally a few μ W, which is normally not enough to induce saturation in the Na saturation spectroscopy experiments. Therefore, the previous study performed the Na saturation spectroscopy experiments using the amplified 589 nm light source composed of a configuration of master oscillator fiber amplifier and a high-efficiency wavelength conversion module, which is a waveguide periodically poled lithium niobate.

In this study, we have developed a new optical system for Na-saturation spectroscopy using a low-output power 589 nm light source with a few μ W obtained in SFG by mixing two DFB lasers, without the fiber amplifier and the high-efficiency wavelength conversion module used in the previous study. First, based on the theory of Na hyperfine structures, we modeled Na transitions inside of the Na vapor cell in Na-saturation spectroscopy experiments and investigated the Na saturation by changing the model parameters. As the result, we found the importance of the beam waist size of the laser (i.e., the 589-nm coherent light), which can affect the laser intensity as well as the advection rate. Then, based on the theoretical investigations, we developed an efficient optical system, in which we added lenses to increase the intensity in the Na cell. With the increase in the intensity, the Na D2 hyperfine structures such as Lamb-dips and crossover-peaks were successfully observed with an input power of 6 μ W. In further experiments, we optimize the tuning method of the laser frequency and the cell temperature, the measurements, and the data analysis of measured data. These experiments can be compared with theoretical calculations by the developed model, and thus we evaluate the performance of our Na saturation spectroscopy for further improvements.

In the presentation, we will present experimental results from the developed optical system along with theoretical calculations from the developed model, and then discuss the current performance of our Na-saturation spectroscopy experiments.

R005-P29
ポスター 3 ：11/6　AM1/AM2 （9:00-12:30）

#江尻　省 [1,2)], 桂川　眞幸 [3)], 橋本　彩香 [3)], 小林　蒼汰 [3)], 津田　卓雄 [3)], 中村　卓司 [1,2)]
([1] 極地研,[2] 総研大,[3] 電通大

Development of a resonance scattering lidar for simultaneous observation of meteoric metal atom and ion

#Mitsumu K. Ejiri[1,2)], Masayuki Katsuragawa[3)], Ayaka Hashimoto[3)], Sota Kobayashi[3)], Takuo Tsuda[3)], Takuji Nakamura[1,2)]
([1]NIPR,[2]SOKENDAI,[3]UEC

In a transition region between neutral atmosphere and geospace plasma (80 - 500 km), the vertical mass transport process has still to be revealed because simultaneous measurement of neutral atmosphere and plasma is quite difficult. There are layers of metal atoms and ions in the mesosphere and lower-thermosphere region produced by meteoric ablation. The meteoric ablation occurs mainly around 80-120 km, so metal layers are usually observed below 120 km. However, there have been many recent reports confirming the presence of metal atoms at altitudes higher than that by resonant scattering lidar observations. A simulation study conducted by Chu and Yu (2017) to investigate a possible source of thermospheric iron layers observed at McMurdo Station in Antarctica suggested that metal atoms may be incorporated into vertical transport in geospace with ionization and neutralization, moving over a wide altitude range. Simultaneous observation of the vertical density profiles of metal atoms and ions and tracking their temporal changes could provide observational evidence of large-scale vertical mass transport in the transition region. Calcium is the only metal that can be observed in both atom (Ca) and ion (Ca^+) by ground-based resonant scattering lidar observations. To measure temporal variation in vertical density distributions of Ca and Ca^+, as a dynamical tracer in this region, we started to develop a resonance scattering lidar system, which has an injection-locked Ti:Sapphire laser; a multi-frequency, nanosecond pulse, and a broad frequency tenability. In this presentation, we will introduce the new lidar system and show some preliminary results of test observations.

R005-P30
ポスター 3 ：11/6　AM1/AM2 （9:00-12:30）

主成分分析による磁場水平ベクトルの解明

#高山　久美 [1)], 吉川　顕正 [2)], 三好　勉信 [3)]
[(1] 九大,[(2] 九大/理学研究院,[(3] 九大・理・地球惑星

Clarifying Horizontal Vectors of Magnetic Fields Using Principal Component Analysis

#Kumi Takayama[1)], Akimasa Yoshikawa[2)], Yasunobu Miyoshi[3)]
[(1]Kyushu Univ.,[(2]Kyushu Univ.,[(3]Dept. Earth & Planetary Sci, Kyushu Univ.

Principal Component Analysis (PCA) is a statistical technique that transforms and reduces correlated multivariate data into a small number of uncorrelated variables called ”principal components” We are currently investigating the effectiveness of this method using several different approaches.

In this study, we use this method to derive basis functions for each station and each month from the data of the ground magnetic field during magnetic quiet days of the MAGnetic Data Acqusition System/Circum-pan Pacific Magnetometer Network (MAGDAS/CPMN) from 1992 to 2004. Then we reconstruct daily variations using these basis functions. In particular, the global current structure of the horizontal component was reconstructed from the first to the third principal components to visualize the as equivalent current.

In this study, we compared the following two approaches in generating the dispersion matrix to construct this basis function.
(1) Applying PCA to the northward component (H) and the eastward component (D) of the magnetic field, respectively.
(2) Applying PCA as a vector with horizontal components ($\sqrt{\ H^2\ +D^2\ }$).

As a result, the first principal component showed daily variations of the geomagnetic field (Sq-EEJ current system) in both methods, while the second and third principal components, the method (1) more clearly shows the current structure driven by the wind upwelling and suction of the atmospheric semidiurnal tides. On the other hand, the method (2) has a clearer structure of the Interhemispheric Field-Aligned Current (IHFAC) that bridge both the northern and southern hemispheres. In this presentation, we will report the results of a discussion on how these different methods for obtaining basis functions affect the extraction of information from current systems.

These results strongly suggest that principal component analysis is a useful method for understanding ionospheric-atmospheric vertical coupling.

主成分分析（PCA）とは、相関のある多変量データを『主成分』と呼ばれる相関のない少数の変数に変換し縮約する統計手法の一つである。現在我々は、この手法について、いくつかの異なるアプローチを用いて、その有効性の調査を行っている。

本研究では、この手法を用いて、1992〜2004 年の全球的地磁気観測ネットワーク (MAGDAS/CPMN) の磁気的静穏日における地上磁場のデータから、各観測点、各月の基底関数を導出し、この基底関数を用いて日変動を再構成した。特に、第 1 主成分から第 3 主成分までを等価電流法を用いた可視化法により、水平成分のグローバルな電流構造を再現した。

今回は、この基底関数を構成する為の分散行列を生成する際に、以下 2 つのアプローチによる比較研究を行った。
(1)『磁場の南北成分 (H) と東西成分 (D) それぞれに PCA をかける方法』
(2)『水平成分 ($\sqrt{\mathrm{H}^2+\mathrm{D}^2\ }$) を持つベクトルとして PCA をかける方法』

その結果、第 1 主成分はどちらの手法も地磁気の日変動（Sq-EEJ 電流系）が現れていたが、第 2 主成分、第 3 主成分では、前者 (1) の手法の方がより明確に大気の半日潮汐の風の湧き出しと吸い込みによって駆動される電流構造をもつことが明らかになった。一方、後者（2）の手法からは、南北両半球を跨ぐ沿磁力線電流 (IHFAC) の構造が、よりクリアに表現されるなどの特徴を持つことが明らかになった。本講演では、こうした基底関数を求める手法の違いが、電流系の情報抽出においてどのような影響を与えるのかについての考察結果を報告する予定である。

これらの結果は、主成分分析が電離圏-大気圏上下結合を解明する際に役立つ手法であることを強く示唆している。

R005-P31
ポスター 3 ：11/6　AM1/AM2 （9:00-12:30）

2019 年の南半球成層圏突然昇温が中間圏・熱圏の大気大循環に引き起こす影響について

#山本　桂輔 [1)], 三好　勉信 [1)]
([1] 九大・理・地球惑星

The impacts of the 2019 southern hemisphere SSW on the general circulation in the mesosphere and thermosphere

#Keisuke Yamamoto[1)], Yasunobu Miyoshi[1)]
([1]Dept. Earth & Planetary Sci, Kyushu Univ.

Stratospheric Sudden Warming (SSW) is an event in which atmospheric temperature in the polar stratosphere rises by several tens of kelvin within a few days. The previous studies indicated that cooling and warming occurred in the polar mesosphere and lower thermosphere, respectively. In this study, we focus our attention on the impacts of SSW in the southern hemisphere that occurred in September 2019 on the general circulation in the mesosphere and thermosphere, and similarities and differences between southern hemisphere SSW and northern hemisphere SSW. In this study, an atmosphere-ionosphere coupled model (GAIA) simulation was used. Our results indicate that the meridional circulation in the mesosphere and thermosphere are influenced by the 2019 SSW. It is noteworthy that the vertical wind in low latitudes and north hemisphere in the mesosphere and lower thermosphere (MLT) is also affected by the 2019 SSW. These features are similar to those in the northern hemisphere SSW events. However, the magnitude of the meridional circulation in the MLT during the 2019 SSW is somewhat weaker than that during the SSW events in the northern hemisphere. Detailed results and discussions will be shown in the poster.

成層圏突然昇温 (Stratospheric Sudden Warming：SSW) とは極域成層圏において気温が数日の間に数 10K 上昇する現象である。先行研究によると、SSW の影響は極域成層圏だけでなく、中間圏・熱圏にも影響を及ぼすことが分かっている。例えば、中間圏極域では降温、下部熱圏の極域では昇温すると考えられている。本研究では、2019 年の 9 月に発生した南半球の成層圏突然昇温時の中間圏・熱圏の応答に焦点を当てて解析を行った。2002 年以来発生していなかった非常にまれな南半球の成層圏突然昇温が、北半球での成層圏突然昇温が中間圏・熱圏に及ぼす影響と、どの点が同じでどの点が異なるのかについて調べた。本研究では、大気圏－電離圏結合モデル（GAIA）の計算結果を用いた。成層圏突然昇温時の中間圏・熱圏での子午面循環の変化について調べてみたところ、以下のことが分かった。南極域の成層圏と熱圏で下降流が強まり昇温し、中間圏で下降流が強まり降温するという北半球の突然昇温と同じパターンが見られた。しかし、極域での鉛直流の変化量については、北半球の場合と異なっていた。さらに赤道域や北極域（反対半球）でも南極域の循環の変化に対応して子午面循環が変化していることが分かった。このことは、南半球の成層圏突然昇温についても、影響は反対半球にまで及ぶことを示唆している。両半球における成層圏突然昇温に対する中間圏・熱圏の応答の違いについての詳細は当日議論する予定である。

R005-P32
ポスター 3 ：11/6　AM1/AM2 （9:00-12:30）

成層圏準 2 年周期振動が引き起こす中間圏・下部熱圏の東西風変動について

#菅田　凌生 [1)], 三好　勉信 [1)]
([1] 九大・理・地球惑星

The zonal wind variation in the mesosphere and lower thermosphere caused by the stratospheric Quasi-Biennial Oscillation

#Ryo Sugata[1)], Yasunobu Miyoshi[1)]
([1]Dept. Earth & Planetary Sci, Kyushu Univ.

The stratospheric Quasi-Biennial Oscillation (QBO), which is a quasiperiodic oscillation of the equatorial zonal wind with a period of about 27 months, is one of the most prominent phenomena in stratosphere. Previous studies suggested that the QBO affects the general circulation not only in the middle and high latitudes but also in the mesosphere and lower thermosphere (MLT). The purpose of this study is to investigate impacts of the QBO on the general circulation in equatorial MLT region and to identify its excitation mechanism. GAIA model data from July 2007 to June 2017 was used in this study. This analysis focuses on how atmospheric waves originating from the troposphere are modulated by the stratospheric QBO and how they affect the zonal mean flow in the equatorial MLT region. The results showed that the amplitudes of the Kelvin wave with 2-5day periods and were influenced by the QBO. For example, the Kelvin waves has larger amplitudes during the easterly phase of the QBO. By analyzing the zonal wind acceleration due to these waves, we discuss how the QBO affects the general circulation in the equatorial MLT region.

成層圏準 2 年周期振動 (QBO) は、赤道域成層圏において最も顕著な変動で、東西風が約 27 か月周期で交代する現象である。QBO の影響は、成層圏中高緯度域の大気循環のみならず中間圏・下部熱圏領域 (MLT 領域) の大気循環にまで及んでいる可能性が示されている。本研究では、赤道域 MLT 領域における QBO の影響を調べ、その原因を明らかにすることを目的としている。GAIA モデルを用いて、2007 年 7 月から 2017 年 6 月の 10 年間について解析を行った。赤道 MLT 領域の東西風にも、成層圏 QBO と関係のある変動が見られた。そこで、モデルデータを詳しく解析したところ、対流圏を起源とする大気波動が、成層圏 QBO によって変調し、MLT 領域の東西平均場に影響を及ぼしていることが明らかとなった。例えば、東西波数 1 ・2〜5 日周期のケルビン波や 1 日潮汐波の振幅が成層圏 QBO に伴って変動しており、特にケルビン波の振幅は、QBO 東風時に強くなっていることが分かった。これらの大気波動について、東西平均流に対する加速効果を調べることにより、QBO が赤道 MLT 領域の大気大循環にどのような影響を与えているか議論する。

SS-520-3 号機観測ロケットは、方位角 202.4 度、仰角 80.7 度で 10 時 09 分 25 秒 UT に打ち上げられた。打ち上げ前後の電離層の状態を EISCAT スヴァールバル・レーダーの 32m と 42m アンテナでモニターし、ロケット軌道の頂点付近を通る磁力線に沿った高度 350km 付近の位置で電子温度が上昇していることを確認して、打ち上げタイミングを決定した。ロケットの軌道はほぼ計画通りで、打ち上げ 487 秒後（10 時 17 分 32 秒 UT）には最高高度 742km に到達し、打ち上げ 994 秒（10 時 25 分 59 秒 UT）には水平距離 1354km を飛んで着水した。

SS-520-3 号機観測ロケットには、DFG: Digital Flux Gate magnetometer、LFAS: Low Frequency Analyzer System、TSA: Thermal ion Spectrum Analyzer、LEP: Low Energy Particle experiment、IMS: Ion Mass Spectrometer、FLP: Fast Langmuir Probe, NLP: Needle Langmuir Probe, NEI/PWM: Plasma and Wave Monitor, SAS: Sun Aspect Sensor の 9 つの観測装置が搭載されているが、得られたデータから SS-520-3 号機観測ロケットは高度 700km 以上の Apex 付近とそれ以降の時間帯に、マントル、カスプ、LLBL を飛行することに成功したことがわかった。また、SS-520-3 号機観測ロケットがカスプを飛行している間、搭載されたすべての観測機器がデータを取得することに成功した。

SS-520-3 号機観測ロケット実験は、地上レーダや光学観測を含む総合的な観測キャンペーンとして実施した。また、SS-520-3 号機観測ロケットは、カスプ領域の物理の共通理解を深めることを目的とした大規模な国際共同プロジェクト「Grand Challenge Initiative (GCI) Cusp program」に参加するプロジェクトの 1 つでもある。